行政院國家科學委員會專題研究計畫 期中進度報告

寬頻光都會與接取網路之關鍵技術--總計畫:寬頻光都會與接取網路之關鍵技術(2/3)
期中進度報告(精簡版)

計 畫 類 別 ：整合型
計 畫 編 號 ：NSC 95-2221-E-002-185-
執 行 期 間 ：95 年 08 月 01 日至 96 年 07 月 31 日
執 行 單 位 ：國立臺灣大學電機工程學系暨研究所

計 畫 主 持 人：吳靜雄

公 開 資 訊 ：期中報告不提供公開查詢

中 華 民 國 96 年 06 月 01 日

行政院國家科學委員會專題研究計劃成果報告

寬頻光都會與接取網路之關鍵技術—總計劃(2/3)

計劃編號： NSC-95-2221-E-002-185

執行期限：95 年 8 月 1 日至 96 年 7 月 31 日

主持人：吳靜雄教授

共同主持人：曹恆偉教授　李三良教授 李揚漢教授 曹士林教授

執行單位：台大電機系 台科大電子系 淡江電機系 師大光電所

一、 中文摘要

為因應急速增加的頻寬需求，光纖網路已成為建構寬頻資訊網路的主要媒介。為了有效利用光纖的高容量特性，分波多工(WDM)、分碼多工(CDMA)及分時多工(TDMA)為常見的傳輸方式。同時，高速的路由交換與波長轉換元件為發展光纖網路的關鍵技術。本整合型計畫希望能針對高速光通訊系統與元件之設計進行研究。

在高速光通訊系統設計方面，本計畫中研究於馬可夫模型之自相關傳輸量輸入下的光封包交換機之效能；同時本計畫研究及二維光分碼系統之特性，並藉由上述之研究將二維光分碼應用於被動光網路以實現寬頻接取服務。在元件設計方面，本計畫研究異質積體化技術以將製作於不同基材的多功能元件整合在同一基板上，以結合光通訊模組所需的光學與電路，降低成本並增加可靠度；另外本計畫也研究價格低廉且體積小的光學共振腔式(etalon)光濾波器元件及二段式分佈反饋雷射展示其單模與多模競爭之全光時脈回復機制。

關鍵詞：分波多工，分碼多工，被動光網路，可調波長雷射，波長轉換，光封包交換

Abstract

The optical fiber plays an important role in the broadband wireline communication networks. Three techniques: wavelength division multiplex (WDM), code division multiple access (CDMA) and time division multiple access (TDMA) are most commonly used transmission schemes to efficiently utilize the large bandwidth provided by the fiber. The optical communication devices such as high speed packet switch and wavelength converter are the key components in the optical communication networks. This integrated project studies the high-speed optical communication systems and the design of the optical components.

In this project, we investigate optical packet switches under Markovian modeled self-similar traffic input. We also investigate a 2D OCDMA system which can be applied to the passive optical network which is a solution to realize the full service access network. For the design of the optical components, in order to combine the optical communication modules with the required optic components and electrical circuit, to reduce the cost, and to increase the reliability, we investigate the hetero-integration technology to fabricate the devices of different substrates in one substrate. In addition, we also investigate the low cost and small area etalon optic filter and demonstrate all-optical clock recovery under the psuedorandom bit sequence data injection by using a two-section DFB laser when it was biased at the self-pulsating condition in single mode or in multi-mode competition case.

二、 重要研究成果

I. 子計畫一

網際網路已融入人們日常生活中，也是資訊取得及傳播的利器，因其用戶數迅速增加，寬頻需求殷切，一個好的交換技術是必須要的，而光封包交換技術結合了分波多工的技術，具備了高速交換能力，高資料傳輸速度與格式通透性，在未來即將在通訊領域中扮演重要的角色。本研究主題為(1)於馬可夫模型之自相關傳輸量輸入下的光封包交換機之研究及(2)二維光分碼系統特性之探討。

首先，我們研究使用部分緩衝分享機制下之光封包交換機在馬可夫模型之自相關傳輸量輸入下的封包遺失行為。兩種優先權的分類在此被考慮，此兩者都是自然自相關，且靠著兩個獨立的馬可夫抵達程序來近似。緩衝記憶體的門檻值把佔領緩衝記憶體的狀態空間分成兩個部分，當此週期時間被假設成隨意發生，此種分割將依次給予緊要的與非緊要的週期時間。因此，我們研究與分析短時間與長時間的效能估量，恰當的分析結果已被計算出且被模擬結果所驗證，當光交換機在自相關傳輸量輸入下提供不同的服務時，我們的分析對於最佳化的緩衝記憶體控制是有用的。

其次，我們將指出分波多工的光封包交換機若使用波長轉換時，在馬可夫模型之自相關傳輸量輸入下，其效能會因採用波長轉換的技術而有好處。我們已經計算出分析的結果，且被模擬所驗證，我們提出一種程序去計算數值結果，並減少了計算的時間與複雜度，在獲得分波多工之光封包交換機的滿意效能上，我們的分析是非常有用的。

最後，我們探討二維光編碼的特性，並研究系統架構，在光域上分波多工不需考慮同步問題，但在時域編碼分為同步及非同步兩種，我們比較各種編碼之後發現完美差異碼具許多優點，所以我們將其應用在系統中並完整的評估其效益，數值結果顯示此系統之同時使用者數目及錯碼率均優於其他系統。另外，因光纖已被大量使用，我們也提出二維光域及空域接取網路。

詳細內容請參考附件一。

II. 子計畫二

本子計畫研究供都會網路及接取網路應用的光電主動元件模組，並研發異質積體化技術以將製作於不同基材的多功能元件整合在同一基板上，以結合光通訊模組所需的光學與電路，降低成本並增加可靠度。

我們使用一個價格低廉且體積小的光學共振腔式(etalon)光濾波器元件，放置於 10Gbps 直調雷射的輸出端，可以達到抑制頻率啁啾效應進而延伸傳輸距離的目的，從小於 10 公里增加到大於 75 公里，實驗結果可以對 2 個 10Gbps 直調雷射同時進行補償，因此利用 etalon 的週期性頻譜變化的特性，證實可以同時對多個通道的直調雷射傳輸系統達到性能改善的效果。

我們就二段式分佈反饋雷射展示其單模與多模競爭之全光時脈回復機制，且使用光學濾波器可使全光時脈回復機制同時在多模態下進行。

詳細內容請參考附件二。

III. 子計畫三

本計劃中，針對同步光分碼多工存取系統架構做討論，為了讓系統模擬更符合實際上現象，考慮了接收端使用者的功率會隨著傳送距離遠近而有大小差異的條件，因此在傳統發射同步型的訊框格式下，當考慮使用者接收之功率不同時，會影響整體的系統效能。針對此問題我們提出了接收同步型的架構，藉由估測出距離相對之時間使每個使用者到達耦合器之時間相同，並將訊框格式加以改善，加強使用者間相互干擾的偵測，提升系統效能。最後，我們利用模擬軟體，建構及模擬六組使用者之同步光分碼多工存取系統在發射同步型和接收同步型架構下的效能比較。

詳細內容請參考附件三。

IV. 子計畫四

本子計畫研究重點在於光分碼多工（OCDMA）接收機電路製作，以及光通信網路中信號品質監測之研究。為了增加 PON 網路使用者數目及傳輸容量，實際應用多以分時多工機制來達成，然而其仍具有頻寬使用不佳的缺點存在。本計畫根據完美相差碼所建構的分碼多工機制，設計出接收機前端電路並以台積電 0.35 微米 CMOS 製程完成實作。此外，為了進行光信號品質之即時監測，本計畫另一部份利用非同步光域取樣的方式，根據所得之統計資訊來進行光信噪比（OSNR）之估測。

本計畫所製作的光分碼多工接收電路，包括轉阻放大器（TIA）、可變增益放大器（VGA）、後級放大器與類比相關器（Analog Correlator），以上元件均整合於同一晶片上。為了有效提高電路頻寬，我們採用共閘形式的轉阻放大器，在可變增益放大器與後級放大器則採用主動回授的設計方式。在相關器方面，利用改良式 Gilbert 電路的架構，能夠對完美相差碼進行相關運算。經過測試，本電路在 1.25GHz 的展頻碼與 3.3 伏特輸入電壓之下，總消耗功率為 452mW 且可正常工作。

在信號品質監測之研究方面，非同步光域取樣是本計畫的研究主題。藉由光域非同步取樣所得之統計直方圖

（Histogram），我們可以統計與曲線擬合的方法得到與光信噪比（OSNR）有關的參數。然而在即時監控的應用上，如何能以較少的取樣數獲取足夠且可靠的資訊仍是值得研究的課題。因此我們對取樣時脈進行三角波頻率調變，經模擬驗證（OptiSystem）後發現在 10Gb/s 不歸零碼傳輸應用中，在取樣數為 8192 點即可得到良好的監測參數性質。同時在 10Gb/s±50ppm 的系統時脈運作下都可得到一致的結果，達成位元速率透明性（bit-rate transparency）的理想。

詳細內容請參考附件四。

V. 子計畫五

在最近幾年，光子晶體光通訊元件設計上已逐漸廣泛的被研究應用，現行在產業及學術研究上也充分的被應用及開發，然而光通信元件之縮小化亦為必然趨勢，因此，本計畫即是以縮小現有光通信元件，並朝向光學能隙晶格光通信元件的技術進行研發為目的。本計畫為“下世代光子晶體內嵌式光交換器元件設計、製作及應用於寬頻都會與擷取網路平台之研究”總計畫之一部份，並分三年進行，第一年已完成光學能隙晶格光子晶體光波導光通信元件系統之研究，並建立模擬環境及測量元件基礎環境，並建立微細光纖抽拉裝置結合設計及模擬矽上微腔盤光記憶儲存單位，以輸入光至微腔盤的共振條件成立與否去決定信號光是否在腔盤中儲存其光能量。本年度為計劃第二年，目前已完成利用矽上絕緣層矽晶元件建立光學讀取系統結合多模干涉型光學能隙波導光分歧器及光子晶體Mach-Zehnder結構，並與第一年之光學能隙晶格光子晶體光波導光通信元件系統整合。進度正常依計劃進行，未來第三年將進行32x32矽上絕緣層矽晶為基底奈米光學光波導及波長可交換式微波光子晶體光控開關主動元件光通信元件之研究及整合，以應用於新世代高速光通信系統之中。

本計畫完成研究矽上絕緣層矽晶元件建立光學讀取系統結合多模干涉型光學能隙波導光分歧器及光子晶體Mach-Zehnder結構。我們利用二維光子晶體週期性結構及線狀缺陷的技術並針對不同的能隙結構來控制光在光子晶體波導中行進的路徑，以便達到縮小積體光學元件之體積。多模干涉型光學能隙波導光分歧器是基於自成像現象設計而成。我們利用自成像現象在矽上絕緣層矽晶脊狀光波導設計多模干涉光分歧器並進一步研究自成像現象在光子晶體傳播情形來設計光學能隙波導光分歧器。此外，我們利用六角形晶格光子晶體的Mach-Zehnder結構來達成干涉現象，並藉此設計光學信號讀取系統。

詳細內容請參考附件五。

三、 計畫成果自評與討論

本計畫在光纖通訊研究上有相當多的成果，包括了高速光通訊系統之效能分析，光分碼多工之編碼研究，光封包交換技術及其效能，異質積體化技術光學共振腔式(etalon)光濾波器元件，已有許多專利及論文發表，成果豐富。

附件一

行政院國家科學委員會專題研究計劃成果報告

高速光子交換及被動接取光網路之研究—子計畫一

(2/3)

計劃編號： NSC-95-2221-E-002-184

執行期限：95 年 8 月 1 日至 96 年 7 月 31 日

主持人：吳靜雄教授

參與人員：Malla Reddy Perati、黃富源、邱建林、楊有為、陳仲軒、吳柏毅、余靖涵、陳培霖、戴嘉瑩

中文摘要

網際網路已融入人們日常生活中，也是資訊取得及傳播的利器，因其用戶數迅速增加，寬頻需求殷切，一個好的交換技術是必須要的，而光封包交換技術結合了分波多工的技術，具備了高速交換能力，高資料傳輸速度與格式通透性，在未來即將在通訊領域中扮演重要的角色。本研究主題為(1)於馬可夫模型之自相關傳輸量輸入下的光封包交換機之研究及(2)二維光分碼系統特性之探討。

首先，我們研究使用部分緩衝分享機制下之光封包交換機在馬可夫模型之自相關傳輸量輸入下的封包遺失行為。兩種優先權的分類在此被考慮，此兩者都是自然自相關，且靠著兩個獨立的馬可夫抵達程序來近似。緩衝記憶體的門檻值把佔領緩衝記憶體的狀態空間分成兩個部分，當此週期時間被假設成隨意發生，此種分割將依次給予緊要的與非緊要的週期時間。因此，我們研究與分析短時間與長時間的效能估量，恰當的分析結果已被計算出且被模擬結果所驗證，當光交換機在自相關傳輸量輸入下提供不同的服務時，我們的分析對於最佳化的緩衝記憶體控制是有用的。

其次，我們將指出分波多工的光封包交換機若使用波長轉換時，在馬可夫模型之自相關傳輸量輸入下，其效能會因採用波長轉換的技術而有好處。我們已經計算出分析的結果，且被模擬所驗證，我們提出一種程序去計算數值結果，並減少了計算的時間與複雜度，在獲得分波多工之光封包交換機的滿意效能上，我們的分析是非常有用的。

最後，我們探討二維光編碼的特性，並研究系統架構，在光域上分波多工不需考慮同步問題，但在時域編碼分為同步及非同步兩種，我們比較各種編碼之後發現完美差異碼具許多優點，所以我們將其應用在系統中並完整的評估其效益，數值結果顯示此系統之同時使用者數目及錯碼率均優於其他系統。另外，因光纖已被大量使用，我們也提出二維光域及空域接取網路。

Abstract

Internet has been utilized worldwide, the number of users grow rapidly. The demand of bandwidth increases tremendously. A good switching technology is required, and optical packet switching (OPS) incorporating with wavelength division multiplexing (WDM) technology, which has high-speed switching capability, high data rate and format transparency, is an attractive in the near future. The topics of this search are to investigate optical packet switches under Markovian modeled self-similar traffic input and optical code division multiple access (OCDMA) system.

First, we investigate the loss behavior of optical packet switches (OPSes) employing partial buffer sharing (PBS) mechanism to provide differentiated services under Markovian modeled self-similar traffic input. Two priority classes are considered; both are self-similar in nature and are fitted by two independent Markovian arrival processes (MAPs). The level of buffer threshold divides the state space of the buffer occupancy into two parts. Such a partition in turn gives the critical and non-critical periods which are assumed to occur alternatively. Accordingly, we investigate and analyze both the short term and long term performance measures. Pertinent analytical results are computed and then verified by simulation. Our analysis is useful in telling the optimal control of buffer of OPS handling self-similar traffic to provide differentiated services.

Second, we make the switching performance of wavelength division multiplexing (WDM) optical packet switch (OPS) employing wavelength conversion (WC) techniques under Markovian modeled self-similar traffic input to point the benefit of wavelength conversion. The analytical results are calculated and verified by simulation. We propose a procedure to calculate the numerical results in order to reduce the effort of computation. The computation complexity of the analysis is then presented. Our analysis is useful in dimensioning the WDM OPS to obtain satisfactory performance.

Last, we study two-dimensioned (2-D) Optical Code Division Multiple Access (OCDMA) techniques, several 2-D OCDMA systems were investigated, we have found that the Perfect Difference Code (PDC) have many advantages. Therefore the spectral/time OCDMA system utilizing PDC is investigated completely. The results show that this system has good performance. In addition, because the fibers are deployed in the cities and many residential areas, we also propose a spectral/spatial 2D OCDMA system, which may also applicable for wideband access network.

Keywords: *Differentiated service, Markovian arrival process, matrix-analytic method, partial buffer sharing, self-similar traffic, MAM, MAP,*

self-similar traffic, WDM optical packet switch, wavelength conversion, OCDMA, perfect difference code.

一、 研究內容與討論

(1) Loss Behavior Analysis of Optical Packet Switches Employing Partial Buffer Sharing Mechanism under Markovian Modeled Self-Similar Traffic Input

I. Queiueing Model of OPS Employing PBS Mechanism

Currently, due to the lack of optical random access memory (ORAM), only the passive type buffer management schemes are feasible to be realized in the high-speed optical switching nodes. Among the passive buffer management schemes, PBS mechanism is the most suitable one for OPS. This is because (1) optical buffers consisting of FDLs with fixed delay granularity can not arbitrarily hold the packets for a random amount of time, (2) the erasable optical buffers are not available yet for implementing push-out scheme. Also, due to the implementation, OPS of output queueing type is most feasible. Hence, the equivalent queueing model of a specific output port of the OPS with a service discipline of first-come-first-serve (FCFS) is equal to that of a multiplexer.

A general block diagram of OPS employing PBS mechanism is shown in the left hand side of Fig. 1, where there are N input ports and N output ports each having K +1 fiber delay lines (FDLs) constituting the optical buffers with buffer depth K. When the input traffic is with a fixed packet length and the OPS is operating at a synchronous mode, then the suitable choice of the delay unit, h, in each FDL is to let h equal the packet length of the input traffic measured in time. Consequently, the equivalent queueing model of one specific output port of the OPS employing PBS mechanism can be depicted in the right hand side of Fig. 1, in which, a buffer with buffer depth K and a threshold set at the buffer level $K-d$, $d \geq 0$ [21]. As shown in Fig. 1, the low priority packets can only access the '$K-d-1$' buffer spaces, whereas the high priority packets can utilize the whole buffer space regardless of the threshold level $K-d$. Accordingly, we can define the "critical period" as the time period during which the buffer occupancy is greater than or equal to $K-d$, and the "non-critical period" as the time interval during which the buffer occupancy is less than $K-d$ [19], [21]. In this report, we assume that the packet length is fixed and constant. Hence the resultant queueing system of OPS employing PBS mechanism handling Markovian modeled self-similar traffic with fixed packet length is equivalent to an *MAP/D/1/K* queue with PBS policy.

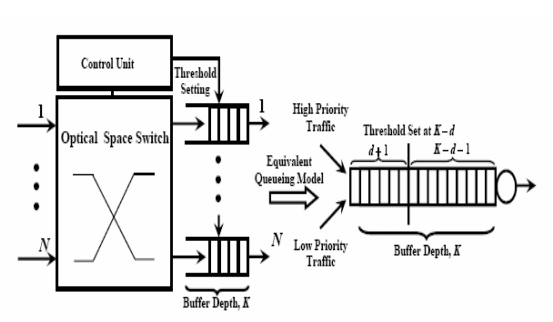

Fig. 1 A general block diagram of the OPS employing PBS mechanism and the equivalent queueing model of a specific output port of the same one with two different priority traffic input.

II Loss Behavior Analysis

Now we could analyze the loss behavior of OPS employing PBS mechanism with MAP modeled self-similar input traffic. For the sake of simplicity, two priorities are considered. Each priority traffic is characterized by a MAP emulating self-similar process. Higher priority (class 1) and lower priority (class 2) packets arrive at the system according to MAPs of states m_1 and m_2, respectively. The above MAPs are characterized by the matrices $\{C(1), D(1)\}$ and $\{C(2), D(2)\}$, respectively. The service time is generally and identically distributed with distribution function $H(t)$. Let $D_m^{(k)}(t)(m \geq 0, k = 1, 2)$ denote the matrices whose (i, j) th element is the probability that given departure of class k at time 0, there is at least one packet left in the system and the process is in state i, the next departure of class k occurs no later than time t with the arrival process in state j, and during that service time there are m arrivals. Then $D_m^{(k)}(t)$ satisfies the following equation

$$\sum_{m=0}^{\infty} D_m^{(k)}(t) z^m = \int_0^t e^{[C(k)+D(k)z]\tau} dH(\tau), \quad k = 1, 2.$$

When service time is deterministic and is h units/packet, then we have

$$\sum_{m=0}^{\infty} D_m^{(k)}(t) z^m = e^{[C(k)+D(k)z]h} u(t-h), \quad k = 1, 2.$$

where $u(t)$ is the unit step function. Therefore, we obtain

$$\sum_{m=0}^{\infty} D_m^{(k)}(h) z^m = e^{[C(k)+D(k)z]h}, \ k = 1, 2.$$

It is obvious that the matrices $D_m^{(k)}$ can be evaluated by comparing the coefficient of z^m on both sides of the above equation. This procedure is outlined in [18], wherein the complete proof or reference is not given. We shall prove the procedure in a simple way and propose a method to tell when the procedure could be terminated. We drop the index k for both classes. Then can be written as

$$\sum_{m=0}^{\infty} D_m(h) z^m = e^{[C+Dz]h}$$

As $e^{[C+Dz]h}$ is analytic, we utilize the decay proposition (Cauchy's estimate) of complex variables as follows.

Proposition 1: **Cauchy's Estimate**

Let the matrix function $a(z) = \sum_{m=0}^{\infty} a_m z^m$ be analytic for

$|z| < R$. Then for any ρ such that $0 < \rho < R$, one has $|a_n| \le M(\rho)\rho^{-n}, n = 0,1,2,3,\ldots,$ where $M(\rho) = \max_{|z|=\rho} |a(z)|$. More precisely, for a given $\varepsilon > 0$ (in our context, ε is the machine precision of the floating point arithmetic) $\exists N$ such that $\sum_{i=N+1}^{\infty} |a_i|$ has elements at most ε. In view of the Proposition 1 and Taylor series, $\sum_{m=0}^{\infty} D_m(h) z^m = e^{[C+Dz]h}$ can be rewritten as

$$\sum_{m=0}^{N} D_m(h) z^m + R_{\varepsilon}(z) = \sum_{r=0}^{\infty} \frac{1}{r!}(A+Bz)^r$$

where $A = Ch$, $B = Dh$ and has coefficients with small moduli at most ε. Hereafter, we drop the argument h in rest of the report for the sake of easiness.

From $\sum_{m=0}^{\infty} D_m(h) z^m = e^{[C+Dz]h}$, for m=0, we have

$$D_0 = I + \sum_{r=1}^{\infty} \frac{Ar}{r!}$$

where I is the unit matrix of appropriate dimension. For $m.n \ge 1$, let $T(n;m)$ be the coefficient of z^{m-1} in $(A+Bz)^n$, the nth term of the series on the right hand side of $\sum_{m=0}^{\infty} D_m(h) z^m = e^{[C+Dz]h}$, then we have

$$T(1,1) = A,\ T(1,2) = B,\ T(n,1) = A^n$$
$$T(n,m) = 0,\ if\ \ m > n+1,$$

and

$$T(n,1) + T(n,2)z + T(n,3)z^2 + \ldots + T(n,m)z^{m-1} + \ldots + T(n,n+1)z^n = (A+Bz)^n$$

Multiplying both sides by (A + Bz), we obtain

$$[T(n,1) + T(n,2)z + T(n,3)z^2 + \ldots + T(n,m)z^{m-1} + \ldots + T(n,n+1)z^n](A+Bz) = [A+Bz]^{n+1}$$

which could be re-written as

$$[T(n,1) + T(n,2)z + T(n,3)z^2 + \ldots + T(n,m)z^{m-1} + \ldots + T(n,n+1)z^n](A+Bz) = T(n+1,1) + T(n+1,2) + \ldots + T(n+1,n+2)z^{n+1}.$$

Equating the coefficients of like powers of z, we obtain

$$\begin{aligned} T(n+1,1) &= T(n,1)A, \\ T(n+1,2) &= T(n,2)A + T(n,1)B, \\ &\vdots \quad\ \vdots \quad\ \vdots \\ T(n+1,q) &= T(n,q)A + T(n,q-1)B, \\ & q \in \mathbf{N} \end{aligned}$$

For any positive integer m, D_m = coefficient of z^m in $\frac{(A+Bz)^m}{m!}$ + coefficient of z^m in $\frac{(A+Bz)^{m+1}}{(m+1)!}$ + coefficient of z^m in $\frac{(A+Bz)^{m+2}}{(m+2)!}$ + …

,i.e.,

$$D_m = \frac{T(m,m+1)}{m!} + \frac{T(m+1,m+1)}{(m+1)!} + \frac{T(m+2,m+1)}{(m+2)!} + \ldots .$$

Consequently, we obtain

$$D_m = \sum_{k=m}^{\infty} \frac{T(k,m+1)}{k!},\ for\ m = 1,2,\ldots,N$$

We then could compute the matrices $D_m s$ for both high priority and low priority packets. Though the above equation involves infinite number of

terms, due to the presence of $k!$ in the denominator, only finite number of terms are required to compute the matrices $D_m s$. The procedure of computing the matrices $D_m s$ can be terminated using Proposition 1. The procedure of computing the matrices $D_m s$ can be terminated using Proposition 1. This is an alternative method to the method proposed in [10], [12], which works well too.

Now consider the embedded Markov chain $\{L_n, J_n \mid n \geq 0\}$ at the departure epochs of the queueing system on the state space $S = \{(b,i,j) \mid 0 \leq b \leq K,\ 1 \leq i \leq m_1,\ 1 \leq j \leq m_2\}$, where L_n denotes the buffer occupancy and J_n denotes the phase of superposed MAP. For the sake of convenience, a queueing system is said to be at level b, if its buffer occupancy is equal to $b-1$ (excluding the one at service). Under the operation of PBS mechanism with the level of threshold $K-d,\ d \geq 0$, the embedded Markov chain has an irreducible transition probability matrix P that is given by

$$\begin{bmatrix}
GD & GD & \cdots & GD & GC & G(D \otimes D) & \cdots & G(D \otimes D) & GE(K) \\
D & D & \cdots & D & C & D \otimes D & \cdots & D \otimes D & E(K) \\
0 & D & \cdots & D & C & D \otimes D & \cdots & D \otimes D & E(K-1) \\
0 & 0 & \cdots & D & C & D \otimes D & \cdots & D \otimes D & E(K-2) \\
\vdots & \vdots & \ddots & \vdots & \vdots & \vdots & \ddots & \vdots & \vdots \\
0 & 0 & \cdots & D & C & D \otimes D & \cdots & D \otimes D & E(d+2) \\
0 & 0 & \cdots & D & C & D \otimes D & \cdots & D \otimes D & E(d+1) \\
0 & 0 & \cdots & 0 & D \otimes D & D \otimes D & \cdots & D \otimes D & E(d) \\
\vdots & \vdots & \ddots & \vdots & \vdots & \vdots & \ddots & \vdots & \vdots \\
0 & 0 & \cdots & 0 & 0 & 0 & \cdots & D \otimes D & E(1)
\end{bmatrix},$$

where

$$\begin{cases}
D_i &= \sum_{i'=0}^{i} (D_{i'}^{(1)} \otimes D_{i-i'}^{(2)}), \\
D_{-2} &= \sum_{i=0}^{\infty} D_i^{(2)}, \\
C_l &= \sum_{i'=0}^{l} (D_i^{(1)} \otimes D_{-2}^{(l-i)}), \\
E(p) &= D_{-1}^{(p)} \otimes D_{-2},\ p = 1,2,3,\ldots,K, \\
G &= (-C)^{-1} D, \\
\mathrm{C} &= \mathrm{C}(1) \otimes C(2), \\
D &= D(1) \otimes D(2),
\end{cases}$$

In above, the matrix G consists of the conditional probabilities that system is idle. The fundamental arrival rate of class k packets is $\lambda^{(k)} = \pi(k) D(k) e,\ k = 1,2,$ where $\pi(k)$ is the steady probability vector of $C(k)+D(k)$. Then the traffic intensity is given as $\rho = (\lambda^{(1)} + \lambda^{(2)}) E[H(t)]$.

From the operation of PBS mechanism, it is clear that high priority packet loss occurs buffer is full, whereas low priority packet loss happens due to the buffer occupancy threshold. Then, by definition, the steady state high priority packet loss probability (P^{hp}) and the steady state low priority packet loss probability (P^{lp}) are respectively given as

$$P^{hp} = \frac{Mean\ of\ \ high\ priority\ packet\ loss}{Mean\ of\ \ high\ priority\ packet\ arrival}$$

$$P^{lp} = \frac{Mean\ of\ \ low\ priority\ packet\ loss}{Mean\ of\ \ low\ priority\ packet\ arrival}$$

Firstly, the mean number of high priority and low priority packet arrivals are $\lambda^{(1)} E[H(t)]$ and $\lambda^{(2)} E[H(t)]$, respectively. Secondly, let $y = (y_0, y_1, \ldots, y_K)$, where $y_k = (y_{k,1,1}, y_{k,1,2}, \ldots, y_{k,m_1,m_2})$, $\forall k$, is the

probability that departing packet leaves k packets in the system, i.e., $yP = y$, $ye = 1$. And then following [19], the mean of high priority packet loss and the mean of low priority packets loss are respectively given as follows:

$$\sum_{i=1}^{\infty} iy_0 G(D_{K+i}^{(1)} \otimes D_{-2})e + \sum_{k=1}^{K}\sum_{i=1}^{\infty} iy_k (D_{K-k+1+i}^{(1)} \otimes D_{-2})e,$$

$$\sum_{i=1}^{\infty} iy_0 G[\sum_{j=0}^{K-d} D_j^{(1)} \otimes D_{K-d-j+i}^{(2)} + D_{-1}^{(K-d+1)} \otimes D_{-2}]e + \sum_{k=1}^{K-d}\sum_{i=1}^{\infty} iy_k [\sum_{j=0}^{K-d-k+1} D_j^{(1)} \otimes D_{K-d-k+1-j+i}^{(2)} + D_{-1}^{(K-d+k+2)} \otimes D_i^{(2)}]e + \sum_{k=K-d+1}^{K}\sum_{i=1}^{\infty} iy_k [D_{-1} \otimes D_i^{(2)}]e$$

where $D_{-1} = \sum_{i=0}^{\infty} D_i^{(1)}$. Thus we can calculate the steady state high priority packet loss probability, P^{hp}, and the steady state low priority packet loss probability, P^{lp}.

Next, we proceed to calculate the mean lengths of critical and non-critical periods which are assumed to occur alternatively. Since the non-critical period is defined as the time period over which the number of packets in buffer (with buffer depth, K) is less than the threshold $K-d$, and the critical period is defined as the time period over which the number of packets in buffer is greater than or equal to the threshold $K-d$, we could decompose the state space S into two subsets:

$$S_{nc} = \{(b,i,j) \mid 0 \le b \le K-d-1, 1 \le i \le m_1, 1 \le j \le m_2\},$$
$$S_c = \{(b,i,j) \mid K-d \le b \le K, 1 \le i \le m_1, 1 \le j \le m_2\}.$$

This partition of S makes the matrix P decomposed as follows:

$$P = \begin{bmatrix} P_{nc} & P_{nc,c} \\ P_{c,nc} & P_c \end{bmatrix}$$

where

$$P_{nc} = \begin{bmatrix} GD_0 & GD_1 & \cdots & GD_{K-d-2} & GD_{K-d-1} \\ D_0 & D_1 & \cdots & D_{K-d-2} & D_{K-d-1} \\ 0 & D_0 & \cdots & D_{K-d-3} & D_{K-d-2} \\ 0 & 0 & \cdots & D_{K-d-4} & D_{K-d-3} \\ \vdots & \vdots & \ddots & \vdots & \vdots \\ 0 & 0 & \cdots & D_0 & D_1 \end{bmatrix},$$

$$P_{nc,c} = \begin{bmatrix} GC_{K-d} & G(D_{K-d+1}^{(1)} \otimes D_{-2}) & \cdots & G(D_{K-1}^{(1)} \otimes D_{-2}) & GE(K) \\ C_{K-d} & D_{K-d+1}^{(1)} \otimes D_{-2} & \cdots & D_{K-1}^{(1)} \otimes D_{-2} & E(K) \\ C_{K-d-1} & D_{K-d}^{(1)} \otimes D_{-2} & \cdots & D_{K-2}^{(1)} \otimes D_{-2} & E(K-1) \\ C_{K-d-2} & D_{K-d-1}^{(1)} \otimes D_{-2} & \cdots & D_{K-3}^{(1)} \otimes D_{-2} & E(K-2) \\ \vdots & \vdots & \ddots & \vdots & \vdots \\ C_2 & D_3^{(1)} \otimes D_{-2} & \cdots & D_{d+1}^{(1)} \otimes D_{-2} & E(d+2) \end{bmatrix},$$

$$P_{c,nc} = \begin{bmatrix} 0 & 0 & 0 & \cdots & D_0 \\ 0 & 0 & 0 & \cdots & 0 \\ \vdots & \vdots & \vdots & \ddots & \vdots \\ 0 & 0 & 0 & \cdots & 0 \end{bmatrix}, \text{ and}$$

$$P_c = \begin{bmatrix} C_1 & D_2^{(1)} \otimes D_{-2} & D_d^{(1)} \otimes D_{-2} & \cdots & E(d+1) \\ D_0^{(1)} \otimes D_{-2} & D_1^{(1)} \otimes D_{-2} & D_{d-1}^{(1)} \otimes D_{-2} & \cdots & E(d) \\ \vdots & \vdots & \vdots & \ddots & \vdots \\ 0 & 0 & D_0^{(1)} \otimes D_{-2} & \cdots & E(1) \end{bmatrix}$$

The sub-matrices P_{nc}, $P_{nc;c}$, $P_{c;nc}$, and P_c are the left upper part, right upper part, left lower part, and right lower part of the matrix P, that correspond to the transitions of those from S_{nc} into itself, from S_{nc} into S_c, from S_c into S_{nc}, and from S_c into itself, respectively.

For the case of non-critical period, consider the transition probability matrix of absorbing Markov chain with transient states S_{nc} and absorbing states S_c,

$$P^{nc} = \begin{bmatrix} P_{nc} & P_{nc,c} \\ 0 & I \end{bmatrix},$$

where I and 0 are the unit matrix and zero matrix of appropriate dimensions. If Y is the random variable standing for the number of steps taken prior to

absorption, then the *k*th factorial moment of *Y* following from the probabilistic arguments is as follows [22],

$$E = [Y(Y-1)\ldots(Y-k+1)]$$
$$= k!\overline{\beta}P_{nc}^{k-1}(I-P_{nc})^{-k}e$$

where $\overline{\beta}$ is the initial probability vector of transient states and is of the form $[\overline{0},\overline{0},\ldots,\overline{0,\beta_{K-d-1}}]$. This is followed from the fact that buffer occupancy starts at $K-d-1$ in every non-critical period except the first one. The vector ¹0 is the zero vector of appropriate dimension. Similarly, for the case of critical period, consider the transition probability matrix of absorbing Markov chain that has transient states S_c and absorbing states S_{nc},

$$P^c = \begin{bmatrix} I & 0 \\ P_{nc,c} & P_c \end{bmatrix}$$

If *Z* is the random variable standing for the number of steps taken prior to absorption, then the *k*th factorial moment of *Z* is given by [22]

$$E = [Z(Z-1)\ldots(Z-k+1)]$$
$$= k!\overline{\alpha}P_c^{k-1}(I-P_c)^{-k}e,$$

where $\overline{\alpha}$ is the initial probability vector of the transient states. Now the problem of finding the mean lengths of critical and non-critical periods are reduced to the problem of finding the initial probability vectors $\overline{\alpha}$ and $\overline{\beta}$, which can be computed as follows.

Consider the first absorbing Markov chain. Let r_{ij} be the probability of being absorbed in the state $i, j \in S_c$, starting in transient state $i, j \in S_{nc}$. Then for each $j \in S_c$, we have the following relation

$$r_{ij} = q_{ij} + \sum_{s \in S_{nc}} q_{is} r_{sj}$$

In the above relation, the first term corresponds to a transition from transient state to absorbing state directly, whereas the second term corresponds to the transitions from a transient state to other transient states and then to absorbing state. The above relation can be written in matrix form as follows:

$$R_{nc} = P_{nc,c} + P_{nc}R_{nc},$$

$$i.e., \quad R_{nc} = (I-P_{nc})^{-1}P_{nc,c}.$$

The matrix $(I-P_{nc})^{-1}$ is the fundamental matrix of the absorbing Markov chain under consideration. R_{nc} is the transition matrix where the chain starts in transient states and ends up in an absorbing state. Similarly for the case of the second absorbing Markov chain, analogous to R_{nc}, we have the matrix R_c that can be obtained as

$$R_c = (I-P_c)^{-1}P'_{nc,c},$$

where $P'_{nc,c}$ is the last column of the matrix $P_{c;nc}$ and is equal to $[D_0, 0, \ldots, 0]$. The matrix $P'_{nc,c}$ is followed from the fact that for a non-critical period, it

suffices to attain the buffer $K-d-1$ level rather than all other below levels, the level of buffer occupancy $K-d-1$ is the starting point of non-critical period of each cycle except the first one. The matrix $(I-P_c)^{-1}$ is the fundamental matrix of the second absorbing Markov chain. Since the critical and non-critical periods are assumed to occur alternatively, the initial distribution vector of transient states of one of the two aforementioned absorbing Markov chains would be the absorbing probability vector of the other. Hence, we have

$$\overline{\beta_{K-d-1}} = \overline{\alpha} R_c \quad \text{and} \quad \overline{\alpha} = \overline{\beta} R_{nc}.$$

Taking the definition of $\overline{\beta}$ into account, the above equation can be written as

$$\overline{\beta_{K-d-1}} = \overline{\alpha} R_c \quad \text{and} \quad \overline{\alpha} = \overline{\beta_{K-d-1}} R'_{nc},$$

where R'_{nc} is the product of the last $m_1 m_2$ rows of $R_c = (I-P_{nc})^{-1}$ and $P_{nc;c}$.

The two vectors $\overline{\beta_{K-d-1}}$ and $\overline{\alpha}$ can be computed by solving $\overline{\beta_{K-d-1}} = \overline{\alpha} R_c$ and $\overline{\alpha} = \overline{\beta_{K-d-1}} R'_{nc}$, iteratively, on assigning arbitrary values to either $\overline{\beta_{K-d-1}}$ or $\overline{\alpha}$ first. Following the above discussions and the matrix analytic methods [12], [19], [22], [23], we could compute the following performance measures:

1) Steady state packet loss probabilities,

2) Mean lengths of critical and non-critical periods.

These two performance measures characterize the long-time and the short-term loss behavior, respectively.

III Approximate Model for Low Priority Traffic

In this report, we further propose an approximate model for the performance analysis of OPS employing PBS mechanism under Markovian modeled self-similar traffic input. Our proposed model is to retain the same high dimensional MAP for high priority traffic, but to reduce the dimension of the resultant MAP of low priority traffic. Obviously, as the number of states of the resultant MAP of low priority traffic decreases, the computation complexity decreases cubically. However, we could not straightforwardly reduce the number of superposed MAPs in fitting the self-similarity for low priority traffic, since this will severely reduce the accuracy of the queueing based performance measures of the resultant MAP.

We have considered three self-similar traffic pertaining to H = 0.7, H = 0.8, and H = 0.9, all with the mean arrival rate, λ = 1, variance, σ^2 = 0.6, over the time-scale range $[10^2, 10^7]$ .. For each case, we have a 16-state MAP obtained by using the fitting method discussed in [9]. For all the cases,

correlation decay rate, ρ, squared coefficient of variation, c^2, the first three moments, $m1$, $m2$, and $m3$, have been calculated. The correlation decay rate ρ is positive in each case, hence one could achieve the desired 2-state MAP with these high dimensional MAPs [24]. Moreover, all the cases satisfy the inequalities $c^2 > 1$ and $\frac{m3}{m_1^3} > \frac{3}{2}(c^2+1)$ which are the necessary conditions to be satisfied by the original distribution in order to have phase-type distribution by matching the first three moments [25]. Following [25], we could have phase type distribution, thereby the approximated 2-state MAP could be obtained.

Table I lists the values of aforementioned traffic descriptors of the original 16-state MAPs, for which we follow the algorithms in [9] to fit a self-similar traffic with mean arrival rate, λ = 1, variance, σ^2 = 0.6, over the time-scale range [10^2; 10^7] in three different traffic cases with Hurst parameters, H = 0.7, H = 0.8, and H = 0.9, and the corresponding ones of the approximated 2-state MAPs.

Table I: Statistics of Original MAPs and Approximated 2-State MAPs.

Hurst Parameter, H=0.7		
Traffic Descriptor	***Original 16-state MAP***	***Approximated 2-state MAP***
Decay Rate	0.98740609009536029	0.98740609009535918
First Moment	1.0000000000002134	1.0000000000000009
Second Moment	2.0878870559162794	2.0878870559153939
Third moment	6.8296241194314407	6.8296241194271055
Hurst Parameter, H=0.8		
Traffic Descriptor	***Original 16-state MAP***	***Approximated 2-state MAP***
Decay Rate	0.98200142470558727	0.98200142470558549
First Moment	0.99999999999626443	1.0000000000000002
Second Moment	2.5492714330618096	2.5492714330808561
Third Moment	14.698932185224454	14.698932185389186
Hurst Parameter, H=0.9		
Traffic Descriptor	***Original 16-state MAP***	***Approximated 2-state MAP***
Decay Rate	0.99992779499313622	0.99992779499313611
First Moment	1.0000000000887637	0.99999999999993183
Second Moment	11.72485772057437	11.7248577184757 84
Third Moment	2799.5512163629924	2799.5512156127179

We illustrate the packet loss probability against the traffic load for the *MAP/D/1/K* queues under the inputs of the above two MAPs with traffic descriptors shown in Table I, when buffer depth equals 10 and H = 0.7 in Fig. 2. From Fig. 2, we observe how accurate the approximated 2-state MAP is. The figures in the cases of H = 0.8 and H = 0.9 could not be shown here. However, we do observe that the accuracy of the approximation becomes worse when H increases. By applying this approximate model, it is obvious that the computation complexity is reduced by 8^3 = 512 times.

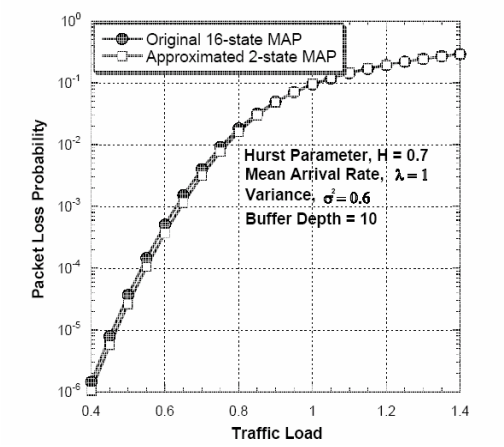

Fig. 2. Packet loss probability against traffic load for the *MAP/D/1/K* queues under the inputs of the two MAPs with traffic descriptors as shown in Table I, at buffer depth equals 10 and $H = 0.7$.

IV Simulation Results

We first validate the approximate model by illustrating the comparisons of long term steady state packet loss probabilities against the variable of threshold level, d, at traffic load, $L = 0.85$, and buffer depth, $K = 15$, between the analytical results of the approximate model and the simulation results without approximation in Fig. 3. The parameters of the high priority and low priority MAP traffic are the same ones as we shown in Table I.

Fig. 4 depicts the mean lengths of the critical and non-critical periods against the threshold level variable, d, for $H = 0.7$, 0.8, and 0.9. Fig. 5 illustrates the mean lengths of the critical and non-critical periods against the threshold variable, d, when $H = 0.8$, over 2 different buffer depths. Fig. 6 depicts the mean lengths of the critical and non-critical periods against the traffic load, when $K = 15$, $d = 9$, and $H = 0.8$. In these figures, the unit time means one unit of the average service time.

From these results, we observe that (1) as d increases, the mean length of non-critical period decreases while the average length of critical period seems to increase slowly (this observation is consistent with the results found in [19], [27], [28]); (2) both the mean lengths of critical and non-critical periods increase, as the buffer depth increases; (3) the mean length of non-critical period decreases drastically as traffic load increases whereas the mean length of critical period increases moderately as traffic load increases; (4) the higher the Hurst parameter is, the lower the mean length of non-critical period is; while the mean length of critical period increases as Hurst parameter increases.

From the information of the mean lengths of critical and non-critical periods, it is very likely that we could adopt these measures as a trigger event of initializing call admission control scheme in OPS to improve the switching performance to greater extent.

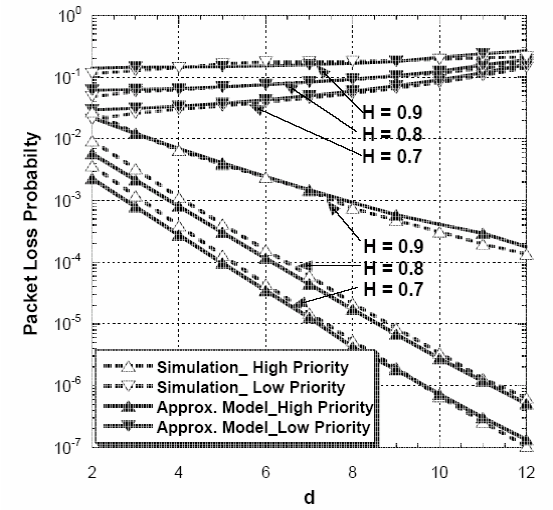

Fig.3 The steady state packet loss probabilities against the variable of threshold level, *d*, at traffic load $L = 0.85$ at various H.

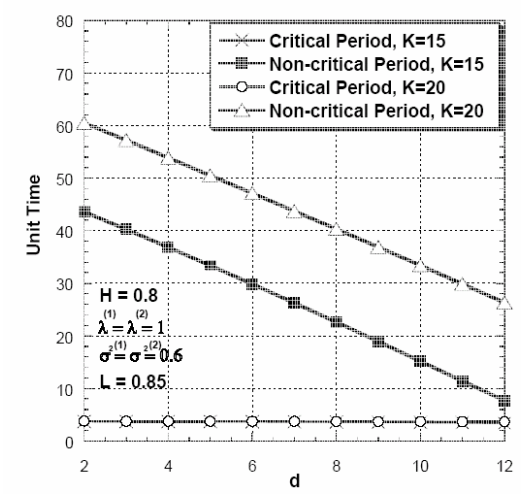

Fig. 5 The mean lengths of critical and non-critical periods against the threshold variable, *d*, at $L = 0.85$, $H = 0.8$, and over two different buffer depths.

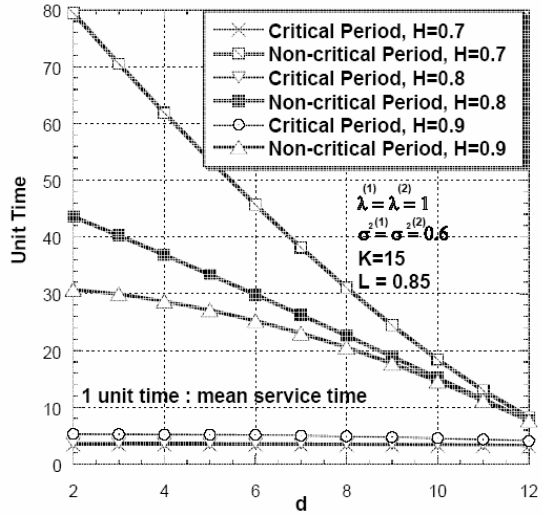

Fig. 4 The mean lengths of critical and non-critical periods against the threshold variable, *d*, at buffer depth $K = 15$, traffic load $L = 0.85$, and over three different Hurst parameters.

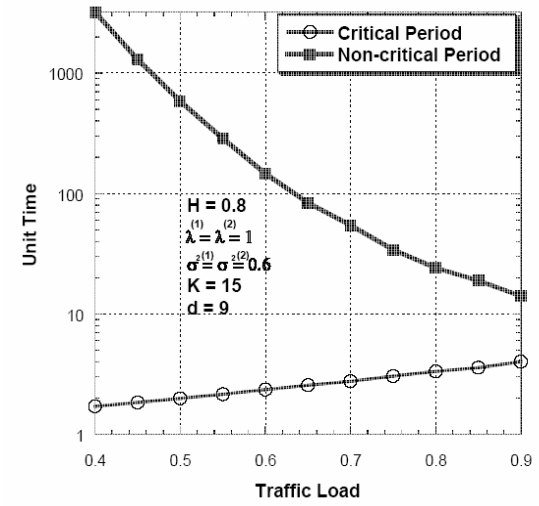

Fig. 6 The mean lengths of critical and non-critical periods against the threshold variable, *d*, at $K = 15$, $d = 9$, and $H = 0.8$.

(2) WDM Optical Packet Switches Employing Wavelength Conversion in Conjunction with Markovian Modeled Self-Similar Traffic Input

I Queueing Model and Related Formulae

The architecture of WDM OPS employing wavelength conversion techniques implemented in a broadcast-and-select architecture is shown in Fig. 7(a), in which, there are *N* input ports and *N* output ports, and each port has *n* wavelength channels, $\lambda_1, \lambda_2, \ldots, \lambda_n$ in it. *B* FDLs constitute the optical buffers with buffer depth ($B-1$). For the sake of simplicity, we assume that the packet length is fixed and constant, and that the packet length is equal to *h* units when it is measured in time. Further, we assume that the WDM OPS is operating at a synchronous mode with delay time unit, *T*, for the FDLs of optical buffers, where the suitable value of delay time unit, *T*, is chosen to be *h*, the packet length measured in time. No specific scheduling algorithm is applied, only the service discipline of first-come-first-serve (FCFS) is adopted. Hence, the queueing model of a specific output port of such OPS is equivalent to the one of a multiplexer. When the wavelength conversion is employed, the equivalent queueing model is shown in Fig. 7(b). When the traffic aggregated at the input end of the optical buffers of one of the specific output ports is MAP modeled self-similar processes, then, the final queueing model is a *MAP/D/c/K* queueing system as shown in Fig. 7(c). As illustrated in Fig. 7(c), the number of wavelength channels per port, *n*, is equal to the number of servers, *c*, and the total effective buffer size of optical buffers, $(B-1)n$ as shown in Fig. 7(b), is equal to the buffer depth of the *MAP/D/c/K* queue, $K-c$. Therefore, the problem of analyzing WDM OPS employing wavelength conversion techniques is equivalent to solving the *MAP/D/c/K* queueing systems with the parameters mentioned above.

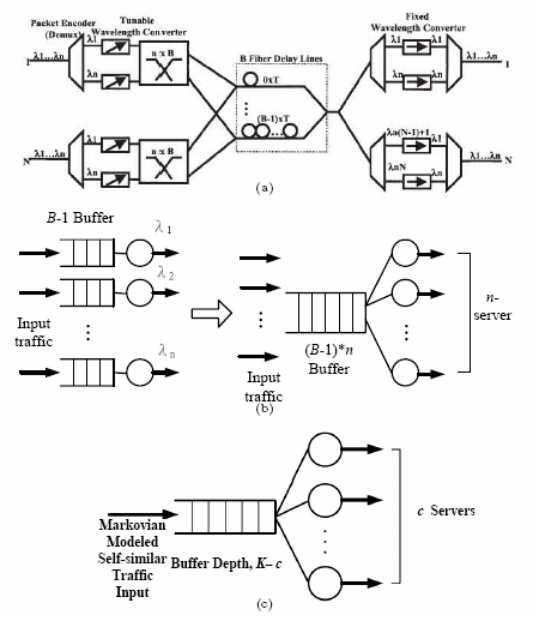

Fig. 7 (a) A block diagram of WDM OPS implemented in broadcast-and-select architecture; (b) the equivalent queueing model of a specific output port of WDM OPS employing wavelength conversion; (c) the final equivalent *MAP/D/c/K* queue.

Let $H(t)$ be the generally and identically distributed service time. Let $A_n(t)$, $n \geq 0$, denote an $m \times m$ matrix

whose (i, j) th element represents the conditional probability that *n* customers arrive at the system during service time and the underlying Markov chain is in phase *j* at the end of service given that the underlying Markov chain is in phase *i* at the beginning of the service. Then $A_n(t)$ satisfies the following equation

$$\sum_{n=0}^{\infty} A_n(t) z^n = \int_0^t e^{[C+Dz]\tau} dH(\tau).$$

When the service time is deterministic and is *h* units/packet, then the above formula is reduced to

$$\sum_{n=0}^{\infty} A_n(t) z^n = e^{[C+Dz]h} = \sum_{r=0}^{\infty} \frac{1}{r!} [A + Bz]^r,$$

where $A = Ch$, $B = Dh$.

It is obvious that the matrices $A_n s$ of counting function can be obtained by comparing the coefficients of z^n on both sides of the above equation. A procedure to calculate the matrices of counting functions [19] is briefed as follows. Hereafter, for the sake of easiness, we drop the argument *h* in rest of the report. For *n* = 0, the above formula will be

$$A_0 = I + \sum_{r=1}^{\infty} \frac{A^r}{r!},$$

where *I* is the unit matrix of appropriate dimension. And the rest of $A_n s$ can be obtained as follows.

$$A_n = \sum_{k=n}^{\infty} \frac{T(k, n+1)}{k!}, \text{ for } n = 1, 2, \ldots, N$$

where $T(i, j)$ can be calculated using the recurrence formulae as follows

$$T(i+1, j) = T(i, j)A + T(i, j-1)B, \; j \in \mathbf{N}$$

Though A_n involves infinite number of terms, due to the presence of *k*! in the denominator, only finite number of terms are required to compute the matrices $A_n s$. The procedure of computing the matrices $A_n s$ can be terminated using Cauchy estimate as shown in the *Proposition* 1 to avoid lots of computation efforts.

Next, we consider the embedded Markov chain $\{L(n), J(n)\}$, $n \geq 0$, at the departures of the queueing system on the state space $\{0,1,2,\ldots,K-c\} \times \{1,2,\ldots,m\}$, where $L(n)$ and $J(n)$ denote the buffer occupancy and the state of MAP, respectively. At the steady state, the transition probability matrix corresponding to the departure points, *P* (with the dimension $(K-c+1)m \times (K-c+1)m$), is as follows:

$$P = \begin{bmatrix}
A_0 & A_1 & \cdots & A_{K-2c} & \cdots & A_{K-c-1} & B_{K-c} \\
A_0 & A_1 & \cdots & A_{K-2c} & \cdots & A_{K-c-1} & B_{K-c} \\
\vdots & \vdots & \ddots & \vdots & \ddots & \vdots & \vdots \\
A_0 & A_1 & \cdots & A_{K-2c} & \cdots & A_{K-c-1} & B_{K-c} \\
A_0 & A_1 & \cdots & A_{K-2c} & \cdots & A_{K-c-1} & B_{K-c} \\
0 & A_0 & \cdots & A_{K-2c-1} & \cdots & A_{K-c-2} & B_{K-c-1} \\
\vdots & \vdots & \ddots & \vdots & \ddots & \vdots & \vdots \\
0 & 0 & \cdots & A_0 & \cdots & A_{c-1} & B_c
\end{bmatrix}.$$

In the matrix, P, elements of the first (*c* + 1) rows are identical and $B_n = \sum_{i=n}^{\infty} A_i$ denote the probability that there are at least *n* arrivals. $A_n s$ are computed following the algorithm in the aforementioned procedure. Next, let $\mathbf{x}_k, 0 \leq k \leq K-c$, denote a $1 \times m$ vector whose *i*th element represents the

steady state probability that the number of packets in the system at departures is *k* and the phase of the arrival process is *i*. At the steady state, we could find the vector $\mathbf{x} = \{\mathbf{x}_k\}$, according to the steady state equations x*P* = x, xe = 1.

Although the general relationship between the probability generating function of queue length at arbitrary time points and at departure points holds good [33] in the case of multiple server queues with finite buffer, the nature of multi-server makes it hard to establish an explicit formula for packet loss probability unlike the single server case in conventional researches [8]. Instead, we compute the loss probability using the steady state probability vector at departure epochs owing to fact that packet loss is due to buffer overflow.

Let *PL* denote the number of packets lost due to the fact that buffer is full. Then the expected value of *PL* is given as

$$E[PL] = \sum_{i=0}^{K-c} \sum_{j=1}^{\infty} j\mathbf{x}_i A_{K-i+j}\mathbf{e}$$

by considering the last column of the $(K-c+1)\times(K-c+1)$ block transition probability matrix *P*. Then the packet loss probability, *PLP*, can be obtained by

$$PLP = \frac{E[PL]}{\lambda E[H(t)]}$$

where , λ $E[H(t)]$ is the number of packet arrivals during the mean service time.

II Steady state Probability Vector

From the above subsection it is clear that problem of finding packet loss probability is reduced to the problem of finding steady state vector. It is worthwhile and interesting to investigate the required computation complexity of calculating the steady state probability vector. To the best of our knowledge, this analysis of the computation complexity pertaining to the *MAP/D/c/K* queueing systems is not available yet and is useful in deciding the necessary platform for analyzing WDM OPS employing wavelength conversion under Markovian modeled self-similar traffic input.

First, we shall present a method to compute the steady state probability vector, and then we derive the computation complexity of the same as follows. The matrix *P* is not of the canonical *M/G/*1 type. However, it is possible to exploit Schur-Banachiewicz inversion formula to *P*, which has been used to compute the steady state probability vector when *P* is in canonical form [12]. Accordingly, the steady state probability vector x is given by x = $[0,0,\ldots,0,1](I-P_1)^{-1}$, where *I* is the unit matrix of appropriate dimension and P_1 is the matrix *P* in which the last column is replaced by $[-1,-1,\ldots,-1,0]^T$. Let $[E_{K-c}, E_{K-c},\ldots,E_{K-c},E_{K-c-1},\ldots,E_c]^T$ be the last column of P_1. Multiplying the permutation matrix *S* by $(I-P_1)$, we have

$$S(I-P_1)=\begin{bmatrix} -A_0 & -A_1 & \cdots & -A_{K-2c} & \cdots & -A_{K-c-1} & -E_{K-c} \\ 0 & -A_0 & \cdots & -A_{K-2c+1} & \cdots & -A_{K-c-2} & E_{K-c-1} \\ \vdots & \vdots & \ddots & \vdots & \ddots & \vdots & \vdots \\ 0 & 0 & \cdots & -A_0 & \cdots & -A_{c-1} & I-E_c \\ I-A_0 & -A_1 & \cdots & -A_{K-2c} & \cdots & A_{K-c-1} & -E_{K-c} \\ -A_0 & I-A_1 & \cdots & -A_{K-2c} & \cdots & -A_{K-c-1} & -E_{K-c} \\ \vdots & \vdots & \ddots & \vdots & \ddots & \vdots & \vdots \\ -A_0 & -A_1 & \cdots & I-A_{K-2c} & \cdots & A_{K-c-1} & -E_{K-c} \end{bmatrix},$$

where

$$S=\begin{bmatrix} 0 & 0 & \cdots & 0 & I & 0 & \cdots & 0 \\ 0 & 0 & \cdots & 0 & 0 & I & \cdots & 0 \\ \vdots & \vdots & \ddots & \vdots & \vdots & \vdots & \ddots & \vdots \\ 0 & 0 & \cdots & 0 & 0 & 0 & \cdots & \mathrm{I} \\ I & 0 & \cdots & 0 & 0 & 0 & \cdots & 0 \\ 0 & I & \cdots & 0 & 0 & 0 & \cdots & 0 \\ \vdots & \vdots & \ddots & \vdots & \vdots & \ddots & \ddots & \vdots \\ 0 & 0 & \cdots & I & 0 & 0 & \cdots & 0 \end{bmatrix}.$$

Note that in the the first row of *S*, *I* is placed in the (*c* + 1)th column.

The matrix $S(I-P_1)$ can be represented by the following form:

$$S(I-P_1)=\begin{bmatrix} \mathbf{A} & \mathbf{B} \\ \mathbf{C} & \mathbf{D} \end{bmatrix}.$$

Dimensions of A, B, C, and D are $(K-2c+1)m\times(K-2c+1)$, $(K-2c+1)m\times cm$, $cm\times(K-2c+1)$, and $cm\times cm$, respectively. Using the Schur-Banachiewicz formula for the inverse of block matrices, we could obtain

$$S(I-P_1)^{-1}=\begin{bmatrix} \mathbf{A^{-1}+E\Delta^{-1}F} & \mathbf{-E\Delta^{-1}} \\ \mathbf{\Delta^{-1}F} & \mathbf{\Delta^{-1}} \end{bmatrix}$$

where $\mathbf{\Delta = D - CA^{-1}B}$, Schur complement of $\mathbf{A}$, $\mathbf{E = A^{-1}B}$, and $\mathbf{F = CA^{-1}}$.

Since $(I-P_1)^{-1}=[S(I-P_1)]^{-1}S$, steady state probability vector is the last row of the matrix $\mathbf{(\Delta^{-1}-\Delta^{-1}-F)}$. The matrix $\mathbf{\Delta}$ is non-singular, if A is non-singular. The matrix $\mathbf{A}$ is upper-triangular Toeplitz matrix whose inverse is easy to compute. The computation complexity to compute its inverse is of the order $O((K-2c)^2m^3)$. The computation complexity to compute $\mathbf{F}$ is of the order $O(c(K-2c)^2m^3)$. The computation complexities to compute $\mathbf{FB}$ and $\mathbf{\Delta^{-1}F}$ is of the order $O(c^2(K-2c)m^3)$. Therefore, the overall complexity to compute the steady state vector is of the order $O(\max[c(K-2c)^2, c^2(K-2c)]m^3)$.

III Simulation Results

We first illustrate the loss probabilities against the traffic intensity pertaining to the analytical and the simulation results of *MAP/D/c/K* queues and the simulation ones of the same queues under the fractional Brownian traffic (FBT) input in Figs. 8(a)-9(c). The MAP shown in Figs. 8(a)-9(c) is obtained by fitting the FBT traffic with mean arrival rate λ = 1, variance σ^2 = 0.6, and Hurst parameter *H* = 0.7 over a typical time-scale $[10^2, 10^7]$ following the method proposed in [9]. From these figures, we observe that our analysis is pretty accurate.

By showing the accuracy of our analysis, we then analyze the performance of WDM OPS employing wavelength conversion under Markovian modeled self-similar traffic input, according to the related system

parameters and traffic descriptors in Figs. 9(a)-11.

Figs. 9(a) and 9(b) illustrate the comparisons of packet loss probability against the load per wavelength channel at the number of FDLs, B = 10, Hurst parameters, H = 0.7 and H = 0.9, respectively. The MAP input is obtained by emulating self-similar traffic with λ = 1 and σ^2 = 0.6 in each case. From these results, the benefit of adopting wavelength conversion is apparent when the load is moderate, i.e., employing more number of tunable wavelength channels leads to better performance. When the load is high, the advantage of employing wavelength conversion is limited.

Figs. 10(a) and 10 (b) depict the comparisons of packet loss probability against the number of FDLs. The input traffic is the same as the ones in Figs. 10 (a) and 10 (b) with load set to 0.8. From these results, we observe that when H increases, the benefit of wavelength conversion becomes less prominent. We also observe that increasing the number of FDLs has limited improvement on performance. This coincides with the impact of self-similar traffic upon the storage models [34] Fig. 11 shows the comparisons of packet loss probability against the number of tunable wavelength channels when B = 10 and load per wavelength channel is 0.8 in both H = 0.7 and H = 0.9 cases. From Fig. 11, we observe that the benefit of wavelength conversion is remarkable when the input traffic is moderate self-similar. However, this benefit decreases drastically when H increases. This is the same as the conclusions shown in [35] by simulations.

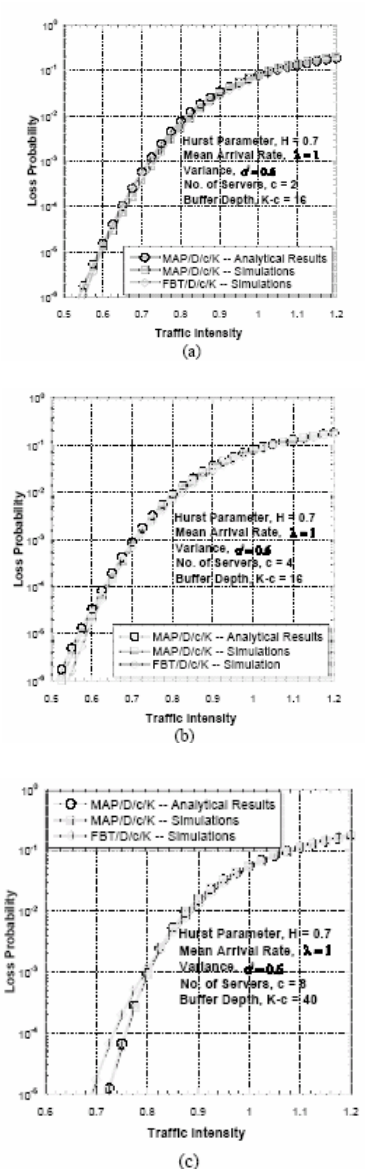

Fig. 8 Comparisons of loss probability against traffic intensity between the analytical and simulation results of *MAP/D/c/K* queues and the simulation ones of the same queues under FBT input, (a) c = 2 and K = 18; (b) c = 4 and K = 20; (c) c = 8 and K = 48.

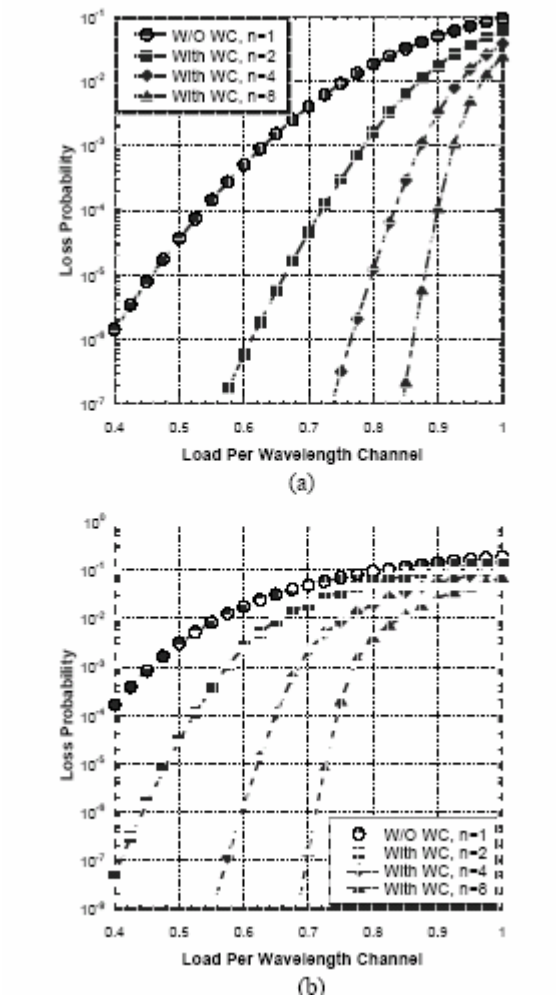

Fig. 9 Packet loss probability versus channel load for a OPS with FDLs = 10, (a) H = 0.7; (b) H = 0.9.

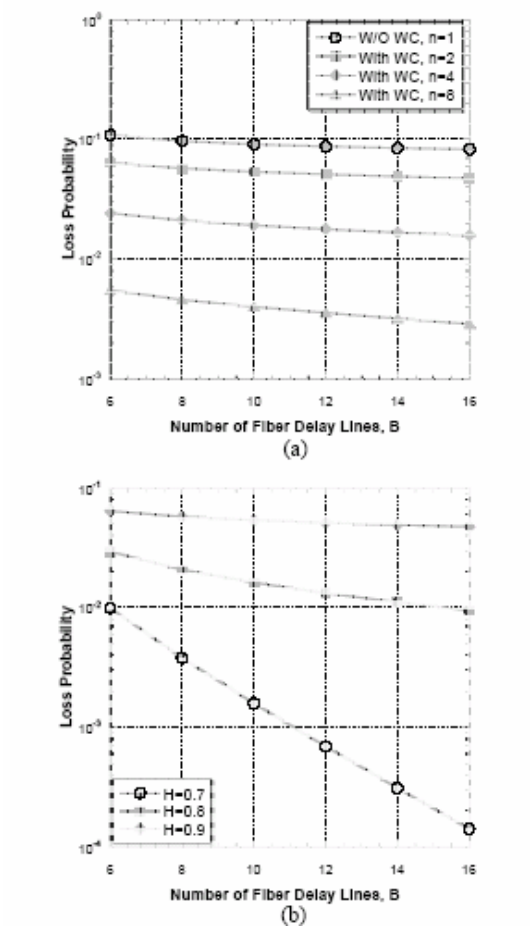

Fig. 10 (a) Packet loss probability versus the number of FDLs for various tunable wavelengths when the load per wavelength channel is 0.8 and H = 0:9; (b) packet loss probability versus the number of FDLs for various Hurst parameters at load per wavelength channel is 0.8 and number of tunable wavelengths is 2.

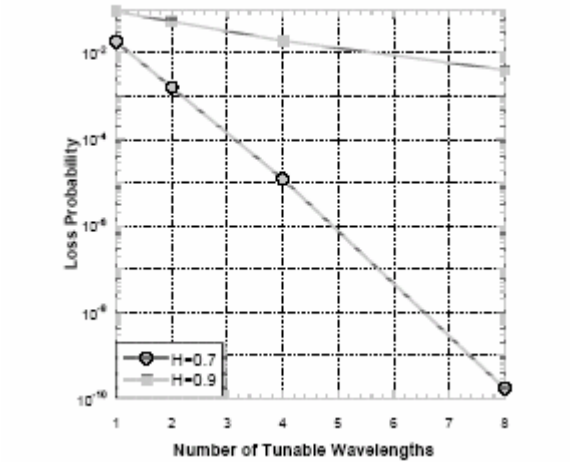

Fig. 11 Packet loss probability versus the number of tunable wavelengths for input traffic when the number of FDLs is set to be 10 and the load per wavelength is 0.8 at H = 0.7 and H = 0.9.

(3) Noncoherent Spatial/Spectral Optical CDMA System With Two-Dimensional Perfect Difference Codes

Ⅰ Introduction

Because the demand of bandwidth increases rapidly, the access network becomes the bottle neck of the internet. PON has many advantages, currently most of PONs employ Time Division Multiple Access (TDMA) techniques. However, OCDMA has many benefits such as security, flexible transmission and no need for high speed electronics devices. OCDMA has attracted a lot of attention. OCDMA PON is a promising candidates for broadband access network applications. Because of non-negative power for amplitude modulation/direct detect optical signals, optical orthogonal codes (OOCs) are a family of (0, 1) sequences with good autocorrelation and cross correlation properties. $(n, w, \lambda_a, \lambda_c)$ – OOCs denotes the OOCs with code length n, code weight w, autocorrelation λ_a and cross correlation λ_c. For $\lambda_a = \lambda_c = \lambda$, we may simply the notation as (n, w, λ) – OOCs. The code size Φ is given by [36]

$$\Phi \le \left\lfloor \frac{1}{w} \left\lfloor \frac{n-1}{w-1} \right\rfloor \cdots \left\lfloor \frac{n-\lambda}{w-\lambda} \right\rfloor \cdots \right\rfloor$$

By relaxing the cross correlation constrain, the code size of $(n, w, 1, 2)$ - OOCs is about 10 times larger than that of $(n, w, 1)$ – OOCs [37]. However the bit error rate (BER) performance of the later is better than that of the former.

The one-dimensional $(n, w, \lambda_a, \lambda_c)$ – OOCs, which speads the input data bits in time domain, have been studied intensively. Recently the 2-D spectral/time OOCs were proposed [42]. The 2-D spectral/time OOCs can support a large number of users. The 2-D OOCs can be considered as an *mxn* matrix with (0, 1) elements. An example of 2-D OOCs is shown in Fig. 12 [42].

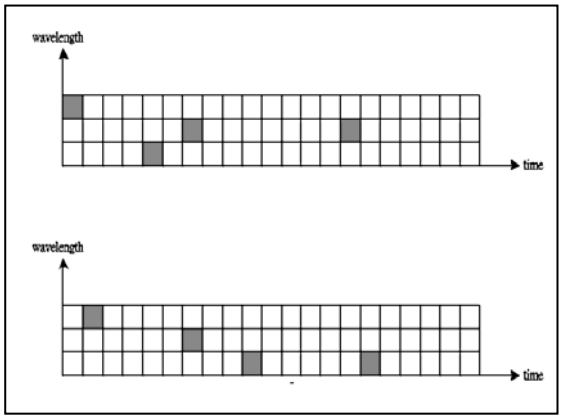

Fig. 12 An example of two (3×21, 4, 1, 1)-MWOOCs

For any codeword X= { X_{ij} } of the ($mxn, w, \lambda_a, \lambda_c$) – OOCs. The periodic autocorrelation λ_a satisfies

$$\sum_{i=1}^{m-1}\sum_{j=0}^{n-1} X_{ij} X_{ij\oplus f} \le \lambda_a$$

where f is the asynchronous time shift and $\oplus$ represents the modulo- n addition.

For any code words X= { X_{ij} } and Y= { Y_{ij} }, the periodic cross correlation λ_c satisfies.

$$\sum_{i=1}^{m-1}\sum_{j=0}^{n-1} X_{ij} Y_{iy\oplus f} \le \lambda_c$$

The mxn of many 2-D OOCs are constrained by certain relations [42]. The 2-D OOCs with arbitrary combination of m and n are proposed [43], where m≤n, we have applied the proposed 2-D OOCs to the spectral/time OCDMA systems.

Another type of 2-D OCDMA systems employ multi-fibers. Therefore the data bits are spread in the time domain and spatial domain. The partial modified prime (PMP) codes are applied in the system. Because the system can suppress the phase-induced intensity noise (PIIN), it also has very good performance [44].

Ⅱ The 2-D spectral/time OCDMA system

The receiver structure of the 2-D spectral/time OCDMA system using Pd codes is shown in Fig. 13 [43]. We assume the system is chip synchronous among users since it is the worst case of the performance. The average photon arrival rate Σ per pulse is given by

$$\Sigma = \frac{\eta p w}{h f}$$

where η is the APD quantum efficiency, p_w is the received optical signal power, h is the plauck's constant, and f is the optical frequency. The optical signal at the output of the second hard limiter has "on" and "off" two level which are denoted by state S_1 and S_0. The photon arrival rates for state S_1 and S_0 are Σ and zero. With the Gaussian probability density function (pdf) assumption, the output current φ_b of the photo detector is given by [45]

$$P_{\varphi_b}(\varphi) = \frac{1}{\sqrt{2\pi\sigma_b^2}} e - (\varphi - \mu_b)^2 \Big/ 2\sigma_b^2$$

where bE{0, 1} for state ω_b, μ_b is the mean value of the detector output current given by

$\mu_b = GT_c(b\varepsilon + I_b/e) + T_c I_s/e$

have G is the average APD gain, T_c is the chip time, e is the electron charge, I_b and I_c are the bulk and surface leakage currents of the APD.

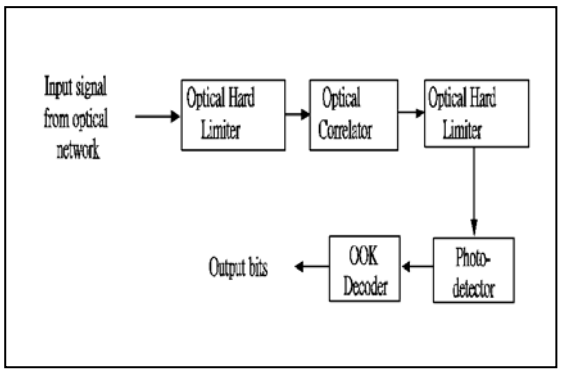

Fig. 13 The receiver structure of asynchronous OCDMA systems using double optical hard limiters

The variance of the photo current, σ_b^2 is expressed as

$$\sigma_b^2 = G^2 F_e T_c(b\varepsilon + I_b/e) + T_c I_s/e$$

$$T_e = k_{eff} G + (2 - 1/G)(1 - k_{eff})$$

here k_{eff} is the APD effective ionization ratio. The variance of thermal noise is given by

$$\sigma_b^2 = 2K_b T_r T_c / e^2 R_L$$

Where K_B is the Boltzmann's constant, T_r and R_L are the receiver noise temperature and load resistance. The threshold is set at

$$\theta = \frac{\mu_0\sigma_1 + \mu_1\sigma_0}{\sigma_1 + \sigma_2}$$

The probabilities that the desired signal bit by the interfering user at one work and λ_c works are q_1 and q_λ which are given by

$$q_1 = \frac{w^2 - \lambda_c}{2mn}$$

and

$$q_{\lambda c} = \frac{1}{2mn}$$

The number of code weights interfered by α interfering users can be modeled by the Markov chain [46]. The state transition occurs, when a new interfering user appears. The transition probability P_{ij} is

$$P_{ij}\begin{cases} q_0 + q_1\dfrac{i}{w} + q_\lambda \dfrac{\binom{i}{w}}{\binom{w}{\lambda_c}} & \text{if } j = i \\ q_1\dfrac{w-i}{w} + q_\lambda \dfrac{\binom{i}{\lambda_c - 1}\binom{w-i}{1}}{\binom{w}{\lambda_c}} & \text{if } j = i+1 \\ q_{\lambda_c}\dfrac{\binom{w-i}{\sigma_c}}{\binom{w}{\lambda_c}} & \text{if } j = i+\lambda_c \\ 0 & \text{otherwise} \end{cases}$$

where $q_0 = 1 - q_1 - q_{\lambda_c}$

Let $K^{(\alpha)} = [K_0^{(\alpha)} K_1^{(\alpha)} \ldots K_w^{(\alpha)}]$ represent the state probability of the Markov chain given α [44]. Let $\underline{P}$ demote the state transition matrix where $\underline{P} = \{P_{ij}\}$ for $0 \le i,\ j \le w$, therefore we have

$K^{(\alpha)} = K^{(\alpha-1)}\underline{P}$, where $K^{(0)}$ is the initial state and is given by $K^{(0)} = [1, 0, \ldots 0]$ [44]. Because the second can completely remove the multiuser interference (MUI) when data bit "i" is transmitted. If "o" is sent, the second limiter can not entirely remove the MUI if the number of interfering marks exceeds or equal to w. When the simultaneously users are N, the probability of error is expressed as

$$P_e = P_r(S_1 \mid b = 0)$$
$$= K_w^{N-1}$$

The total BER is given by

$$BER = \frac{1}{2} erfc(\frac{\theta -$$
$$+ \frac{1}{2}(1 - erfc$$

where $P_r(S_0 \mid b = 0) = 1 - P_r(S_1 \mid b = 0)$ [44].

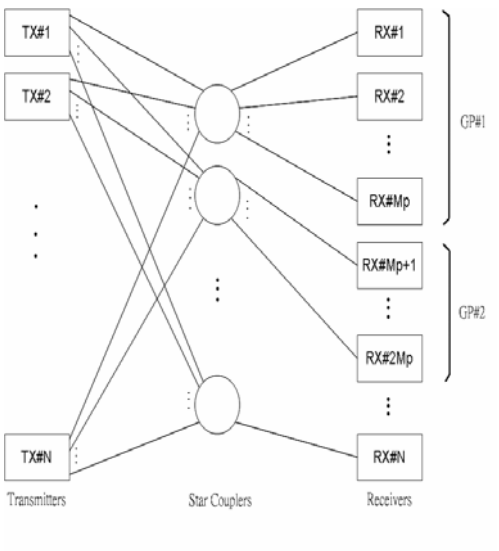

Fig. 14: A schematic of a newly constructed spectral/spatial OCDMA network.

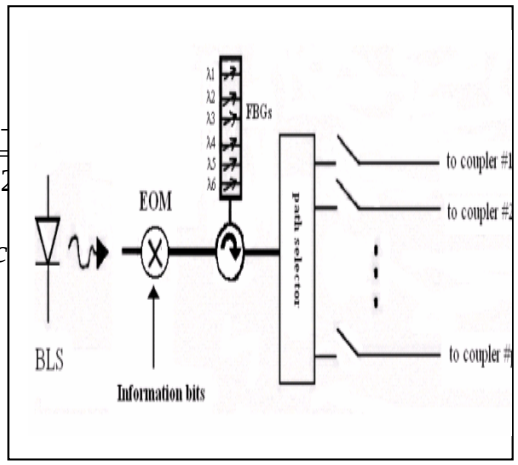

Fig. 15: The transmitter structure of the proposed spectral/spatial OCDMA system.

Ⅲ The 2-Dspectral/spatial OCDM system

Ⅲ-1 System Architecture

The proposed system Architecture is shown in Fig 14. The structures of the transmitter and receiver are depicted in Figs 15 and 16 [43].

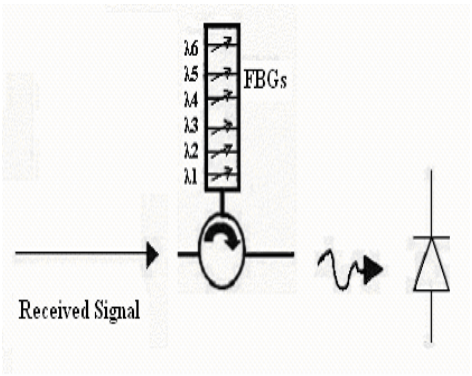

Fig. 16: The receiver structure of the proposed spectral/spatial OCDMA system.

The transmitter has a broadband light source (BLS), an electro-optic modulator (EOM), a spectral encoder composed of a set of fiber Bragg gratings (FBGs), and a path selector. Therein, the EOM is used to perform the ON-OFF keying scheme to convert the incoming information bits into an optical broadband pulse stream. The spectral encoder is used to encode the broadband pulse stream spectrally according to the assigned code sequence of the PMP codes. The path selector is used to choose a signal transmission path according to the code group of the assigned code sequence [43].

If the information bit inputted into the EOM is “1”, the EMO will provide an optical broadband pulse for the spectral encoder. Otherwise, no optical pulse will be provided. When an optical broadband pulse is inputted into the spectral encoder, the spectral components corresponding to the assigned code sequence are reflected back and the other unwanted spectral components are filtered out. After that, the reflected spectral components, i.e. the spectrally encoded signals, are delivered to the path selector, which will select an optical fiber connected to the star coupler corresponding to the code group of the assigned code sequence and then pass the encoded signals via the selected optical fiber.

As shown in Fig. 14, the receiver structure has a spectral decoder composed of a set of FBGs and a photodiode. Therein, the spectral decoder is used to decode the received optical signals in the spectral domain according to an assigned code sequence of the PMP codes and the photodiode is used to convert the decoded optical signals into electrical ones. It should be noted that the grating arrangement of the spectral decoder is contrary to that of the spectral encoder to compensate the round-trip delays of different spectral components. When the encoded optical signals are passed into the spectral decoder, the spectral components corresponding to the assigned code sequence are reflected back and the other unwanted spectral components are filtered out. Then, the reflected optical signals, i.e. the spectrally decoded signals, are passed to the photodiode for electro-optic conversion to recover the original information bit stream.

According to the 2-D OCDAM network architecture shown in Fig. 14, a receiver is only connected to a start coupler corresponding to the code group of the assigned PMP code sequence via an optical fiber. An example of the PMP Codes for GF(5) and M=2 is listed in TableII. Hence, the receiver can only receive the optical signals encoded according to the PMP code sequences belonging to the same code group. As mentioned above, the PMP code sequences of the same code group are mutually orthogonal. Hence, the spectral decoder of the receiver can completely

filter out the undesired optical signals sent from other users and thus eliminate MUI. Moreover, since no undesired optical signal sent from other users can be delivered to the photodiode of the receiver, the PIIN is suppressed greatly.

Ⅲ-2 Performance Analysis

In order to simplify the analysis, some assumptions are given as follows [48-50]:

1) The broadband light source is ideally unpolarized and has a flat spectrum over [f_c-$\Delta f/2$, f_c+$\Delta f/2$], where f_c is the central frequency and Δf is the bandwidth of the light source;
2) Each spectral slice of the encoded signals has identical bandwidth;
3) Each user has equal transmission power at the receiver; and
4) Bit streams sent from different users reach the receiver synchronously.

In the following analysis, the intensity noise, the shot noise, and thermal noise are considered. The effect of receiver's dark current is neglected. In general, the photocurrent noise that occurs during the detection of thermal light, which is produced by a broadband light source, can be expressed as [48]

$$\left\langle i^2 \right\rangle = G^2 P_{in}^2 R^2 B \tau_c + 2eG^2 F_e P_{in} R B + 4K_b T_n B / R_L \quad ,$$

where G and F_e are average gain and excess noise factor of an avalanche photodiode (APD), e is the electron's charge, B is the noise-equivalent electrical bandwidth of the receiver, τ_c is the coherence time of the light source, K_b is the Boltzmann's constant, T_n is the absolute receiver noise temperature, R_L is the receiver load resistance, P_{in} is the optical power incident on the APD, and R is the responsivity of the APD.

Therein, R is given by $R=\eta e/hf_c$, where η is the quantum efficiency of the APD and h is the Planck's constant. P_{in} can be expressed as

$$P_{in} = \int_0^\infty S(f)df \, ,$$

where $S(f)$ is the single sideband power spectral density of the broadband light source. The excess noise factor, F_e, can be written as

$$F_e = k_e G + (1-k_e)(2-G^{-1}) \, ,$$

where k_e is the effective ionization ratio of the APD. In (16), the items at right hand side result from the PIIN, shot noise, and thermal noise, respectively. Note that the coherence time can be expressed as [44]

$$\tau_c = \frac{\int_0^\infty S^2(f)df}{\left[\int_0^\infty S(f)df\right]^2} \, .$$

If the power loss caused by the optical fibers used for signal transmission is ignored, the power spectral density (PSD) of the received optical signal of the h-th receiver can be written as

$$R_h(f) = \frac{1}{Mp}\frac{P_s}{\Delta f}\sum_{k=1}^{K} b_k \sum_{i=1}^{L} C_k(i) F(i,f),$$

where P_s is the output power of a broadband light source, K is the number of simultaneous users in the system, b_k is

a data bit sent from the *k*-th user and can be 1 or 0, *p* is a prime number used in the PMP codes, *L* is the code length of the PMP codes, $C_k(i)$ denotes the *i*-th element of the *k*-th PMP code sequence, $F(i, f)$ represents the *i*-th slice of the spectrum used in signal transmission and can be expressed as

$$F(i,f)=\left\{u\left[f-f_0-\frac{\Delta f}{2L}(-L+2i-2)\right]-u\left[f-f_0-\frac{\Delta f}{2L}(-L+2i)\right]\right\}$$

where $u(f)$ is the unit step function, defined as

$$u(f)=\begin{cases}1, & f\ge 0\\ 0, & f<0\end{cases}.$$

After being received, the optical signals are decoded by the spectral decoder of the *h*-th receiver. The transfer function of the spectral decoder of the *h*-th receiver can be written as

$$H_h(f)=\sum_{i=1}^{L}C_h(i)F(i,f),$$

where $C_h(i)$ denotes the *i*-th element of the *h*-th PMP code sequence. Thus, the PSD of the decoded optical signals incident on the photo-detector of the *h*-th receiver can be written as

$$G_h(f)=R_h(f)H_h(f)$$

$$=\frac{\frac{1}{Mp}P_s}{\Delta f}\sum_{k=1}^{K}b_k\sum_{i=1}^{L}C_k(i)C_h(f)F(i,f),$$

Due to the orthogonal property, $G_h(f)$ can be rewritten as

$$G_h(f)=\frac{\frac{1}{Mp}P_s}{\Delta f}b_h\sum_{i=1}^{L}C_h(i)F(i,f)$$

$$=\frac{\frac{1}{Mp}P_s}{\Delta f}b_h\sum_{i=1}^{L}C_h(i)\begin{Bmatrix}u\left[f-f_0-\frac{\Delta f}{2L}(-L+2i-2)\right]\\ -u\left[f-f_0-\frac{\Delta f}{2L}(-L+2i)\right]\end{Bmatrix}.$$

Therefore, the optical power incident on the APD is

$$P_{in}=\int_0^{\infty}G_h(f)df$$

$$=\frac{\frac{1}{Mp}P_s}{\Delta f}b_h\int_0^{\infty}\sum_{i=1}^{L}C_h(i)\begin{Bmatrix}u\left[f-f_0-\frac{\Delta f}{2L}(-L+2i-2)\right]\\ -u\left[f-f_0-\frac{\Delta f}{2L}(-L+2i)\right]\end{Bmatrix}df$$

$$=\frac{P_s(p-1)}{M^2pL}b_h.$$

Since the code length *L* is equal to p^2, we have

$$P_{in}=\frac{P_s(p-1)}{M^2p^3}b_h.$$

Finally, the photocurrent can be expressed as

$$I_h=GRP_{in}=\frac{GRP_s(p-1)}{M^2p^3}b_h.$$

And the PIIN can be expressed as

$$\left\langle i_{PIIN}{}^2\right\rangle=G^2P_{in}^2R^2B\tau_c$$

By substituting these above equations, the PIIN can be rewritten as

$$\left\langle i_{PIIN}{}^2\right\rangle=G^2R^2BP_{in}^2\frac{\int_0^{\infty}G_h^2(f)df}{\left[\int_0^{\infty}G_h(f)df\right]^2}.$$

Since $P_{in}=\int_0^{\infty}G_h(f)df$, we get

$$\left\langle i_{PIIN}{}^2\right\rangle=G^2R^2B\int_0^{\infty}G_h^2(f)df.$$

Therein,

$$\int_0^{\infty}G_h^2(f)df=b_h^2\frac{P_s^2}{M^2p^2\Delta f^2}\times$$

$$\int_0^{\infty}\left(\sum_{i=1}^{L}C_h(i)\left\{u\left[f-f_0-\frac{\Delta f}{2L}(-L+2i-2)\right]-u\left[f-f_0-\frac{\Delta f}{2L}(-L+2i)\right]\right\}\right)^2df$$

$$= b_h^2 \frac{P_s^2}{M^2 p^2 \Delta f^2} \times \frac{(p-1)\Delta f}{ML}$$

Due to $L=p^2$, $\int_0^\infty G_h^2(f)\,df$ can be further simplified as

$$\int_0^\infty G_h^2(f)df = b_h^2 \frac{P_s^2(p-1)}{M^3 p^4 \Delta f}.$$

Hence, the PIIN can be expressed as

$$\left\langle i_{PIIN}{}^2 \right\rangle = G^2 R^2 B \frac{P_s^2(p-1)}{M^3 p^4 \Delta f} b_h^2.$$

The shot noise can be expressed as

$$\left\langle i_{shot}{}^2 \right\rangle = 2eG^2 F_e P_{in} RB.$$

By substituting these above equations, we have

$$\left\langle i_{shot}{}^2 \right\rangle = \frac{2P_s(p-1)eG^2 F_e RB}{M^2 p^3} b_h.$$

Since the noise power of the phototcurrrent is composed of PIIN, shot noise, and thermal noise, the total noise power can be expressed as

$$\left\langle i^2 \right\rangle = \left\langle i_{PIIN}{}^2 \right\rangle + \left\langle i_{shot}{}^2 \right\rangle + \left\langle i_{thermal}{}^2 \right\rangle =$$
$$G^2 R^2 B \frac{P_s^2(p-1)}{M^3 p^4 \Delta f} b_h^2 + \frac{2P_s(p-1)eG^2 F_e RB}{M^2 p^3} b_h + 4K_b T_n B / R_L$$

Since b_k can be 1 or 0, $\left\langle i^2 \right\rangle$ can be rewritten as

$$\left\langle i^2 \right\rangle = \left(\begin{array}{l} G^2 R^2 B \frac{P_s^2(p-1)}{M^3 p^4 \Delta f} \\ + \frac{2P_s(p-1)eG^2 F_e RB}{M^2 p^3} \end{array} \right) b_h + 4K_b T_n B / R_L$$

Because b_h has the same probability to be 0 or 1, we have

$$\left\langle i^2 \right\rangle = G^2 R^2 B \frac{P_s^2(p-1)}{2M^3 p^4 \Delta f}$$
$$+ \frac{P_s(p-1)eG^2 F_e RB}{M^2 p^3} + 4K_b T_n B / R_L.$$

Consequently, the signal-to-noise ratio (SNR) at a receiver of the proposed system can be obtained as

$$SNR = \frac{I^2}{\left\langle i^2 \right\rangle} = \frac{\frac{G^2 R^2 P_s^2 (p-1)^2}{M^4 p^6}}{G^2 R^2 B \frac{P_s^2(p-1)}{2M^3 p^4 \Delta f} + \frac{P_s(p-1)eG^2 F_e RB}{M^2 p^3} + 4K_b T_n B / R_L}$$

By using well-known Gaussian approximation, the bit-error-rate (BER) of the proposed system can be written:

$$BER = \frac{1}{2} erfc\left(\frac{SNR}{8} \right),$$

where the complementary error function is defined as

$$erfc(x) = \frac{2}{\sqrt{\pi}} \int_x^\infty \exp(-z^2) dz.$$

Table II: An example of the PMP codes for GF(5) and M=2.

Group x	i 01234	Sequence	Code Sequence
0	X0X0X	$S_{0,0,0}$	$C_{0,0,0}$= 00000
	X4X4X	$S_{0,1,0}$	10000
	X3X3X	$S_{0,2,0}$	00000
	X2X2X	$S_{0,3,0}$	10000
	X1X1X	$S_{0,4,0}$	00000
	XX0X0	$S_{0,0,1}$	$C_{0,1,0}$= 00000
	XX4X4	$S_{0,1,1}$	00001
	XX3X3	$S_{0,2,1}$	00000
	XX2X2	$S_{0,3,1}$	00001
	XX1X1	$S_{0,4,1}$	00000
			$C_{0,2,0}$= 00000
			00010
			00000
			00010
			00000
			$C_{0,3,0}$= 00000
			00100
			00000
			00100
			00000
			$C_{0,4,0}$= 00000
			01000
			00000
			01000
			00000
			$C_{0,0,1}$= 00000
			00000
			10000
			00000
			10000
			$C_{0,1,1}$= 00000

			00000 00001 00000 00001 $C_{0,2,1}$= 00000 00000 00010 00000 00010 $C_{0,3,1}$= 00000 00000 00100 00000 00100 $C_{0,4,1}$= 00000 00000 01000 00000 01000
1	0XX3X 1XX4X 2XX0X 3XX1X 4XX2X XX2X4 XX3X0 XX4X1 XX0X2 XX1X3	$S_{1,0,0}$ $S_{1,1,0}$ $S_{1,2,0}$ $S_{1,3,0}$ $S_{1,4,0}$ $S_{1,0,1}$ $S_{1,1,1}$ $S_{1,2,1}$ $S_{1,3,1}$ $S_{1,4,1}$	$C_{1,0,0}$= 10000 00000 00000 00010 00000 $C_{1,1,0}$= 01000 00000 00000 00001 00000 $C_{1,2,0}$= 00100 00000 00000 10000 00000 $C_{1,3,0}$= 00010 00000 00000 01000 00000 $C_{1,4,0}$= 00001 00000 00000 00100 00000 $C_{1,0,1}$= 00000 00000 00100 00000 00001 $C_{1,1,1}$= 00000 00000 00010 00000 10000 $C_{1,2,1}$= 00000 00000 00001 00000 01000 $C_{1,3,1}$= 00000 00000 10000 00000 00100 $C_{1,4,1}$= 00000 00000 01000 00000
			00010
2	0XX1X 2XX3X 4XX0X 1XX2X 3XX4X X2XX3 X4XX0 X1XX2 X3XX4 X0XX1	$S_{2,0,0}$ $S_{2,1,0}$ $S_{2,2,0}$ $S_{2,3,0}$ $S_{2,4,0}$ $S_{2,0,1}$ $S_{2,1,1}$ $S_{2,2,1}$ $S_{2,3,1}$ $S_{2,4,1}$	$C_{2,0,0}$= 10000 00000 00000 01000 00000 $C_{2,1,0}$= 00100 00000 00000 00010 00000 $C_{2,2,0}$= 00001 00000 00000 10000 00000 $C_{2,3,0}$= 01000 00000 00000 00100 00000 $C_{2,4,0}$= 00010 00000 00000 00001 00000 $C_{2,0,1}$= 00000 00100 00000 00000 00010 $C_{2,1,1}$= 00000 00001 00000 00000 10000 $C_{2,2,1}$= 00000 01000 00000 00000 00100 $C_{2,3,1}$= 00000 00010 00000 00000 00001 $C_{2,4,1}$= 00000 10000 00000 00000 01000
3	0X1XX 3X4XX 1X2XX 4X0XX 2X3XX X3XX2 X1XX0 X4XX3 X2XX1 X0XX4	$S_{3,0,0}$ $S_{3,1,0}$ $S_{3,2,0}$ $S_{3,3,0}$ $S_{3,4,0}$ $S_{3,0,1}$ $S_{3,1,1}$ $S_{3,2,1}$ $S_{3,3,1}$ $S_{3,4,1}$	$C_{3,0,0}$= 10000 00000 01000 00000 00000 $C_{3,1,0}$= 00010 00000 00001 00000 00000 $C_{3,2,0}$= 01000 00000 00100 00000 00000 $C_{3,3,0}$= 00001

			00000 10000 00000 00000 $C_{3,4,0}$= 00100 00000 00010 00000 00000 $C_{3,0,1}$= 00000 00010 00000 00000 00100 $C_{3,1,1}$= 00000 01000 00000 00000 10000 $C_{3,2,1}$= 00000 00001 00000 00000 00010 $C_{3,3,1}$= 00000 00100 00000 00000 01000 $C_{3,4,1}$= 00000 10000 00000 00000 00001
4	0X3XX 4X2XX 3X1XX 2X0XX 1X4XX X4X2X X3X1X X2X0X X1X4X X0X3X	$S_{4,0,0}$ $S_{4,1,0}$ $S_{4,2,0}$ $S_{4,3,0}$ $S_{4,4,0}$ $S_{4,0,1}$ $S_{4,1,1}$ $S_{4,2,1}$ $S_{4,3,1}$ $S_{4,4,1}$	$C_{4,0,0}$= 10000 00000 00010 00000 00000 $C_{4,1,0}$= 00001 00000 00100 00000 00000 $C_{4,2,0}$= 00010 00000 01000 00000 00000 $C_{4,3,0}$= 00100 00000 10000 00000 00000 $C_{4,4,0}$= 01000 00000 00001 00000 00000 $C_{4,0,1}$= 00000 00001 00000 00100 00000 $C_{4,1,1}$= 00000 00010 00000 01000

00000 $C_{4,2,1}$= 00000 00100 00000 10000 00000 $C_{4,3,1}$= 00000 01000 00000 00001 00000 $C_{4,4,1}$= 00000 10000 00000 00010 00000

Ⅲ-3 Numerical Results

The system parameters used to obtain the numerical results are listed in Table III. The quantum efficiency, average gain, excess noise factor and effective ionization ration of the APDs are η=0.6, G=40, F_e=21and k_e=0.5, respectively. The receiver noise temperature and load resistance are T_n=300K and R_L=1030Ω. The spectrum of the broadband light source is centered at 1.55μm with spectral width $\Delta\lambda$=*30*nm and coherence time is about τ_c≈0.267ps. The data transmission rate is 155Mbps and the electrical bandwidth of receivers is 80MHz.

Table III: Parameters used in the numerical calculation

PD quantum efficiency	η=0.6
Spectral width of broadband light source	$\Delta\lambda$=30nm (i.e. Δf=3.75THz)
Wavelength location	1.55μm
Electrical bandwidth	B=80MHz
Data transmission rate	155Mbps
Receiver noise temperature	T_n=300K
Receiver load resistor	R_L=1030Ω

Fig. 17 shows the number of simultaneous users that can be accommodated in the proposed system versus BER for p=7, M=3, and P_s=5dBm. For convenience of comparison, the numerical results of the OCDMA systems using MQC codes, M-matrices codes, and 2-D perfect difference codes are also shown. As depicted in Fig. 17, the maximum number of simultaneous users that can be accommodated in the proposed system is limited to 147 due to the code size. It is clear that the proposed system can support more simultaneous users than the systems using MQC codes and M-matrices codes. Although the OCDMA system using 2-D perfect difference codes can support more simultaneous users than the proposed system, its BER is much higher and increases rapidly with the number of simultaneous users.

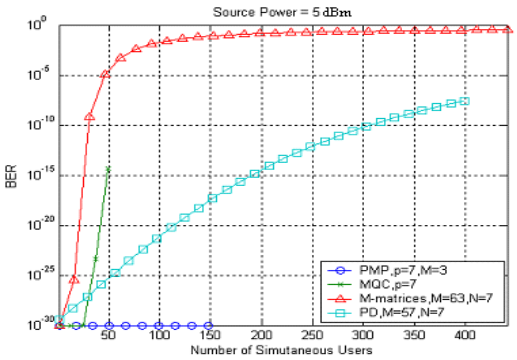

Fig. 17: The number of simultaneous users versus BER for p=7, M=3, and P_s=5dBm.

In Fig. 18, the source power is set to 0dBm. It shows that the OCDMA system using 2-D perfect difference codes has a dramatic performance drop because of insufficient source power. In Fig. 19, the source power is set to -10dBm. As we can see, the performances of the systems using MQC

codes and M-matrices codes are also degraded to a unusable extent. Only the proposed system can still keep its performance in an acceptable level, i.e. the BER is smaller than 10^{-9}. In Fig. 8, the source power is set to -15dBm. We can find that the proposed system can still accommodate 147 simultaneous users at BER around 10^{-9}.

In Fig. 19, the BER versus the source power is shown at the number of simultaneous users equal to 130. As we can see, the systems using 2-D perfect different codes and the M-matrices codes cannot make BER lower than 10^{-9} when the source power is below 0dBm. However, the proposed system can well meet this requirement even when the power is around -15dBm.

According to the numerical results shown in Figs. 17-19, it can be concluded that the proposed system is of much better performance when the optical power is low. In other words, the power demand of the proposed system is much lower than that of other systems.

Fig. 20 shows the BER of the proposed system versus the source power as the number of simultaneous users is 49 and the parameters of the PMP codes are set to (p, M) = (5, 2), (7, 3), (11, 2), or (11, 5). It is easy to find that the proposed system with the setting of (p, M) = (5, 2) needs the least source power to meet the requirement of BER=10^{-9} while the one with the setting of (p, M) = (11, 5) needs the most. This is because that, when the source power is fixed, the transmitter of the proposed system using the PMP codes with (p, M) = (5, 2) causes the least power loss during spectral encoding and thus has the largest output signal power.

As the transmitted digital data is 1, the power loss resulting from spectral encoding can be expressed as

$$P_{loss} = \left(1 - \frac{p-1}{Mp^2}\right) \cdot P_s .$$

In condition that the code length is fixed, i.e. the value of p is fixed, decreasing the value of M can reduce the encoding power loss and thus to reduce the required source power. However, decreasing the value of M will also reduce the code size and hence the number of simultaneous user that can be accommodated in the proposed system is also reduced. Therefore, there is a tradeoff in selection of the value of M.

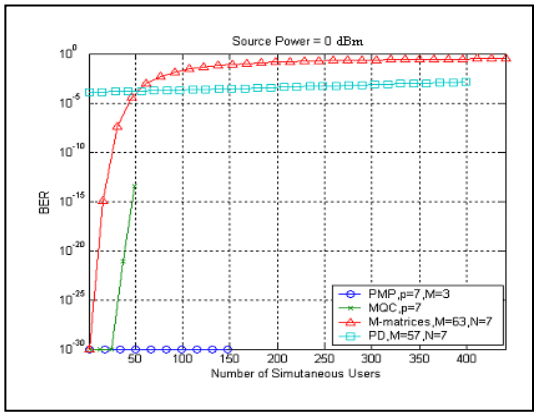

Fig. 18: The number of simultaneous users versus BER for p=7, M=3, and P_s=0dBm.

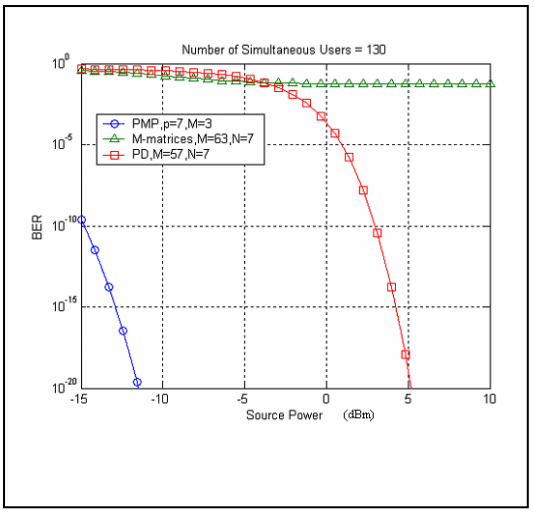

Fig. 19: BER versus the source power as the number of simultaneous users is 130.

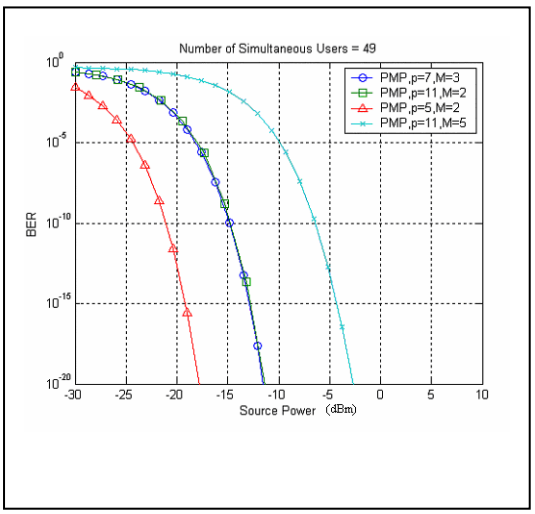

Fig. 20: BER versus the source power as the number of simultaneous users=49.

二、 計畫成果自評與結論

First, we have investigated the loss behavior of OPS employing PBS mechanism to provide DiffServ under Markovian modeled self-similar traffic input. The computation complexity has been shown to increase cubically as the state of MAP increases. To reduce the computation complexity, we propose an approximate model for OPS employing PBS mechanism under Markovian modeled self-similar traffic input. Our proposed model is to retain the same high dimensional MAP for high priority traffic, but to reduce the dimension of MAP of low priority traffic following the methods in [24]. By applying the approximate model, it is obvious that the computation complexity is reduced by $8^3 = 512$ times while retaining satisfactory accuracy. Accordingly, we investigate and analyze both the short term and long term performance measures. Our model is useful in performing the optimal buffer control for OPS employing PBS to provide differentiated services under self-similar traffic input. With our model and analysis, we could find out the optimal threshold level to obtain the greatest DiffServ performance and the utilization of the buffers simultaneously for OPS employing PBS mechanism under self-similar traffic input. We could also utilize the information of the mean lengths of critical and non-critical periods to be an event trigger mechanism for initializing the related call admission control schemes in OPS to improve the switching performance to greater extent.

Second, we investigate analytically the switching performance of WDM OPS employing wavelength conversion techniques under Markovian modeled self-similar traffic input. We leverage

the results of using MAPs to emulate self-similar traffic and apply them to the investigation of performance analysis of WDM OPS employing wavelength conversion techniques. Our analysis is pretty accurate and can capture the impact of self-similar traffic upon the switching performance of WDM OPS employing wavelength conversion techniques to some extent. We also propose an efficient procedure to avoid large computation efforts in solving the resultant *MAP/D/c/K* queues and analyze the computation complexity in a concise way. Our analysis holds good and is in line with the conclusions of other investigations made by simulations. This feature makes our analysis valuable and useful in dimensioning WDM OPS employing wavelength conversion techniques under self-similar traffic input.

Last, we study the Spectral/time OCDMA system employing PDC. This system is applicable to the access network such as PON. In addition, we propose a novel 2-D OCDMA network architecture to further suppress PIIN and lower the demand of source power. In the proposed network architecture, the receivers are divided into p groups. The receivers in each group correspond to one code group of the PMP codes and connect to the outputs of the same star coupler. Since the cross-correlation between any two of the PMP code sequences in the same group is zero, the code sequences assigned to the receivers in the same group are mutually orthogonal. The transmitters of the proposed network architecture only transmit the spectrally encoded signals to the receivers via the start coupler corresponding to the code group of the adopted code sequence. Hence, the receivers can use the orthogonal property of the code groups of the PMP codes to completely filter out the undesired signals sent from other users. In this way, the MUI and PIIN caused by other users can be eliminated. Moreover, since the transmitters only need to transmit the spectrally encoded signals to one group of the receivers, the signal power lost in the start coupler can be reduced. Thus, the demand of source power is greatly reduced. According to the numerical results, it is proven that the source power of the proposed system can be much lower than that of the system using MQC codes, M-matrices codes, and 2-D perfect difference codes. When the parameters of the PMP codes are set to p=7 and M=3, the spectral width is 30nm, and the transmission rate is 155Mbps, the proposed system can still accommodate 147 simultaneous users with the source power equal to −15dBm. Because the proposed system can function well with low source power, it is possible to employ low-cost light-emitting diodes (LEDs) in practical implementation. Moreover, by using the group orthogonal property of PMP codes, the receivers can use a set of FBGs to remove MUI and PIIN

caused by other users. Hence, the complexity of the receivers of the proposed system is lower than that of other non-coherent OCDMA systems. Therefore, the proposed system can be used to realize a low-cost and high-performance optical access network.

三、 發表之論文

[1] Chun-Yang Chen, Chih-How Chang, Malla Reddy Perati, Shou-Kuo Shao , Jingshown Wu, ” Performance Analysis of WDM Optical Packet Switches Employing Wavelength Conversion under Markovian Modeled Self-Similar Traffic Input”, HPSR Conference, Thursday, May 31, 2007, New York, USA

[2] Chih-How Chang, Malla Reddy Perati, Shou-Kuo Shao , Jingshown Wu,” An Efficient Approximate Markovian Model for Optical Packet Switches Employing Partial Buffer Sharing Mechanism under Self-Similar Traffic Input”, HPSR Conference, Thursday, May 31, 2007, New York USA

[3] Chih-How Chang, Shou- Kuo Shao, Malla Reddy Perati and J. Wu, “Performance Study of Various Packet Scheduling Algorithms of Variable-Packet-Length Feedback Type WDM Optical Packet Switches”, Proceeding of the Workshop on High Performance Switching and Routing, June 2006, Poznan, Poland

[4] C. H. Lin and J. Wu, “Comments on "Novel Combinatorial Constructions of Optical Orthogonal Codes for Incoherent Optical CDMA Systems,” *IEEE Journal of Lightwave Technology*, Vol. 24, No. 2, PP. 1064, Feb. 2006

[5] Yen-Chun Liao, Chia-Chu Ho, Hen-Wai Tsao, and Jingshown Wu, “Design and Experimental Demonstration of a Synchronous OCDMA-Based 10Gbps/1.25Gbps EPON with a Novel Synchronization Scheme”, Journal of Selected Topics in Quantum Electronics, Submitted

[6] Wen-Jeng Huang, Cheing-hong Lin, and Jingshown Wu, “Spatial/Spectral OCDMA System Using Partial Modified Prime Code and Error Correcting Code”, JLT, Submitted

[7]Chun-tao Niu, Cheing-hong Lin, and Jingshown Wu, “Novel Architecture of Non-coherent Spectral/Spatial OCDMA System Using Partial Modified Prime Codes”, JLT, Submitted

[8] Chih-How Chang, Meng-Guang Tsai, Shou-Kuo Shao, Hen-Wai Tsao, Malla Reddy Perati and J. Wu, “An Efficient Void Filling Algorithm for WDM Optical Packet Switches Operating under Variable-Packet-Length Self-Similar Traffic,” IEICE Transaction on Communications, Vol. E88-B, No. 12, PP. 4659-4663, Dec. 2005

[9] F. R. Gu and J. Wu, “Construction of Two-Dimensional Wavelength/Time Optical Orthogonal Codes Using Difference Family,” IEEE Journal of Lightwave Technology, Vol. 23, No. 11, PP. 3642-3652, Nov. 2005

四、 參考文獻

[1] Chih-How Chang, Shou- Kuo Shao, Malla Reddy Perati and J. Wu, "Performance Study of Various Packet Scheduling Algorithms of Variable-Packet-Length Feedback Type WDM Optical Packet Switches", Proceeding of the Workshop on High Performance Switching and Routing, June 2006, Poznan, Poland

[2] F. Callegati, G. Corazza, and C. Raffaelli, "Exploitation of DWDM for optical packet switching with quality of service guarantees," *IEEE J. Select. Areas Commun.*, vol. 20, no. 1, pp. 190–201, Jan. 2002.

[3] M.R.N. Ribeiro, and M.J. O'Mahony, "Improvements on performance of photonic packet switching nodes by priority assignment and buffer sharing," in *Proc. ICC'2000*, vol. 3, pp. 1738–1742, New Orleans, USA, June 2000.

[4] W.E. Leland, M.S. Taqqu, W. Willinger, and D.V. Wilson, "On the self-similar nature of ethernet traffic (extended version)," *IEEE/ACM Trans. Networking*, vol. 2, no. 1, pp. 1–15, Feb. 1994.

[5] V. Paxson and Sally Floyd, "Wide area traffic: the failure of Poisson modeling," *IEEE/ACM Trans. Networking*, vol. 3, no. 3, pp. 226–244, June 1995.

[6] M.E. Crovella and A. Bestavros, "Self-similarity in world wide web traffic: Evidence and possible causes, "*IEEE/ACM Trans. Networking*, vol. 5, no. 6, pp. 835–846, Dec. 1997.

[7] A.T. Andersen and B.F. Nielsen, "A Markovian approach for modeling packet traffic with long-range dependence," *IEEE J. Select. Areas in Commun.*, vol. 16, no. 5, pp. 719–732, June 1998.

[8] S. Kasahara, "Internet traffic modeling: Markovian approach to

[10] C. H. Lin, J. Wu, H. W. Tsao, and C. L. Yang, "Spectral Amplitude-Coding Optical CDMA System Using Mach-Zehnder Interferometers," IEEE Journal of Lightwave Technology, Vol. 23, No. 4, PP. 1543-1555, Apr. 2005

[11] Shou-Kuo Shao, Malla Reddy Perati, Meng-Guang Tsai, Hen-Wai Tsao, and J. Wu, "Generalized Variance-Based Markovian Fitting for Self-Similar Traffic Modelling," IEICE Transaction on Communications, Vol. E88-B, No. 4, PP. 1493-1502, Apr. 2005

[12] Shou-Kuo Shao, Meng-Guang Tsai, Hen-Wai Tsao, Paruvelli Sreedevi, Malla Reddy Perati, and J. Wu, **"**Performance evaluation of feedback Type WDM optical routers under asynchronous and variable packet length self-similar traffic," IEICE Transaction on Communications, Vol. E88-B, No. 3, PP. 1072-1083, Mar. 2005

[13] F. R. Gu and J. Wu, "Construction and Performance Analysis of variable-Weight optical Orthogonal Codes for Asynchronous Optical CDMA Systems," IEEE Journal of Lightwave Technology, Vol. 23, No. 2, PP. 740-748, Feb. 2005

self-similar traffic and prediction of loss probability for finite queues," *IEICE Trans. Commun.*, vol. E84–B, no. 8, pp. 2134–2141, Aug. 2001.

[9] S.K. Shao, M.R. Perati, M.G. Tsai, H.W. Tsao, and J. Wu, "Generalized variance-based Markovian fitting for self-similar traffic modeling," *IEICE Trans. Commun.*, vol. E84–B, no. 8, pp. 4659–4663, Dec. 2005.

[10] D.M. Lucantoni, K.S. Meier-Hellstern, and M.F. Neuts, "A single-server queue with server vacations and a class of nonrenewal arrival processes," *Adv. Appl. Prob.*, vol. 22, pp. 676–705, 1990.

[11] D.M. Lucantoni, "New results on the single server queue with a batch Markovian arrival process," *Commun. Statist. –Stochastic Models*, vol. 7, pp. 1–46, 1991.

[12] C. Blondia, "The N/G/1 finite capacity queue," *Commum. Statist. Stochastic Models*, vol. 5, pp. 273–294, 1989.

[13] M.F. Neuts, "Models based on the Markovian arrival process," *IEICE Trans. Commun.*, vol. E75-B, pp. 1255–1265, Dec. 1992.

[14] S.H. Kang, Y.H. Kim, D.K. Sung, and B.D. Choi, "An application of Markovian arrival process (MAP) to modeling superposed ATM cell streams," *IEEE Trans. Commun.*, vol. 50, no. 4, pp. 633–642, Apr. 2002.

[15] H. Heffes and D.M. Lucantoni, "A Markov modulated characterization of packetized voice and data traffic and related statistical multiplexer performance," *IEEE J. Select. Areas Commun.*, vol. 4, no. 6, pp. 856–868, Sept. 1986.

[16] I. Ide, "Superposition of interrupted Poisson processes and its application to packetized voice multiplexers," In *Proc. ITC-12*, vol. 3, pp. 3.1B.2, Torino, Italy, 1988.

[17] Y.H. Kim and S.Q. Li, "Timescale of interest in traffic measurement for link bandwidth allocation design," in *Proc. Infocom'96*, vol. 2, pp. 738–748, San Francisco, USA, Mar. 1996.

[18] B. Venkataramani, S.K. Bose, K.R. Srivathsan "Queuing analysis of a non-pre-emptive MMPP/D/1 priority system," *Computer Commun.*, vol. 20, no. 11, pp. 999–1018, Oct. 1997.

[19] Y.C. Wang, C.W. Lin, and C.C. Lu, "Loss behavior in space queue with batch Markovian arrival process – discrete time case," *Performance Evaluation*, vol. 41, no. 4, pp.269–293, Aug. 2000.

[20] H. Kr¨oner, "Comparative performance study of space priority mechanisms for ATM networks," in *Proc. IEEE INFOCOM' 90*, vol. 3, pp. 1136–1143, San Francisco, USA, June 1990.

[21] M.R. Perati, C.H. Chang, S.K. Shao, and J. Wu, "Loss behavior analysis of optical packet Switches Employing Partial Buffer Sharing Mechanism in conjuction with Markovian Modeled Self-Similar Traffic," submitted to *WOCN*'2007.

[22] G. Latouche and V. Ramaswami, *Introduction to Matrix Analytic Methods in Stochastic Modeling,* SIAM Press, Philadelphia, Pennsylvania, 1999.

[23] M.F. Neuts, *Matrix-Geometric Solutions in Stochastic Models: An Algorithmic Approach*, Dover Publications, 1995.

[24] J.E. Diamond, and A.S. Alfa, "On approximating higher order MAPs with MAPs of order two," *Queueing Systems*, vol. 34, pp. 269–288, 2000.

[25] T. Altiok, "On the phase-type approximations of general distributions," *IIE Trans.*, vol. 17, pp. 110–116, 1985.

[26] A.N. Dudin, V.L. Kilmenok, and G.V. Tsarenkov, "Software Sirius++ for performance evaluation of modern communication networks," in *Proc. ESM'2002*, pp. 489–493, Fachhochschule Darmstadt, Germany, June 2002.

[27] V. Ramaswami and W. Willinger, "Efficient traffic performance strategies for packet multiplexer," *Comput. Networks and ISDN Systems*, vol. 20, pp. 401–407, 1990.

[28] H. Yamada, "Cell/packet loss behavior in a statistical multiplexer with bursty input," *Performance Evaluation*, vol. 17, no. 2 pp.77–90, Mar. 1993.

[29] S.L. Danielsen, B. Mikkelsen, C. Joergensen, T. Durhuus, K. Stubkjaer, "WDM packet switch architecture and analysis of the influence of tunable wavelength converters on the performance," *J. Lightw. Technol.,* vol. 15, pp. 219-227, Feb. 1997.

[30] S.L. Danielsen, P.B. Hansen, and K.E. Stubkjaer, "Wavelength conversion in optical packet switching, " *J. Lightw .Technol.,* vol. 11, no. 12, pp. 2095-2108, Dec. 1998.

[31] L. Tancevski, S. Yegnanarayanan, G. Castanon, L. Tamil, F. Masetti, and T. McDermott, "Optical routing of asynchronous, variable length packets, " *IEEE J. Select. Areas Commun.*, vol. 18, no. 10, pp. 2084-2093, Oct. 2000.

[32] J.J. He and D. Simeonidou, "Contention resolution in optical packet-switching networks: Under long-range dependent traffic," in *Proc. OFC'2000*, ThU4-1/295, pp. 295-297,2000.

[33] T. Takine, and Y. Takahashi, "On the relationship between queue lengths at a random instant and at a departure in the stationary queue with BMAP arrivals, " Stochastic Models, vol. 14, no. 3, pp. 601-610, 1998.

[34] I. Norros, "A storage model with self-similar input," Queueing Systems, vol. 16, pp. 387-396, 1994.

[35] G. Shen, S.K. Bose, T.H. Cheng, C. Lu, T.Y. Chai, "Performance study on a WDM packet switch with limited-range wavelength converters, " *IEEE Commun. Letters,* vol. 5, no. 10, pp. 432-434, Oct. 2001.

[36] G. C. Yang and T. E. Fuja, "Optical orthogonal codes with unequal auto and cross-correlation constrains," IEEE Trans. Inform. Theory, pp.96-106, Jan. 1995.

[37] C. S. Weng and J. Wu, “Optical Orthogonal Codes with Nonideal Cross Correlation”, IEEE Journal of Lightwave Technology Vol. 19, NO.12, PP. 1856-1863, December 2001.

[38] P. R. Prucnal, M. A. Santoro, and T. R. Fan, “Spread spectrum fiber-optic local area network using optical processing,” J. Lightwave Technol., Vol. LT-4, pp. 547~554, May 1986.

[39] Chi-Shun Weng and Jingshown Wu, “Perfect difference codes for synchronous fiber-optic CDMA communication systems,” J. Lightwave Technol., Vol. 19, pp. 186 -194, Feb. 2001.

[40] J. A. Salehi, “Code division multiple-access techniques in optical fiber networks-Part I: Fundamental principles,” IEEE Trans. Comm., Vol. 37, pp. 824-833, Aug. 1989.

[41] F. R. K. Chung, J. A. Salehi, and V. K. Wei, “Optical orthogonal codes: Design, analysis, and applications,” IEEE Trans. Inform. Theory, Vol. 35, pp. 595-604, May 1989.

[42] Elie Inaty, Hossam M. H. Shalaby and Paul Fortier, “On the cutoff rates of a multiclass OFFH-CDMA system,” IEEE Trans. Comm., Vol. 53, No. 2, pp. 323-334, Feb. 2005.

[43] F. R. Gu and J. Wu, “Construction of Two-Dimensional Wavelength/Time Optical Orthogonal Codes Using Difference Family”, IEEE Journal of Lightwave Technology, Vol. 23, No. 11, PP. 3642-3652, November 2005

[44] Chun-tao Niu, Cheing-hong Lin, and J. Wu, “Novel Architecture of Non-coherent Spectral/Spatial OCDMA System Using Partial Modified Prime Codes,” submitted to IEEE Journal of Lightwave Technology.

[45] Elwyn D. J. Smith, Richard J. Blaikie and Desmond P. Taylor, “Performance enhancement of spectral amplitude-coding optical CDMA using pulse-position modulation,” IEEE Trans. Commun., Vol. 46, No. 3, pp. 1176~1185, Sep. 1998.

[46] Xiang Zhou, H.H.M. Shalaby, Chao Lu and Teehiang Cheng, “Code for spectral amplitude coding optical CDMA systems,” Electronics Letters, Vol. 36, No. 8, pp. 728~729, 13th, April 2000.

[47] Zou Wei, H. M. H. Shalaby and H. Ghafouri-Shiraz, “Modified quadratic congruence codes for fiber Bragg-grating-based spectral-amplitude-coding optical CDMA systems,” J. Lightwave Technol., Vol. 19, No. 9, pp. 1274~1281, Sept. 2001.

[48] Cheing-Hong Lin; Jingshown Wu; Hen-Wai Tsao; Chun-Liang Yang, “Spectral amplitude-coding optical CDMA system using Mach-Zehnder interferometers,” J. Lightwave Technol., Vol. 23, No. 4, pp. 1543~1555, April 2005.

[49] Chao-Chin Yang and Jen-Fa Huang, “Two-dimensional M-matrices coding in spatial/frequency optical CDMA networks,” IEEE Photonics Technology Letters, Vol. 15, No. 1, pp. 168~170, Jan.

2003.
[50] Cheing-Hong Lin, Jingshown Wu, and Chun-Liang Yang, “Noncoherent Spatial/Spectral Optical CDMA System with Two-Dimensional Perfect Difference Codes,” J. Lightwave Technol., Vol. 23, No. 12, pp. 3966~3980, December 2005.

行政院國家科學委員會專題研究計劃成果報告

子計畫二：光網路主動元件技術之研究與應用(2/3)

計畫主持人：李三良 博士
執行單位：國立台灣科技大學電子工程系

計畫編號：NSC95-2221-E011-083 (95B0121)

一、計畫摘要：

本子計畫主要使用一個價格低廉且體積小的光學共振腔式(etalon)光濾波器元件，放置於10Gbps直調雷射的輸出端，可以達到抑制頻率啁啾效應進而延伸傳輸距離的目的，從小於 10 公里增加到大於 75 公里，實驗結果可以對2個10Gbps直調雷射同時進行補償，因此利用 etalon 的週期性頻譜變化的特性，證實可以同時對多個通道的直調雷射傳輸系統達到性能改善的效果。

研究光都會網路及接取網路應用的光電主動元件模組,並研發異質積體化技術以將製作於不同基材的多功能元件整合在同一基板上,以結合光通訊模組所需的光學與電路，降低成本並增加可靠度。

區域網路頻寬的需求在過去幾年迅速地增長，從 10/100 Mbps 增加至 1-Gbps，並且很快會進入 10-Gbps 時代，全光時脈回復將會是全光高速光網路的核心技術。我們的研究發現全光時脈回復採用二段式分佈反饋雷射可以藉由布拉格波長調整表現出分散 Q 開關特色。布拉格波長調整源自去除二段式分佈反饋雷射其中一段的薄移層。這種設計破壞了分佈反饋雷射模態衰減，並提供穩定的單模輸出。布拉格波長調整導致了偏激射模態偏移。藉由注入電流，兩個不同區域的自震盪因此產生。

我們就二段式分佈反饋雷射展示其單模與多模競爭之全光時脈回復機制，且使用光學濾波器可使全光時脈回復機制同時在多模態下進行。

二、成果：

首先我們討論只有一個直調雷射通道加上etalon 後的效應，實驗的設置如圖 1 所示，載送的調變的訊號為 9.95328-Gb/s (2^{31}-1 PRBS) NRZ 碼，調變電流設定在20~40mA之間，當加上直流電流 18mA與調變電流 40mA時，雷射輸出的光熄滅比為9dB，相對地平均雷射輸出光功率為 3.5 dBm，雷射的輸出波長落在 1557.294nm附近，etalon 的插入損耗約為 4dB左右，主要是因為耦合損失，藉由較佳的耦光設置就可以大幅地降低損失。

我們選擇的 FP etalon 的穿透頻譜如圖 1 的縮圖，它的 3dB 頻寬為 0.125-nm ，自由頻譜週期(FSR)為 100-GHz，相對地 finesse 為約 0.66，一旦 etalon 的溫度可以穩定控制，它的梳狀頻譜可以涵蓋一個大的波長範圍作為參考用，所以，可以用來作為同時補償多個 WDM 通道，只要它的自由頻譜週期(FSR)符合通道間距。

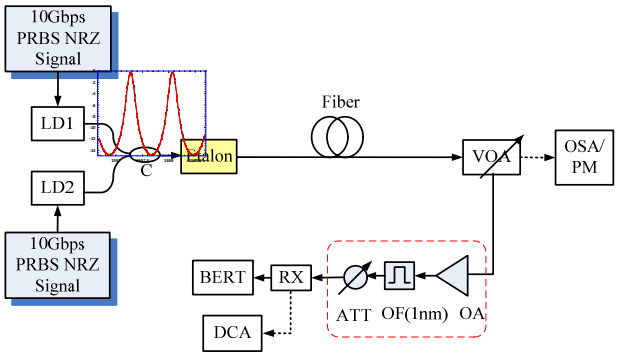

圖1 主要實驗架設圖

在一個嚴重頻率啁啾情形下，雷射輸出頻譜顯示出有兩個峰值代表傳遞訊號"0"與"1"準位有不同中心頻率，應用一窄頻寬的 FP etalon 可以去消減雷射因為調變下而變寬的頻譜，一些以前的研究報告提出使用光濾波器於雷射輸出端可以增進雷射的效能，但是必須將濾波器的中心位置作適當偏移的動作，於我們實驗中，我們只要簡單地將 etalon 的峰值對準雷射輸出"1"的波長。

為了研究啁啾效應及最佳化雷射的操作條件，我們執行時域啁啾值的量測，結果顯示於圖 2，當雷射的光明滅比< 5dB 時，平均的峰對峰的啁啾值幾乎都可以減少一半，在大偏壓電流(40mA)與小偏壓電流(20mA)情況下，可以降低成 10GHz 和 8GHz，雷射的光明滅比>5dB 以上，並且是在較小的調變電流情形下，暫態啁啾是非常嚴重導致光譜分佈呈現一個不對稱的形狀，頻率啁啾值會超過 20GHz 以上，再者，從量測的啁啾值可進一步計算出相對應的線寬增強因子 α ，比較在一般的條件與加上 etalon 後的差異。

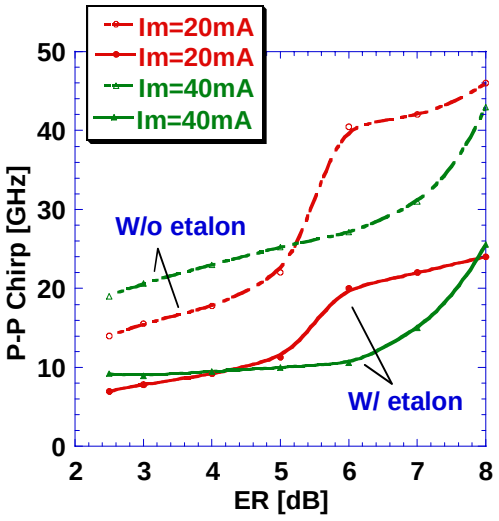

圖2 雷射設定在不同光明滅比之下，比較沒有與加入etalon後，頻率啁啾的變化情形。

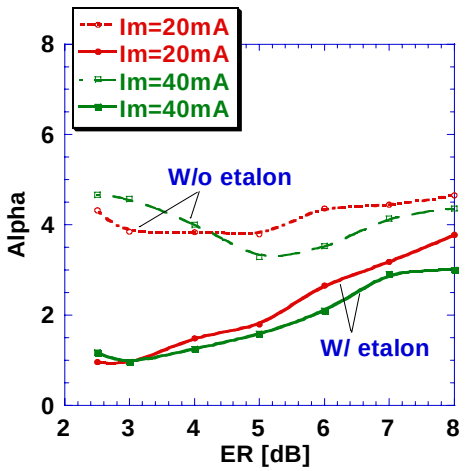

圖3 雷射設定在不同光明滅比之下，比較沒有與加入etalon後，線寬增強因子 α 的變化情形。

結果顯示於圖 3，一般情形之下，直接調變雷射的線寬增強因子 α 是介於 3.5 ~ 4.5，使用 FP etalon 後，雷射工作在光明滅比越小的條件下，可以將線寬增強因子 α 抑制的更小，如此可以得到更大的傳輸距離。

由於雷射輸出具有靜態啁啾效應(即傳送訊號" 0" 準位與訊號 "1" 準位是不同中心頻率)，所以我們將代表訊號"1"準位的波長對準到etalon 的峰值點，因此代表訊號"0"準位的波長會將對準到etalon 濾波器的斜率上，訊號"0"準位的光功率會被抑制，相對地提昇光訊號的明滅比，光明滅比的提升直接地反應在訊號品質的提升，使得量測的誤碼率可以降低。

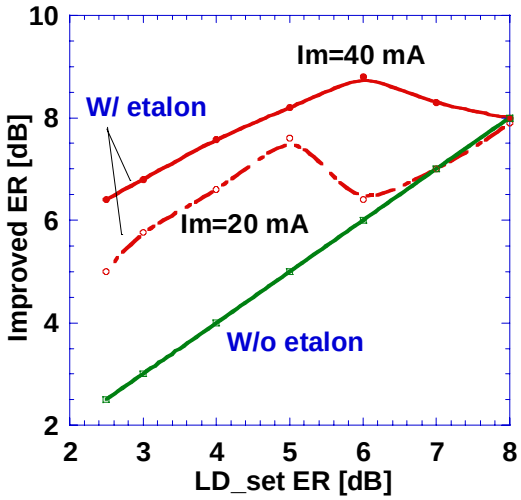

圖4雷射設定在不同光明滅比之下，比較沒有與加入etalon後，輸出光明滅比的改善情形

在圖4中表示，較大的調變電流可以使得兩個訊號波長間距較大，代表訊號"0"準位的波長對準在 FP etalon 頻譜上較陡峭的位置，因此，可以得到較大的光明滅比提升量。反而言之，可以使雷射操作在較小的光明滅比輸出的條件，如此可以具有較小的暫態頻率啁啾值，再藉由etalon的幫助，將光明滅比提升到可以接受的位準，我們可以得知，考慮抑制靜態啁啾值時，最理想的etalon選擇必須是具有很陡峭的斜率，考慮抑制暫態啁啾

值時，訊號”1”位準的波長要穩穩地對準 FP talon 的峰值上。並且etalon 3dB 頻寬只要稍大於訊號頻寬即可。

接著，我們想探討在不同的雷射光明滅比設定下，藉由加上一etalon後對傳輸性能上的改善情形，固定調變電壓有兩個準位—1V(20-mA)及2V(40-mA) 的情況下，利用變化不同的偏壓電流得到各個光明滅比的條件，結果為圖5(a)所示。在小調變電流下，未經光纖傳輸時，加上etalon由於光明滅比的提升，所以將降低功率償付值，但是在設定的明滅比愈大時，反而變差，隨著傳輸距離再增長，要求功率償付值小於2dB以下，只能使用光明滅比為2.5~3dB的條件。圖5(b)中在大調變電流下，靜態啁啾較大，所以光明滅比可以增加到大過6dB後，暫態啁啾值才會超過靜態啁啾值，但是相對地最大的傳輸距離反而縮減。

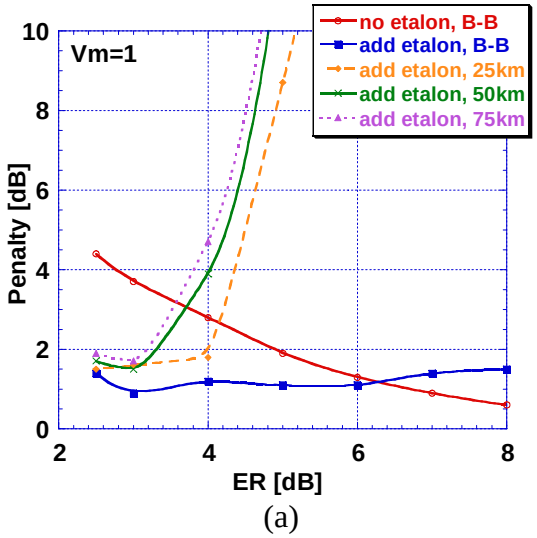

(a)

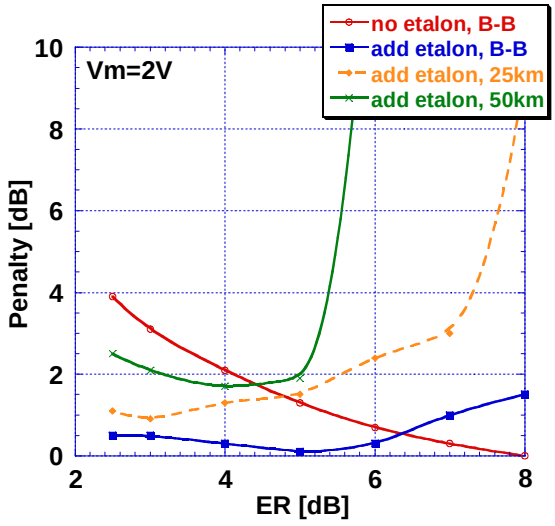

(b)

圖 5 雷射設定在不同光明滅比之下，比較沒有與加入 etalon 後，並變動傳輸距離，付出的功率代償值。(a) 小調變電流 (b)大調變電流。

兩個通道的傳輸系統架設仍然如圖 1 所示，波長分別為 1557.294nm 和 1558.088nm，比較沒有與加入 etalon 後的雷射輸出頻譜分布圖，顯示在圖 6 中，加入 etalon 後，可將兩各通道的頻譜分布變得更窄與更對稱。

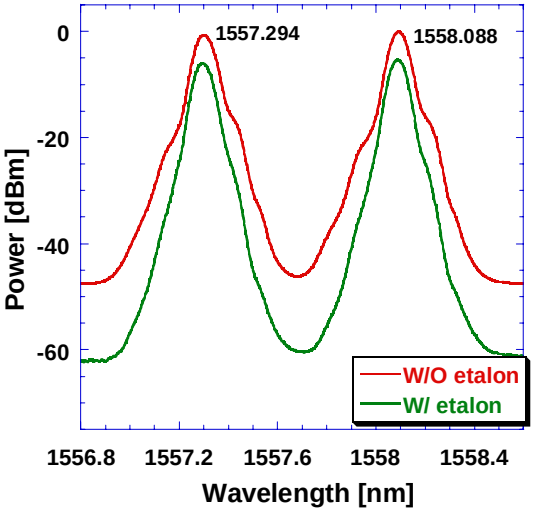

圖 6 兩個直調雷射在未加與加上 etalon 的頻譜比較

從上述結果，我們可以得知要傳輸最長距離，必須選擇光明滅比為3dB 左右，調變電流要小，再加上etalon濾波器後，光明滅比可提升到6.2 和6.5dB。利用此條件進行傳輸，結果如圖7所示，在未加etalon時，位元錯誤率<10-9 的要求下，傳輸8.5公里後就會增加3-dB 的功率償付值，但加上etalon後，即使傳輸75公里後，只產生小於3-dB 的功率償付值。

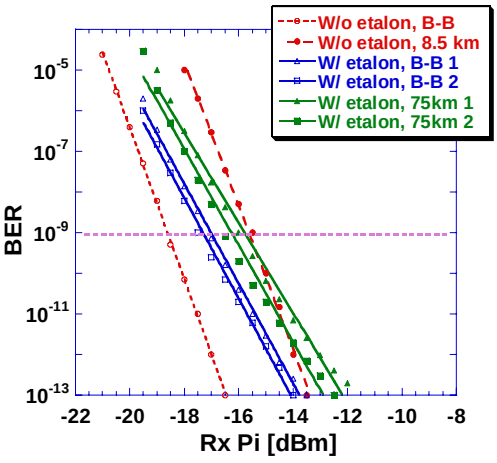

圖 7 在未加與加上 etalon 光濾波器，不同傳輸距離下量測的位元誤碼率。

我們也使用 VPI 系統模擬軟體進行使用 etalon 補償多個通道的效果，結果如圖 8

所示，使用 4 個通道，雷射參數的設定與實驗符合，再傳輸 75 公里之後，各個通道的最大的功率償付值相差不超過 2dB。

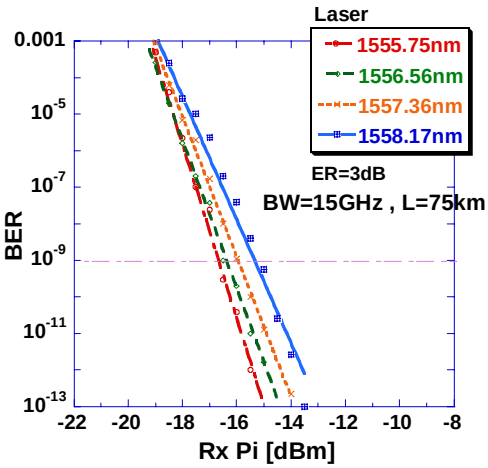

圖 8 使用 VPI 系統模擬軟體進行 4 個通道傳輸的模擬結果

分別依高性能低價位 WDM-PON 模組、高速連續可調波長雷射、高速取樣脈波雷射及光電取樣技術研究之成果報告分述如下：

(1) 高性能低價位 WDM-PON 模組：

(2) 高速連續可調波長雷射：

上一年度的計畫中，我們已經根據理論搭配 PICS3D 雷射模擬軟體來最佳化雷射結構的各項參數，已完成在主動層材料的選擇、量子井厚度和層數的評估以及光侷限層（SCH）的設計等。現階段並將所設計之雷射結構材料交予專業磊晶廠完成晶片的磊晶，而為進一步提升連續可調波長雷射之輸出特性，必須在雷射幾何結構上進行進一步設計。

圖 9(a)為傳統分布式布拉格雷射注入電流與波長變化的簡單示意圖，由示意圖可得之傳統長度(>200 m)的雷射共振腔，在電流注入下對波長的控制只能形成跳動式的階梯變化，在同樣的前提下，如將雷射共振腔的長度縮短(<100 m)，即形成圖 9(b)的示意，在電流注入下，波長能形成區段性的連續可調效果，此情況取決於共振腔之縱模斜率與布拉格模態的斜率的差異度，當兩者差異度越大，則對波長的控制接近於圖 9(a)之情形，反之，當兩者差異度越小，則對波長的控制接近於圖 9(b)之效果。

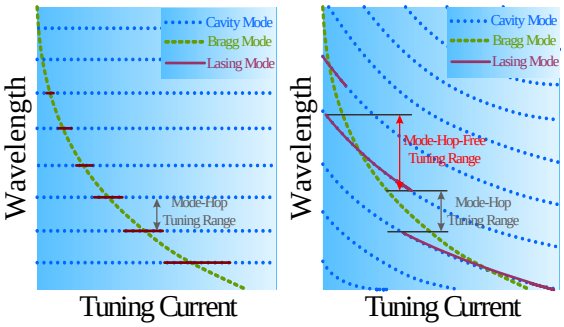

圖 9(a)傳統分布式布拉格雷射(b)短腔分布式布拉格雷射，注入電流與波長變化的簡單示意圖

基於此原理，為增加連續可調之波長範圍，必須使共振腔之縱模斜率與布拉格模態的斜率相近，方能增加連續可調之效果，綜觀國內外之相關研究，均以減短共振腔之長度為設計方向，然而減短共振腔的長度，必然促使臨界增益驟增，極易導致材料結構無法形成有效的共振腔，甚至使元件無法形成激發放射，為此，上一年度的計畫中，已經考量材料上實行的困難度，因此最佳化雷射結構中的每一層組成與參數，同時我們也積極思考進一步改善的研發方向。由於本計畫基於低價位高效率的方向考量，因此摒棄了國外文獻中複雜的磊晶方式，改以雷射結構的設計方向進行研發。

本實驗室提出在短腔式雷射結構中加入相位區，並且將相位區與光柵區的電極一併進行電流的調動，此方式經理論與模擬程式的印證具一定的功效性。現階段國外的研發方向，尚無加入相位區的考量，在經本實驗室積極的印證下，相位區的加入可輔助連續波長的調動範圍，亦對一度再短共振腔的雷射結構提供一個新的研發方向，圖 10 所示為相位區長度對連續可調波長範圍的作圖，隨著相位區的長度增加，連續可調的範圍亦隨著增加，另外，從模擬數據中亦可得知，當腔長為 50μm 時，連續可調的範圍則遠大於腔長為 100μm 時的效果。

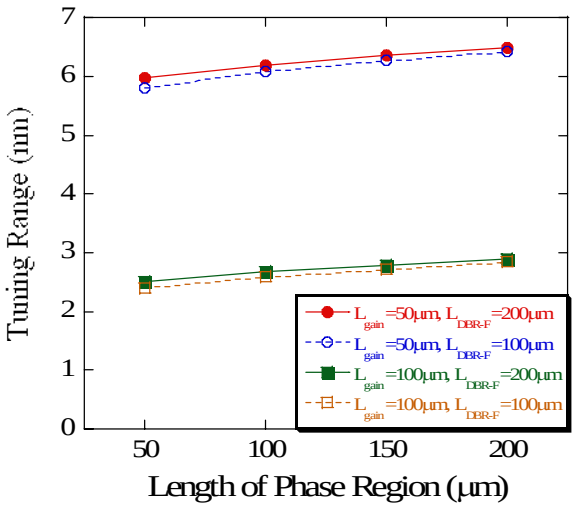

圖 10 相位區長度對連續可調波長範圍之關係圖

關於此階段設計之可調式雷射與半導體放大器積體化之研發方向亦在本階段有了初期的研究成果，由於主被動元件之單石積體化一直是國內外致力研究的方向，本實驗室以既有之量子井混合(Quantum Well Intermixing)技術，應用於現階段之研發。量子井混合效應主要是利用迅速升降溫的系統，對已磊晶完成之雷射晶片作短時間迅速升降溫的操作，藉由短時間高溫的操作，將主動層中原為矩形井狀的量子井，在經過內部擴散作用後，呈較平滑的圓弧形狀，而能隙也變的較大，對元件的輸出特性而言，發光波長會往短波長變動，即一般所稱之藍位移(Blueshift)。因此藉由控制操作溫度以及擴散時間的長短，可在同一個晶片上得到不同程度的能隙變化量。

一般而言，，主要可透過兩大方式來達成量子井混合效應，分別為摻質輔助內部擴散(Impurity-Induced inter-Diffusion, IID)與晶格缺位擴散(Impurity-Free Vacancy Diffusion, IFVD)兩種，在此將針對摻質輔助內部擴散技術進行研究。此技術可應用於所有Ⅲ-Ⅴ族之半導體材質中，主要是利用外界植入之摻質來促進量子井混合效應產生的技術，主要的製程步驟依序為(1)植入摻質到晶片內部(2)對晶片做快速升降溫之操作。相較於其他技術，此方式最大的優點是能對能隙做大幅度的調變。

藉由現階段的量子井混合研究結果，單一晶片中位移的波長，足以設計製作整合主被動元件於單一晶片中，接續的研究方向，將以此階段之研究成果為基礎，整合主被動元件於同一晶片中，以確實完成單石積體化之連續可調波長雷射。

(3) 高速取樣脈波雷射及光電取樣技術：

此計畫主要在研究分佈反饋雷射在高速光學網路的多重角色可能性，包含下列二項:

1. 二段式分佈反饋雷射自震盪現象的成立條件觀察。
2. 二段式分佈反饋雷射利用自震盪現象進行時脈回復之驗證。

全光時脈回復必須就輸入信號的相位與頻率同時鎖定，並且須有一時脈作為取樣信號。幾種全光時脈回復技術已被提出並顯示，如自震盪分佈反饋雷射，光學鎖相迴路，主動鎖模光纖環形雷射，被動鎖模半導體雷射[1]。時脈回復採用自震盪分佈反饋雷射是一有前景的方法，因為它的結構簡單和高速運作。分散 Q 開關以及模態競爭是主要的自震盪機制[2]。自震盪若由分散 Q 開關產生，其震盪頻率範圍是從 2 至 22GHz，而超過 20GHz 則是由模態競爭產生。當我們調整二段式分佈反饋雷射的注入電流時，它會產生自震盪的頻譜，我們由光頻譜分析儀觀察得知。我們將顯示單模及多模競爭的自震盪光頻譜。時脈回復的動態特性，如在回復的時脈與輸入信號在鎖定時間，偏離時間和相位穩定度是非常重要的光網路應用。鎖住時間和偏離時間已就二段式分佈反饋雷射已可達次奈微秒[3]。

使用二段式分佈反饋雷射產生分散 Q 開關自震盪時脈實驗裝置如圖 11 所示。

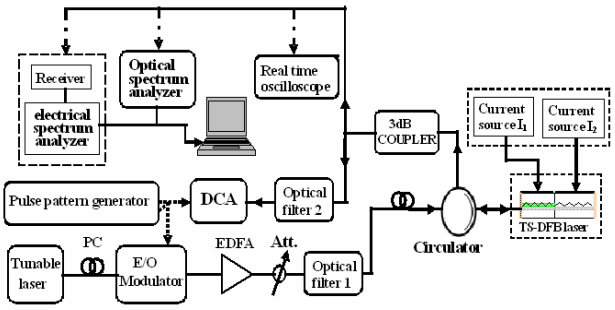

圖 11：研究架構

自震盪可由光頻譜分析儀，射頻頻譜分析儀（22GHz頻寬），和即時示波器（12 GHz頻寬）觀察而得。注入二段式分佈反饋雷射的電流I_1與I_2係由兩個穩定電流源提供。二段式分佈反饋雷射之單模自震盪效應發生在I_1遠大於I_2或I_1遠小於I_2，但這兩種情形的輸出特性是不同的。該二段式分佈反饋雷產生單模自震盪只有在I_2小於 6mA且I_1遠大於I_2的情形，或是I_2介於 11mA與 25mA且I_1遠小於I_2

的情形。

多模競爭的情況下，二段式分佈反饋雷射可能產生自震盪效應，當注入電流選擇非I_1遠大於I_2或I_1遠小於I_2，當I_1等於 15.94mA 而I_2等於 80mA，圖 15 顯示單模自震盪的光頻譜和射頻頻譜。當I_1等於 85mA 而I_2等於 37.6mA。

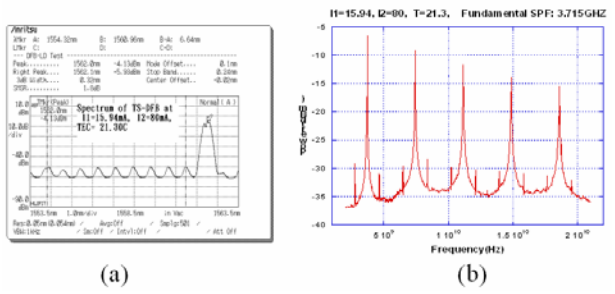

圖 12：單模自震盪機制

（a）光頻譜（b）射頻頻譜

由圖 13 知有三種模態存在。當二段式分佈反饋雷射偏壓在自震盪條件下，我們可以打入一光信號進入二段式分佈反饋雷射。該光信號束攜帶如圖 1 所示由可調適雷射，光電調變器以及信號產生器所產生的二進位制信號。如果輸入信號頻率是接近的自震盪基頻時，則回復之光時脈可從實驗中的即時示波器觀察到。

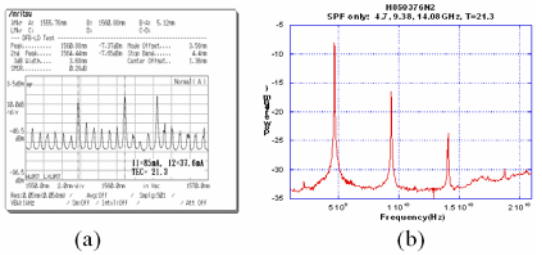

圖 13：多模競爭自震盪機制

（a）光頻譜（b）射頻頻譜

圖 14 顯示單模光時脈回復的實驗結果，當I_1等於 15.94mA 而I_2等於 80mA時，自震盪基頻及輸出波長分別是 3.715GHz和 1562nm。二段式分佈反饋雷射輸出功率約 1.7mW。輸入隨機信號波長和功率分別是 1554.32nm和 8dBm。時脈回復鎖定範圍大約可達±100MHz。時脈回復鎖定範圍經極化最佳化後，在不同的傳輸速度下，最高可達 300MHz。

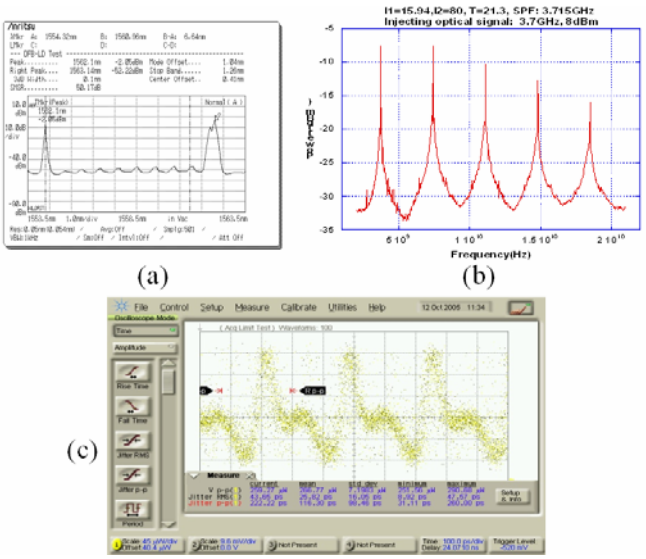

圖 14：注入信號之單模時脈回復機制

（a）光頻譜（b）射頻頻譜（c）即時示波器

圖 15 顯示多模競爭光時鐘回復的射頻頻譜和即時示波器結果。輸入隨機信號波長和功率分別是 1554.32nm 和 10dBm。在這種情況下，利用光學濾波器，我們可以得到每個模態同時進行時鐘回復。但回復效率每個模態仍有不同。

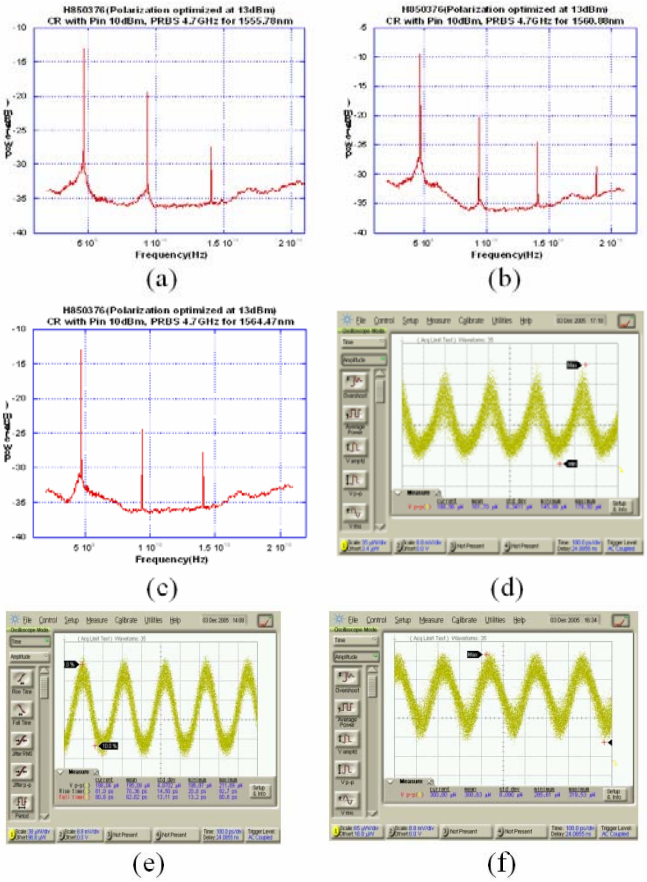

圖 14：注入信號之多模競爭時脈回復機制

a. 注入信號波長 1555.78nm 射頻頻譜

b. 注入信號波長 1560.88nm 射頻頻譜

c. 注入信號波長 1564.44nm 射頻頻譜

d. 注入信號波長 1555.78nm 即時示波器

e. 注入信號波長 1560.88nm 即時示波器

f. 注入信號波長 1564.44nm 即時示波器

三、發表之論文：

1. L.-W. Chung and S.-L. Lee**,** "Multimode-interference-based broad-band demultiplexers with internal photonic crystals," *Optics Express*, vol. 14, no. 11, pp. 4923-4927, 2006.
2. Y.-H. Lee, C.-L. Yang, M.-H. Chuang, H.-W. Tseng, Y.-S. Chou, H.-W. Tsao, and S.-L. Lee, "Analysis and selection of optimum driving current combinations for tunable wavelength laser," *Microwave and Optical Technology Letters*, vol. 48, no. 7, pp. 1417-1423, 2006.
3. C.-L. Yao, S.-L. Lee, I.-F. Jang, W.-J. Ho, "Wavelength selectable lasers with bragg-wavelength detuned sampled-grating reflectors," *J. Lightwave Technol.*, vol. 24, no. 9, pp. 3480-3489, 2006.
4. L.-W. Chung, S.-L. Lee, and Y.-J. Lin, "Principles and application of reduced beat length in MMI couplers," *Optics Express*, vol. 14, no. 19, pp. 8753-8764, 2006.
5. Jer-Shien Chen, Hong-Chang Kung, Hen-Wai Tsao, San-Liang Lee**,** "Performance Enhancement on High-Speed CWDM System by Using Offset-Launch and DFE," The 11th Optoelectronics and Communications Conference (OECC2006), paper 4F1-4, Taiwan, 2006.
6. Shu-Chuan Lin, San-Liang Lee**,** "Simultaneous Improvement on Two 10-Gb/s Channels with Directly Modulated Lasers," The 11th Optoelectronics and Communications Conference (OECC2006), paper 4F1-5, Taiwan, 2006.
7. Jer-Shien Chen, San-Liang Lee, Hong-Chang Kung, Hen-Wai Tsao, Fu-Hsiung Chen**,** "Dynamic Optical Field Analysis for Self-Pulsating Two-Section DFB Lasers," The 11th Optoelectronics and Communications Conference (OECC2006), paper 5E1-5, Taiwan, 2006.
8. San-Liang Lee, Chih-Jen Wang, Pei-Ling Jiang, Hong-Wei Chang, Hong-Chang Kung, Shu-Chuan Lin, Jer-Shien Chen, Hen-Wai Tsao**,** "Two-Section DFB Laser and Applications as Wavelength Converters and Clock Sources," The 11th Optoelectronics and Communications Conference (OECC2006), paper 5F1-1, Taiwan, 2006.
9. Li-Chann Wang, Ming-Feng Hsu, San-Liang Lee**,** "Dynamic Range of Cross-Polarization Modulation Based Multicast Wavelength Converters," The 11th Optoelectronics and Communications Conference (OECC2006), paper 5F1-3, Taiwan, 2006.
10. Yen-Ting Pan, San-Liang Lee, Der-Yuh Lin, Jiun-De Wu**,** "High-Performance InGaAsP Lasers Fabricated by Ion Implantation Induced QW Intermixing," The 11th Optoelectronics and Communications Conference (OECC2006), paper 6C1-2, Taiwan, 2006.
11. Hong-Chang Kung, Jer-Shien Chen, San-Liang Lee, Hen-Wai Tsao**,** "Experimental Investigation of all-optical Clock Recovery in Two-section DFB Lasers," The 11th Optoelectronics and Communications Conference (OECC2006), paper 6E1-3, Taiwan, 2006.
12. Chiu-Lin Yao, Hsiu-Che Wang, Yung-Jr Hung, San-Liang Lee, and Jing-Lyang Jeng, "Novel Tunable Laser Sources with Cascaded DFB Reflectors for Multi-Gas Sensor Applications," The 11th Optoelectronics and Communications Conference (OECC2006), paper 7B1-4, Taiwan, 2006.
13. Lung-Wei Chung, San-Liang Lee**,** "Multimode Interference-based broad-band photonic crystal demultiplexers," The 11th Optoelectronics and Communications Conference (OECC2006), paper 7B2-2, Taiwan, 2006.

四、總結：

本子計畫成果主要包括三部份：直調雷射傳輸特性改善；連續可調波長設計；及高速光電取樣技術。在直調雷射傳輸特性改善方面，使用一個價格低廉且體積小的光學共

振腔式(etalon)光濾波器元件，放置於 10Gbps 直調雷射的輸出端，可以達到抑制頻率啁啾效應進而延伸傳輸距離的目的，從小於 10 公里增加到大於 75 公里，實驗結果可以對 2 個 10Gbps 直調雷射同時進行補償，因此利用 etalon 的週期性頻譜變化的特性，證實可以同時對多個通道的直調雷射傳輸系統達到性能改善的效果。在連續可調雷射設計部分，已完成元件結構分析設計，並完成磊晶工作；在光電取樣技術方面，我們首次展示了二段式分佈反饋雷射自震盪在單模及多模競爭的情形。不論是單模或多模競爭，當二段式分佈反饋雷射偏壓在自震盪，我們得到的實驗結果光時脈下的注入鎖定結果。回復效率在多模態競爭時，每個模態仍有不同。時脈回復鎖定範圍可達 100MHz。由於自震盪機制，二段式分佈反饋雷射可用於作時脈恢復以及波長轉換。在全光網路，它可作為一種多功能元件。

五、成果自評：

本年度所提工作項目大部分皆已順利進行且有很好的成果，並已整理多篇論文，部份已發表於一流期刊與研討會，並有多篇論文投稿或審查中，成果相當豐碩。

行政院國家科學委員會專題研究計畫成果報告

子計劃三：寬頻光都會與接取網路之強健系統與智慧網路之設計(2/3)

計畫編號：NSC-95-2221-E-032-028
執行期限：95 年 8 月 1 日至 96 年 7 月 31 日
主　持　人：李揚漢　　淡江大學電機系

一、　中文摘要

本計劃中，針對同步光分碼多工存取系統架構做討論，為了讓系統模擬更符合實際上現象，考慮了接收端使用者的功率會隨著傳送距離遠近而有大小差異的條件，因此在傳統發射同步型的訊框格式下，當考慮使用者接收之功率不同時，會影響整體的系統效能。針對此問題我們提出了接收同步型的架構，藉由估測出距離相對之時間使每個使用者到達耦合器之時間相同，並將訊框格式加以改善，加強使用者間相互干擾的偵測，提升系統效能。最後，我們利用模擬軟體，建構及模擬六組使用者之同步光分碼多工存取系統在發射同步型和接收同步型架構下的效能比較。

關鍵詞：光分碼多工存取(Optical Code-Division Multiple Access, OCDMA)，平衡編碼(Balanced Encoding)，耦合器(Coupler)。

Abstract

In this project we consider the architecture of a synchronous optical code-division multiplexing system. In order to have the system to mimic the practical situation that the receiving powers at the receiver terminal will have different levels because of various transmission distances. Consequently the system performance will be degraded when we still use at the transmitting side the traditional synchronous frame format and taking into the consideration that every user has different receiving power level. We propose at the receiver a synchronous architecture to encounter this kind of problem by first to estimate the propagation time from each user's distance so that each user's information will arrive at the coupler at the same time, we then modify the frame format and improve the interferences detection among users to improve the system performance. Finally we utilize simulation software to set up a synchronous optical division multiplexing system that consists of six users to compare the system performance under the architectures of synchronous transmitter and synchronous receiver.

二、 研究目的

分碼多工存取(Code-Division Multiple Access, CDMA)最初應用於射頻通訊系統中，但由於光纖通訊系統中之光纖頻寬遠大於電子系統之頻寬，所以從 1980 年開始[1][2]，光分碼多工存取(Optical Code-Division Multiple Access, OCDMA)即為寬頻網路中可行之一種選擇[3]，並且引起廣泛的討論。儘管同步光分碼多工存取網路為了達到同步使得其結構複雜性提高[4]，但它有較大之展頻碼容量，在同時間內容許的使用者數量也較多[5]。

由於發射同步型同步訊框的設計中，在接收端所收到的功率均假設為同等的大小，也就是在彼此各使用者之間所產生的相互干擾量的能量為相同[6-8]，但在實際的傳輸情況下，如圖一所示，假設有六組使用者，各個使用者與耦合器的距離最近的有 1 公里最遠則有 6 公里之差距，由於在距離的遠近影響了耦合器所接收信號的大小，因此在實際的系統中，必須加入接收端所收信號強弱的變異來考量設計出符合實際的架構。針對此一情形本計劃提出接收同步型訊框格式，並設計出較合試的訊框格式，設計來提升 OCDMA 系統的效能。

三、 研究方法

1. 接收同步式 OCDMA

多個使用者連接到星形耦合器所組成的星形網路，如圖一所示，各使用者與耦合器間之距離都不相同，使得各使用者傳送之信號會在不同的時間點到達耦合器，造成在多重使用者干擾(MUI)估算困難，所以提出接收同步式架構，主要藉由傳送前先量測出各使用者至耦合器之間的距離，並將使用者所傳送之信號利用延遲時間之方式使信號同時到達耦合器，以加強多重使用者干擾之估算。

(1). 系統描述

由圖一所示，各個使用者與耦合器之間的距離不盡相同，所以首先量測出每個使用者傳送信號至耦合器所耗費的時間，例如：使用者 1 傳送資料耗費的時間為 Tt1 、使用者 6 傳送信號耗費的時間為 Tt6 ；接著將使用者 1 端加入延遲時間 Td1 之方式並以此類推，讓每個使用者的信號經由延遲後再開始傳輸，使各個使用者的信號同時到達耦合器，如圖二所示。

我們利用使用者 1 與使用者 6 來說明；如式子 (1) 所示， n 代表光纖之群折射率為 1.4795 (雷射光波長為 1310 nm 時的最佳量測狀況)， c 代表光速 3×10^8 m /sec，計算可得介質中群速度 V；如式子 (2) 所示，D 代表使用者與耦合器之距離，計算可得使用者傳送到耦合器之間的時間。經過計算後可知，使用者 6 需要 29.58 μs 信號才能到達耦合器，使用者 1 需要 4.93 μs 信號才能到達，為了讓使用者的信號能同時到達耦合器，我們將兩者時間差距算出後，將使用者 1 經過延遲 24.65 μs (29.58 μs - 4.93 μs = 24.65 μs) 後再送出訊號，則可讓兩者之信號同時到達耦合器。在傳送至接收的能量損耗的方面，我們經由模擬得到 1 Km 大約損耗 0.2 dB ，距離 6 Km 損耗約為 1.2 dB。

$$V = \frac{c}{n} \qquad (1)$$

$$\text{傳送時間} = \frac{D}{V} \qquad (2)$$

(2). 訊框格式

由於在光分碼多工存取系統中，每個使用者傳輸至耦合器的距離不同使得接收到信號的時間也不同，而為了達到多工存取的機制，必須定義出每個使用者的訊框格式，我們將使用發射同步型系統架構下的訊框格式和我們提出的接收同步型架構下的訊框格式互相比

較，找出適當的訊框來提升系統效能。

比較接收同步型訊框與發射同步型訊框之差異，主要在於前者已經先依據各使用者和耦合器的距離調整過時間差，使每個使用者傳送的信號同時到達耦合器，如圖四所示。我們藉由此特性，在前置信號區放入長度為 W0 信號 0 和長度為 W1 信號 1，用來估測使用者之間相互的干擾量，且可有效的利用信號的多寡來增加估測使用者相互干擾量的精準度。

2. 模擬結果與分析

參照前一節所提出的發射同步型與接收同步型兩種型式，建構出了六組使用者做為系統模擬之依據。首先對發射同步型與接收同步型訊框的門檻電流界定方式做詳細說明，接著再按照接收功率大小不同之訊號對系統傳輸的誤碼率比較。

(1).系統模擬方塊圖

圖 五　為傳送端的模擬架構圖。在雷射端供給 60 mA 來驅動單模雷射，此雷射的輸出波段為 1552.52 nm，接著我們採用振幅調變做為外部調變之方式，在信號輸入方面，則是將各個使用者傳送的訊框載入，利用光延遲線將信號延遲，產生出各使用者的展頻碼，最後將信號結合做為輸出。

圖 六 為接收端的模擬架構圖，此接收端主要是先將光經過延遲線產生光相關函數的方式來進行解碼，接著信號經由 APD 檢光器將光信號轉換為電信號，藉由信號取樣找出適當之門檻電流，最後則可依照門檻電流的判斷解出原始的信號。

(2). 門檻電流

根據兩種訊框格式，分別敘述其門檻電流定義。發射同步型訊框格式如圖 三 所示，利用 t_E 到 t_D 時間裡的 10 個信號 0 來做門檻電流的估測，即是在 $W0 = 10$ 的條件下進行分析。

接收同步型訊框格式如圖 四 所示，與發射同步訊框相同都在 t_E 到 t_D 時間裡傳送 10 個信號 0 ，除此之外 t_E 到 t_S 之間又傳送 10 個信號 1 來做門檻電流的估測，即是在 $W0 = 10$、$W1 = 10$ 的條件下進行分析。

四、結果與討論

本節針對發射同步型系統與接收同步型系統架構在不同訊框下做效能分析。藉由圖一各個使用者傳送至耦合器距離不同，我們選擇使用者 1 (距離耦合器最近) 和使用者 6 (距離耦合器最遠) 來做接收端功率大小對誤碼率之比較。在發射同步型訊框 $W0 = 10$ 和接收同步型訊框 $W0 = 10$、$W1 = 10$ 來比較效能之差異。圖 七 則為模擬結果，從結果可明顯的看出，接收同步型訊框下的系統效能不論是在使用者距離遠近下都較先前發射同步型訊框的誤碼率低。

藉由模擬驗證我們提出的接收同步型 OCDMA 系統的設計以及在訊框格式的制定，當接收端功率為 2.8 μW 時，使用者 1 和使用者 6 在接收同步系統與發射同步系統中的錯誤率約略都在 10^{-2} 到 10^{-4} 之間，隨著接收到的信號功率上升，各系統之錯誤率快速下降。當接收端功率到達 3.6 μW 時，使用者 1 在接收同步系統的錯誤率小於 10^{-12}，而在發射同步系統的錯誤率約為 10^{-6}；使用者六在接收同步系統的錯誤率約為 10^{-8}，而在發射同步系統的錯誤率約為 10^{-5}，從模擬的結果發現接收同步系統的錯誤率小於發射同步系統，證明文中提出的接收同步系統具有較好之性能。未來將分析接收同步系統前置信號與門檻電流之關係，探討訊框中 $W0 = 10$ 與 $W1 = 10$ 數目多寡與訂定門檻電流精確性，找出適當前置信號長度，以降低系統錯誤率及提升系統效能。

五、計畫自評

(a) 接收同步型光分碼多工存取系統使用平衡編碼之效能提升與分析(已完成之具體成果 1)

在本計畫中，第二年進行的實現接收同步型光分碼多工存取系統使用平衡編碼之效能提升與分析。在下一個年度會針對此架構進行更詳細的分析與模擬並提出簡單的 MAC 提升系統的效能。

(b) DBR 雷射電流最加組合之分析(已完成之具體成果 2)

本計畫之第一年的研究重點是加強波長穩定的設計，所以我們又提出在不同的 Channel 之間跳動時，搭配不同的組合能找出使雷射輸出波長最穩定的解，在第二年，我們針對第一年的研究作更深入的分析包括同一個 Channel 不同電流組合的跳動分析，找出更好的電流組合。第三年會針對這些電流組合加入系統的模擬與分析。

六、 已完成之具體成果：

1. Rong-Hou Wu and **Yang-Han Lee**, "Specification Study of Optical Transmission System for Commercial Airborne on Board Entertainment Applications," *Tamkang Journal of Science and Engineering* . (Submitted on October 02, 2006) **(EI, Engineering)**
2. **Yang-Han Lee,** Yih-Guang Jan, Shian-Wei Tzeng, Ming-Hsueh Chuang Shiann-Tsong Sheu, Yue-Ru Chuang, and Jei-Jung Shen, "The Hardware Design for a Parallel-Processed Genetic Algorithm Accelerator for Packet Scheduling Problems," *Tamkang Journal of Science and Engineering* . (Revised on December 14, 2006) **(EI, Engineering)**
3. **Yang-Han Lee**, Fun Ye, Yun-Hsih Chou, Ming-Chieh Tsou, Yih-Guang Jan, Jheng-Yao Lin, Hsien-Wei Tseng and Ming-Hsueh Chuang, "The Design of a Linear Digital Pixel Sensors with Wide Dynamic Range and Logarithmic Response," *IEEE Sensors Journal for possible publication, ISJPP.* (Submitted on October 19, 2006).
4. 趙亮琳, **李揚漢,** 溫敏如, 楊淳良, 莊明學, 彭瓊萱, 黃聖博, 董先育, "同步光分碼多工存取系統使用平衡編碼之效能提升與分析" 台灣光電科技研討會暨國科會光電學門研究成果發表會(Optical and Photonics, Taiwan 2006).
5. 楊淳良, 趙亮琳, 周永山, **李揚漢**, 彭瓊萱, 詹益光, 莊明學, 溫敏如, 曾憲威, 董先育, 黃聖博, "DBR雷射波長切換最佳化之驅動電流組合控制方法," *2006 全國電信研討會 - 2006 National Symposium on Telecommunications*, December 1-2, 2006.
6. Rong-Hou Wu, **Yang-Han Lee**, Shiann-Tsong Sheu, Hsien-Wei Tseng, Ming-Hsueh Chuang, and Yung-Kuang Wang, "Application of Hardware Architecture of Genetic Algorithm for Optimal Packet Scheduling," *11th International Conference on Fuzzy Theory and Technology (FTT 2006) in conjunction with 9th Joint Conference on Information Sciences (JCIS 2006)*, Kaohsiung, Taiwan, R.O.C., October 8-11, 2006.

七、 參考文獻

[1] P. R. Prucnal, M. A. Santoro, and T. R. Fan,"Spread spectrum fiber-optic local area network using optical processing," *J. Lightwave Technol.*, vol. LT-4, pp. 547−554, May 1986.

[2] J. A. Salehi, "Code division multiple-access techniques in optical fiber networks－Part I:

Fundamental principles," *IEEE Trans. Commun.*, vol. 37, pp. 824−833, Aug. 1989.

[3] L.-L. Jau and Y.-H. Lee, "Optical code-division multiplexing systems using Manchester Coded Walsh Codes," *IEE Proc.-Optoelectron.*, vol. 151, pp. 81–86, Apr. 2004.

[4] C.-S. Weng and J. Wu, "Perfect difference codes for synchronous fiber-optic CDMA communication systems, " *J. Lightwave Technol.*, vol.19, pp. 186−194, Feb. 2001.

[5] P. R. Prucnal, M. A. Santoro, and S. K. Sehgal,"Ultrafast all-optical synchronous multiple access fiber networks," *IEEE J. Select. Areas Commun.*, vol. SAC-4, pp. 1484−1492, Dec. 1986.

[6]. L.-L. Jau and Y.-H. Lee, "A synchronous optical CDMA system with constant multi-user interference," *Proceedings of the 2004 National Symposium on Telecommunications (NST 2004)*, Keelung, Taiwan, pp.120-125, Dec. 3-4, 2004.

[7]. L.-L. Jau and Y.-H. Lee, "Optical code-division multiplexing systems using common zero codes," *Microwave and Optical Techn. Lett.*, vol. 39-2, pp. 165–167, Oct. 2003.

[8]. L.-L. Jau and Y.-H. Lee, "Synchronous optical-CDMA systems using tunable hard limiters," *J. Optical Commun.* vol. 24, pp. 217–222, Dec. 2003.

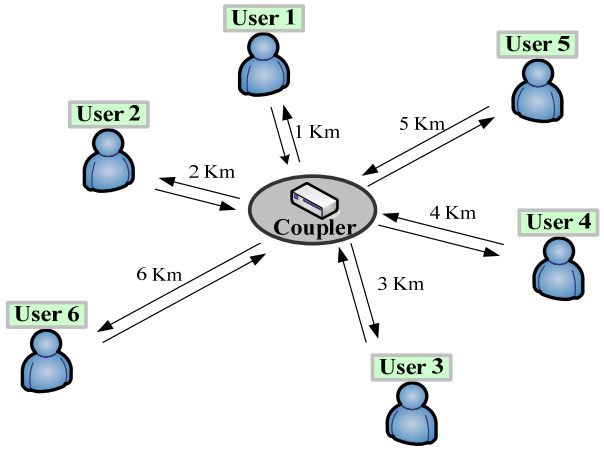

圖一 使用者連接到星形耦合器所組成之星狀網路

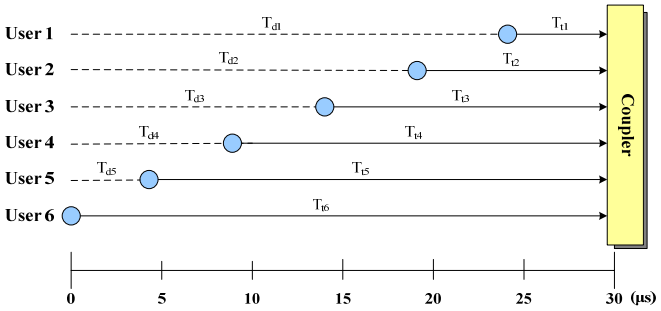

圖二各使用者傳送至耦合器時間之示意圖

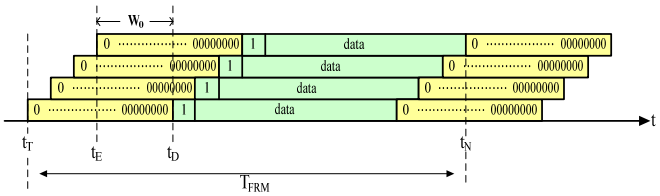

圖 三 發射同步型訊框

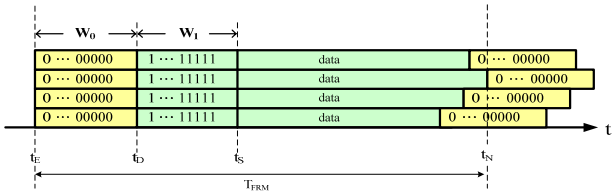

圖四 接收同步型訊框

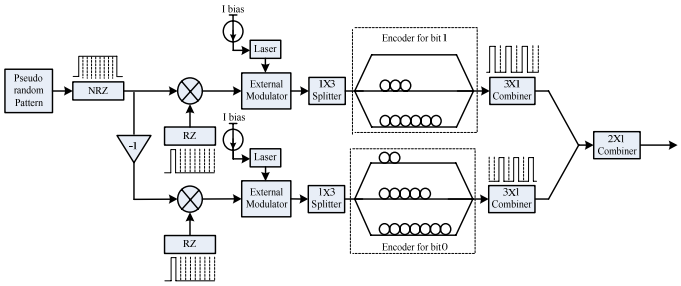

圖五 OCDMA 傳送端模擬架構圖

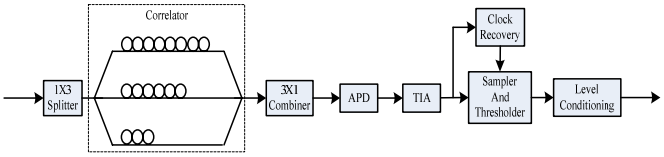

圖 六 OCDMA 接收端模擬架構圖

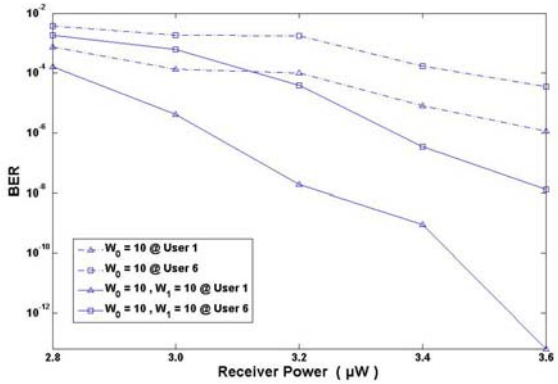

圖 七 BER vs. Powe

光網路分碼多工接收機前級及信號品質監測電路之研製（子計畫四）

"Design and Implementation of Circuits for CDMA PON Receiver and Metro/Access Network Signal Quality Monitoring"

計畫編號：NSC95-2213-E-002-049
執行期間：95 年 08 月 01 日至 96 年 07 月 31 日

主持人：曹恆偉 教授（國立台灣大學）
參與人員：鐘國晉、謝明志、王勝賢、黃乾宗、卓均勇、吳嘉訓（國立台灣大學）

摘要

近幾年為了滿足對頻寬不斷增加的需求，骨幹網路和區域網路都有很大進展，介於兩者之間的擷取網路，其速度的需求也隨著提升，就研究顯示，被動式光網路是寬頻擷取網路的最好選擇，可以作為連接這兩者之間的中介。

光分碼多工乙太被動光網路是乙太被動光網路[1]的一個改良版本，與分時多工相比，能對頻寬作更有效的利用，本報告討論光分碼多工乙太被動光網路接收機前端電路的設計及實作，操作在 1.25Gb/s的速度之下，利用 0.35-μm CMOS 製程，將前端類比電路和類比相關器整合在單一晶片上，前端電路包含轉阻放大器、可變增益放大器和後端放大器，這前端電路具備有高度的動態範圍來保持接收訊號的線性度及工作完整性，模擬結果顯示，整個前段電路的增益有 78.8dB，頻寬約為 1.27GHz，在 3.3 伏特的工作電壓下，總消耗功率為 452 毫瓦，全部的晶片面積佔了 1.0 × 1.4 mm^2。

為了有效對光通信系統進行誤碼率的監控，光域取樣是相當重要的研究議題。本報告第二部份討論非同步取樣在 10Gb/s 非歸零碼傳輸系統中的應用，並對信號原時脈少許之頻率差異對取樣均勻度的影響作探討。此外，為了增加取樣過程之均勻度，我們將取樣時脈進行頻率調變。經模擬後發現，此法能在頻率差量比±50ppm 內提供可靠的誤碼率監控資訊。

關鍵字 – 光纖通訊，光接收機，被動光網路，乙太被動光網路，光分碼多工，類比相關器，非同步取樣，頻率差量比，頻率調變，頻率展開比，直方圖。

Abstract

Recently, the backbone network and the Local-Area Network (LAN) have a great advance up to tens of gigabit per second. However, there is still a gap between backbone and LAN. The progress in access network doesn't keep with the great advance of backbone and LAN. This is a well-known "the First Mile" problem. The passive optical network (PON) has been investigated as the best candidate for the access network, which can bridge this gap.

An Optical CDMA-based EPON is a modified version of EPON, which can utilize the bandwidth better than EPON. In this work, the front end circuit of OLT receiver for Optical CDMA-based EPON system is designed and implemented. The receiver operates at the rate of 1.25Gb/s, and integrates the analog front end and the analog correlateor on the same chip using the 0.35-μm CMOS process. The front end including transimpedance amplifier (TIA), variable gain amplifier (VGA) and post amplifier has a wide dynamic range to preserve the linearity of the received signal. The simulated results show the front end has a transimpedance gain of 78.7dB over the bandwidth of 1.27GHz. Under the supply voltage of 3.3V, the whole chip dissipates a power of 452mW. And the whole chip occupies an area of 1.0 × 1.4 $mm^{2.}$

In order to monitor the bit error rate (BER) of optical communication systems efficiently, optical sampling is an important method. In this report, we will discuss the application of asynchronous sampling in 10 Gb/s nonreturn-to-zero (NRZ)

transmission systems, and the effect of sampling uniformity in signal clock with a small amount of frequency deviation. Moreover, to increase the sampling uniformity, we apply frequency modulation to the sampling pulses. According to simulation results, this method can provide reliable information about BER with frequency deviation ratio within ±50ppm.

Index Terms – Optical communication, optical receivers, passive optical network (PON), Ethernet passive optical network (EPON), Optical CDMA, analog correlator, asynchronous sampling, frequency deviation ratio, frequency modulation, spread ratio, histogram.

【Part A】

前言

目前都會網路對於頻寬的需求與日俱增，提供安全、穩定、高速的寬頻擷取服務是都會網路的一大課題，被動式乙太光網路是制定於 IEEE 802.3ah 的一種新的網路架構，被動式乙太光網路有著低成本、易建置的特性，能將光纖普及到用戶端，提供寬頻擷取，被認定是「最後一哩」最佳的解決方案，本研究將找出被動式乙太光網路 OLT 頭端電路最適合的硬體實現方法。

研究目的

目前 IEEE 所提出的被動式乙太光網路採取分時多工機制來達成上行傳送，但分時多工有頻寬使用效率不佳的缺點，因此本研究根據完美相差碼所架構的分碼多工機制來達成上行傳送，用成本低廉的 TSMC 0.35μm CMOS 製程來實現分碼多工接收機，將前端電路所包含的轉阻放大器、可變增益放大器、後級放大器以及分碼多工相關器整合在單一晶片上。

研究方法

在此光網路分碼多工接收機前端電路的設計上有以下兩大考量：

1.) 線性度以及動態範圍

在 PON 的系統架構中，每一個 OLT 約需服務 32 個 ONU[2]，而系統中處於傳送狀態的 ONU 數目並不固定，因此 OLT 所收到的訊號大小並不固定，在此情況之下，前端電路的訊號路徑部份必須工作在線性區域，需要線性度佳以及高動態範圍的特性。

2.) 分碼多工相關器

光域分碼多工系統之工作原理和無線分碼多工系統類似，主要差別在於展頻碼特性的不同，電域展頻碼有完全正交的特性，而光域的展頻碼最多只能具有準正交的特性[3]，因此在設計上必須加以考慮，一般來說分碼多工相關器可以用數位或類比的方法來實現，在高速電路上，用數位的方法來實現相關器必須使用高速類比數位轉換器，先將類比訊號轉成數位訊號，在數位的領域來實現相關器，倘若以類比的方式來實現，則可以免去高速類比數位轉換器的使用，大大地減低接收機的成本及功率消耗，所以我們將採取類比的方式來實現相關器的設計。

圖一是光網路分碼多工接收機的方塊圖，光纖訊號由光電二極體轉成電流訊號，經過前級放大器轉成電壓訊號，但此級輸出訊號往往過小，所以會接著由後級放大器放大，再輸入至分碼多工相關器，解調出訊號之後，再由類比數位轉換器將訊號取樣送入數位晶片作處理。

本前端電路包含轉阻放大器(TIA)、可變增益放大器(VGA)、後級放大器、和類比相關器(Analog Correlator)，利用 TSMC 0.35μm CMOS 製程將其整合在一個單晶片上，完整架構如圖二所示：

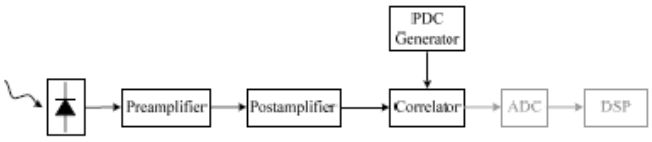

圖一、光網路分碼多工接收機（OLT 端）

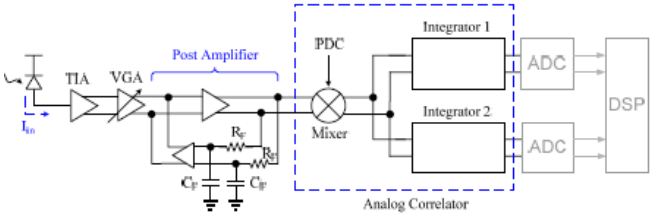

圖二、光網路分碼多工接收機前端電路架構圖

接下來，將介紹光網路分碼多工接收機前端電路各個部份的設計。

A. 轉阻放大器

為了達到比較高的頻寬，我們採用共閘極形式的轉阻放大器(TIA)，除此之外我們還採用調節式堆疊(RGC, Regulated Cascade)的技術[4]，如圖三所示，MB、MT、M2 形成調節式堆疊組態，可以大大減低輸入端的等效阻抗，讓轉阻放大器有更高的操作頻寬。

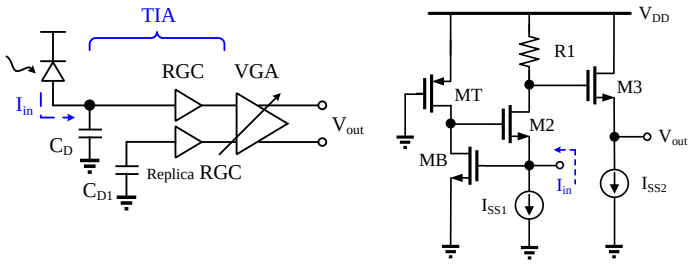

(a) (b)

圖三、轉阻放大器 (a)架構圖 (b)電路圖

B. 可變增益放大器

這是一個折疊式的 Gilbert 放大器[5]，利用控制迴路 M5、M6 來控制通過 M1、M2 以及 M3、M4 的電流，產生不同的轉導增益，相減

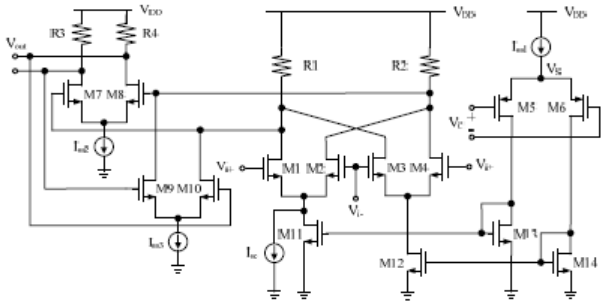

圖四、可變增益放大器電路圖

之後，得到可調式放大器的輸出訊號，此放大器的線性範圍達到輸入±276mV，增益調控的範圍為 18dB 到-34dB，約有 52dB 的動態範圍，為了能操作在高頻的範圍，如圖四所示，我們利用主動回授的方法[6]來提高操作頻寬。

C. 後級放大器

如圖五，後級放大器包含了直流偏差修正電路，在放大器中我們一樣使用主動回授機制 [6]來提高工作頻寬，直流偏差修正電路可以修正因為非理想效應所產生的直流偏差，而且也可以增加輸出訊號的振幅範圍，迴路裡的低通濾波器中我們採用 PMOS 來實現電阻，NMOS 來實現電容，如此一來，可以將被動元件整合在晶片上而不會佔太大的面積。

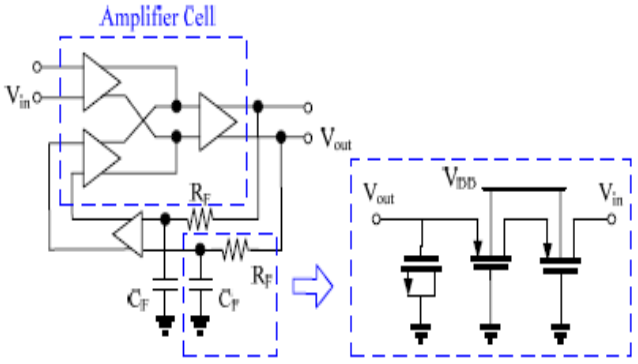

(a)

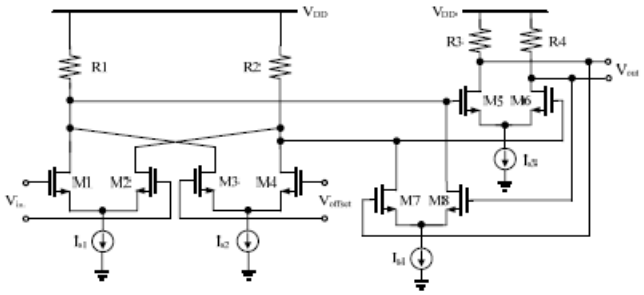

圖五、後級放大器 (a)架構圖 (b)電路圖

D. 類比相關器

相關器(Correlator)包含相乘和累積的運算，相乘部份，我們提出一個改良式Gilbert放大器的架構，當完美相差碼是 ”1” 的時候，可產生放大訊號，在 ”0” 的時候，不產生放大訊號，M_{s1}和M_{s2}能增加此相關器的線性度。透過積分器，可以將此輸出訊號作累加，此類比相關器輸出訊號頻寬約為 22MHz，如圖六所示，我們採用兩個時間交叉式(time interleaved)的積分器，讓一個處於被取樣階段時，另一個仍能正常地處理相關器產生的訊號。

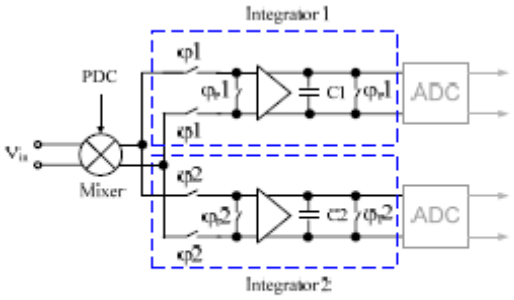

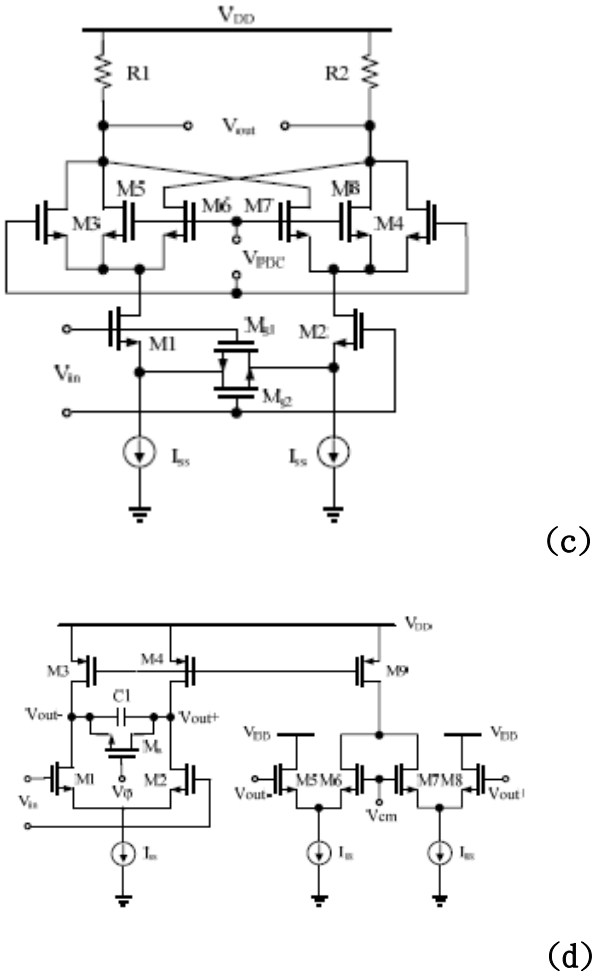

圖六、類比相關器之 (a)架構圖和 (b)控制訊號圖，類比相關器內部中的 (c)相關器和 (d)積分器之電路圖

結果與討論

A. 模擬結果

模擬結果主要針對兩部分，類比前端電路和類比相關器，類比前端電路由轉阻放大器、可變增益放大器和後級放大器組成，我們輸入完美相差碼來觀測前端電路輸出的眼圖，類比相關器部分則觀測在採用和輸入信號相對應的完美相差碼作相關運算之後是否能產生極大值，若輸入非相對應的完美相差碼時應產生極小值。

圖七是類比前端電路的頻率響應圖，可提供78.7dB 的增益，圖八是類比前端電路輸出眼圖，輸入信號為完美相差碼所得輸出的眼圖。圖九是類比相關器的暫態分析圖，由圖可見當

切換開關φ1 打開時，第一個積分器會正常工作，另一個則處於被取樣狀態之後便重置(reset)，Vinte1(pre)和 Vinte2(pre)是 Pre-simulation 的結果 Vinte1(post)和 Vinte2(post)是 Post-simulation 的結果，可看見當類比相關器輸入和輸入訊號相對應的完美相差碼時，類比相關器都能產生極大值，由此可驗證整個晶片的工作正確性，圖十則呈現了最後晶片的微影圖。

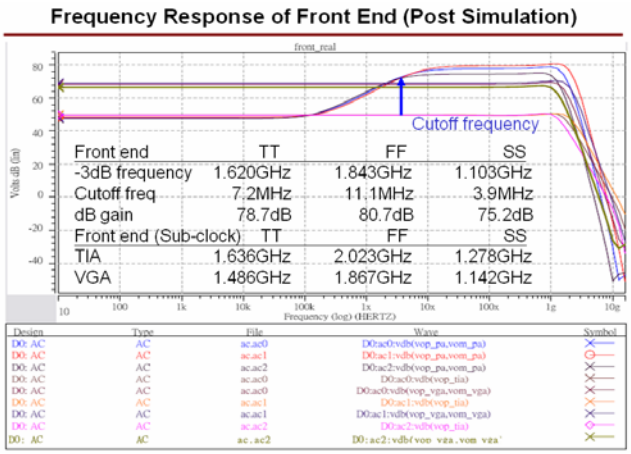

圖七、類比前端電路頻率響應圖(Post Simulation)

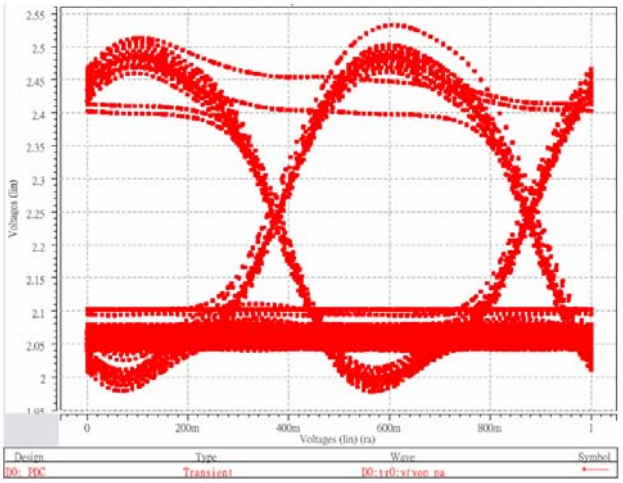

圖八、類比前端電路輸出眼圖(Post Simulation)

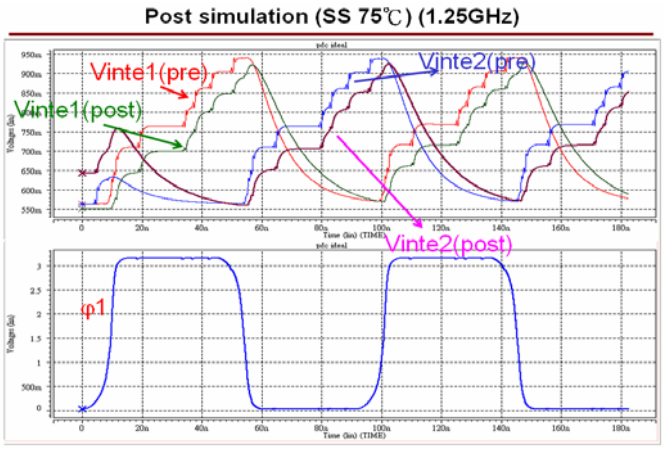

圖九、類比相關器暫態分析圖 (SS 75℃ Post Simulation)

B. 測試結果

在類比前端電路裡各個部份(轉阻放大器、可變增益放大器和後級放大器)都包含一個開汲極(Open Drain)的電晶體，讓在晶片測試時能夠利用 BiasT 接上示波器來觀測輸出眼圖，以便判斷各個部份的正確性，類比相關器部分，可向接收機輸入完美相差碼，利用相對應的完美相差碼和其作相關運算(Correlation)，將輸出端接上示波器可以觀測是否有極大值的出現，若能出現極大值則可代表系統操作是正確的。

以下兩圖是（十一、十二）測試方塊圖，圖中的完美相差碼和開關控制訊號分別由兩台圖樣產生器(Pattern Generator)來產生，並利用任意波形產生器 Tektronix AWG710B 來產生完美相差碼及多階層訊號，而兩台圖樣產生器也透過 Tektronix AWG710B 的驅動來達成同步。

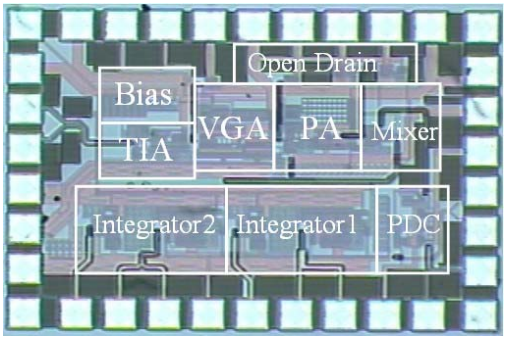

圖十、晶片佈局圖

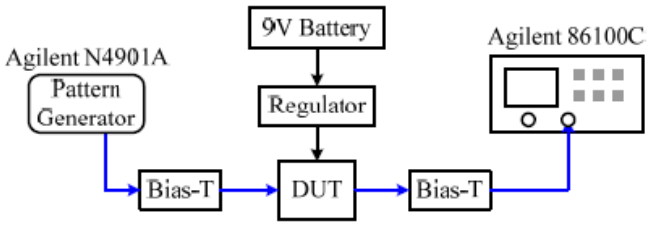

圖十一、在類比前端電路測試方塊圖

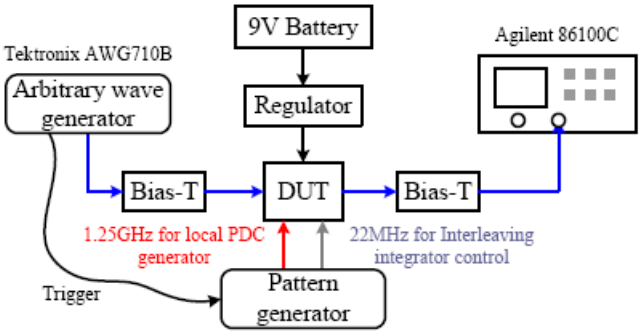

圖十二、類比相關器測試方塊圖

轉阻放大器經由測試之後，可以正確地工作在 1.25Gb/s 的速度之下，下圖分別是轉阻放大器在輸入訊號為 622.5Mb/s 和 1.25Gb/s 的輸出眼圖。

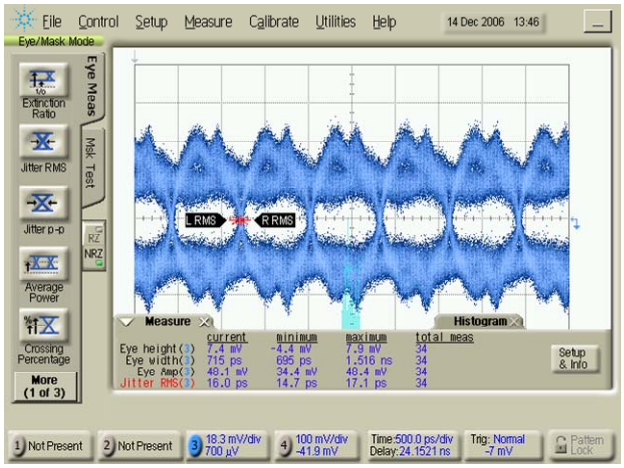

(a)

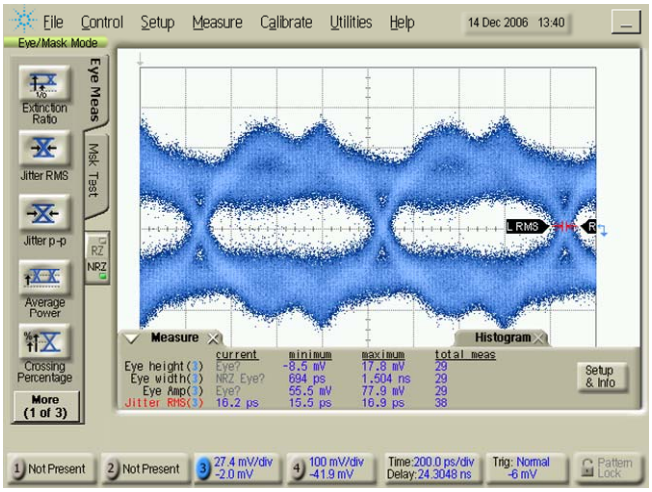

(b)

圖十三、轉阻放大器在輸入訊號 (a)622.5Mb/s 和 (b) 1.25Gb/s 為之輸出眼圖

C. 規格表

表一、規格表

電源供應電壓	3.3V
操作頻率	1.25GHz
消耗功率	452mW
轉阻放大器增益值	50dBΩ
可變增益放大器增益範圍	18dB ~ -34dB
類比前端電路總增益	78.7dB
類比相關器輸出信號頻率	22MHz

D. 結論

本顆晶片整合了乙太被動光網路光分碼多工接收機於單一個晶片，提供了一個低成本的可行方案，這使得乙太被動光網路在擷取網路應用上有很大的幫助，目前而言，該晶片經由測試之後，轉阻放大器可以正確地工作在 1.25G/s 的速度

【Part B】

前言：

光性能監控(Optical performance monitoring, OPM)在高速光纖網路是一門重要的課題，包含光信噪比(Optical signal-to-noise ratio, OSNR)監控、色散監控以及誤碼率監控。通常誤碼率最能真實反應信號品質劣化的情形，因此其相關監控技術亦越來越受到重視。然而直接偵測系統誤碼率相當費時，通常在即時監控的應用中，利用 Q 值(Q_t)以估測誤碼率是普遍的做法。但是以上方法需要以時脈回復裝置維持取樣過程之同步，且一般時脈回復裝置和資料的位元速率相關，在應用上限制頗多。為了簡化監控架構，Shake 等人利用非同步取樣的方式進行 Q 值量測[7]，此時所求出之 Q 值（Q_{avg}）雖然不全等於Q_t，兩者仍存在高度的相關性。由於該架構並不需要時脈回復裝置，使得資料的位元速率不需侷限在特定值而增加了其可用性。

光域取樣（Optical sampling）一般可分為兩大類：全光取樣（All-optical sampling）[8]以及電光取樣（Electro-optical sampling）[9]。前者以光脈波藉由光學元件之非線性效應產生取樣，後者則利用電脈波對光電調制器之電光效應達成。由於一般的光電調制器例如致電-吸光式調制器（Electro-absorption modulator）具有體積小的優點，且電脈波產生相對光脈波容易，因此電光取樣在高速光域取樣的應用相當廣泛。

研究目的：

由於Q_{avg}與取樣值所構成的直方圖（Histogram）有密切的關連，若取樣點數過少會使直方圖無法提供可靠的資訊，過多取樣點數則需要龐大的記憶體容量。因此本計劃將對影響取樣點數的參數進行討論，並採用經頻率調變後的脈波進行取樣，藉以提升取樣過程的均勻性。經電腦模擬，發現此法不僅能改善Q_{avg}的收斂性，同時在系統位元速率在±50ppm 的差異比率之下仍具可靠性，達成位元速率透明性（Bit-rate transparency）的理想。

研究方法：

圖十四是 10-Gb/s 不規零（NRZ）碼傳輸系統的Q_{avg}量測架構。光源採用 1550nm 的外調雷射，驅動信號為週期$2^{23}-1$的 10Gb/s 不歸零碼。經調制後的光信號通過 25km 的單模光纖，由其後的可調式光衰減器以及光放大器改變系統的光信噪比。光放大器的輸出端連接費比-裴洛光濾波器（Fabry-Perot etalon），藉以濾除通帶以外的噪音。為了進行在線監控（in-line monitoring），僅有 5%的光信號功率會被耦合到光電調制器進行取樣。在此使用 25ps 寬且週期為 625MHz 的電取樣脈波，使光電調制器具有光域“及”閘（Optical AND gate）的作用。由於經耦合後光信號相當微弱，我們以有高靈敏度的檢光元件如瀉光二極體（APD）做光電轉換之用。積分器負責將經過轉換的電信號，在取樣脈波的週期進行積分運算，再經過統計分析即可得到取樣分佈的直方圖。

圖十五為典型非同步取樣之分佈之

直方圖。欲計算Q_{avg}可採用與Q_t相同的計算公式；然而與同步取樣不同的是，代表"0"的區域（Space）與代表"1"的區域（Mark）並沒有很明確的分野，因此無法直接判斷"0"與"1"各自的標準差。現行的作法多為刪除直方圖中間區域，再利用高斯曲線擬合的方式分別估計剩餘部份各自的標準差[10][11]。

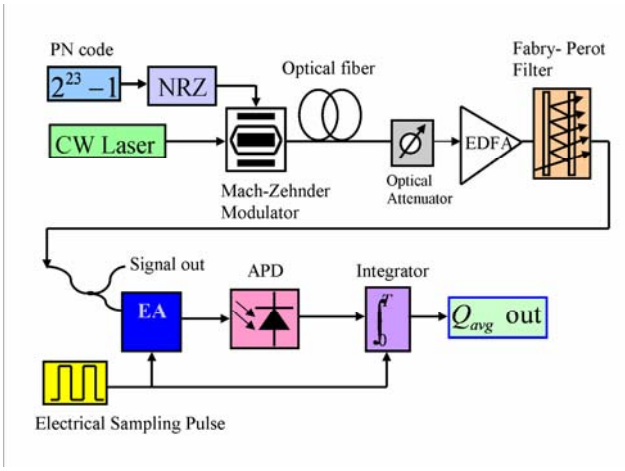

圖十四、Q_{avg}的量測架構示意圖。

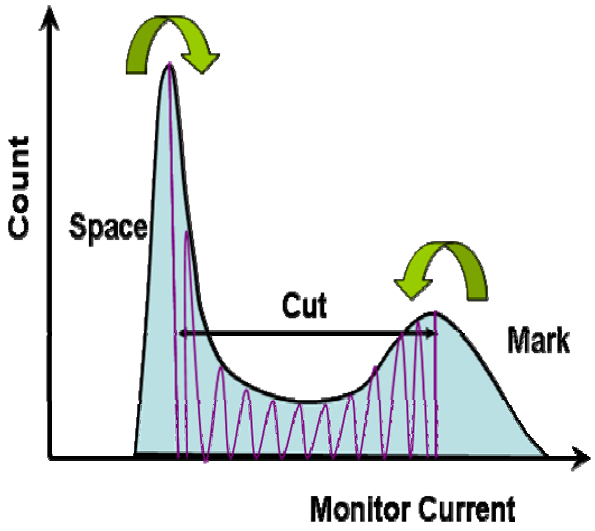

圖十五、典型非同步取樣之分佈直方圖。

模擬結果討論：

在實際系統監控中，若沒有時脈回復裝置則無法準確知道信號源的時脈，因此只能估計其範圍約在±50ppm之內。然而由前法所得到之Q_{avg}，在相同光信噪比之下，與信號源的時脈及取樣點數目（N_s）有關。若信號源時脈為f_s且取樣時脈為f_c，定義一個參數為頻率差量比$R \triangleq \frac{f_s - nf_c}{f_s}$（其中$n$為最接近$\frac{f_s}{f_c}$之整數）。在$Q_t \approx 7.28$的情形之下，由圖十六可以發現在 R=0 的所得到的Q_{avg}較其餘為低且振盪幅度也較大。其原因是由於取樣點均集中某個區域，且取樣脈波寬度並非夠窄使得直方圖產生多個峰值[12]（圖十七），使得經曲線擬合後算出的Q_{avg}較一般為低。若$|R| \leqq 10$ppm，在取樣點較少的情形下也會發生Q_{avg}有顯著起伏的情形；然而取樣點增加，取樣區域也隨之移動使得整個過程更加均勻，Q_{avg}逐漸收斂至到穩定值。若$|R|$持續增加，取樣區域移動更頻繁使直方圖更趨於兩個峰值的高斯分布，Q_{avg}收斂的速度也越快。

然而在系統應用中，R 並非已知。若希望Q_{avg}在$|R| \leqq 50$ppm 的範圍都能有良好的收斂性，若要藉由控制 R 來達成並不可行。本計劃利用將取樣時脈進行三角波頻率調變，其調變頻率為原取樣時脈的$1/2^{12}$倍，頻率展開比

（spread ratio，δ）設為 0.39%、0.78%、1.56%及 2.34%來觀察其對取樣之影響。

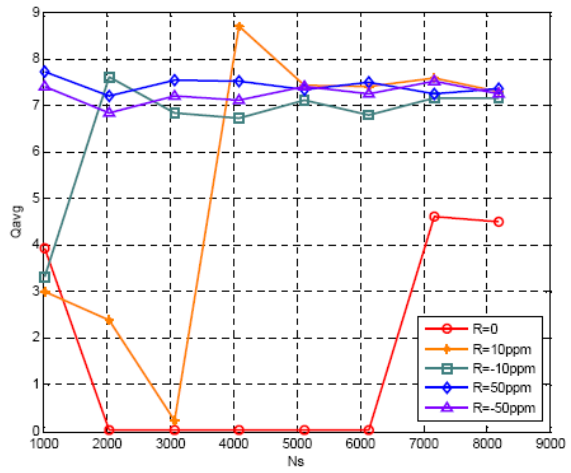

圖十六、在不同 R 值之下，Q_{avg} 與 N_s 之關係圖。（$Q_t \approx 7.28$）

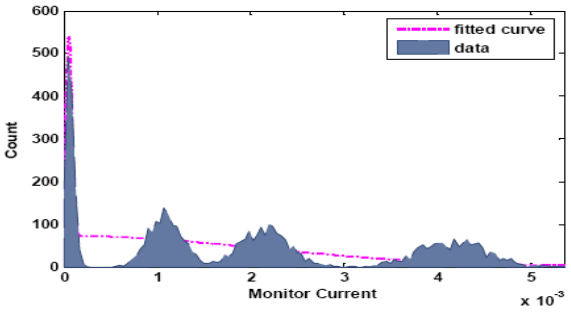

圖十七、非同步取樣之直方圖。（$Q_t \approx 7.28$ N_s=5120 以及 R=0）

由圖十八可發現，在 R=0 且 $Q_t \approx 7.28$ 的操作條件下，經頻率調變後的取樣時脈所求得之 Q_{avg}，其收斂性明顯優於未經調變的取樣時脈。這是由於前者取樣區域不再侷限在特定範圍，使得取樣過程更均勻。我們可更進一步發現在 N_s=8192 時，不論任何 δ 值 Q_{avg} 都會收斂並聚集至同一點。因此再觀察在 N_s=8192 之下，各種 δ 值其 Q_t 與 Q_{avg} 的對應關係（圖十九）。由圖可知，除了 $\delta=0$ 的情形之外，其餘 δ 所求出的 Q_t 與 Q_{avg} 都呈現出高度的線性關係，且該線性分布與 δ 趨近於獨立。此外，圖二十說明了該線性分布與 R 的關連。當 $|R|$=50ppm 時，由於取樣過程夠均勻，無論取樣時脈是否經過頻率調變都不會影響其線性關係，同時也會與 R=0 及 δ=1.56%所對應的直線很接近。由以上可得知，圖十四的架構在 N_s=8192 的狀況下，只要取樣時脈經過頻率調變，且 δ 介於 0.39%與 2.34%之間，所得之 Q_{avg} 在 $|R| \leqq$50ppm 都能與 Q_t 有固定的線性關係。

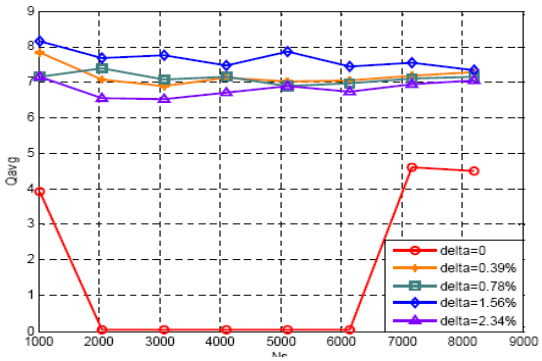

圖十八、在不同 δ 值之下，Q_{avg} 與 N_s 之關係圖。（$Q_t \approx 7.28$）

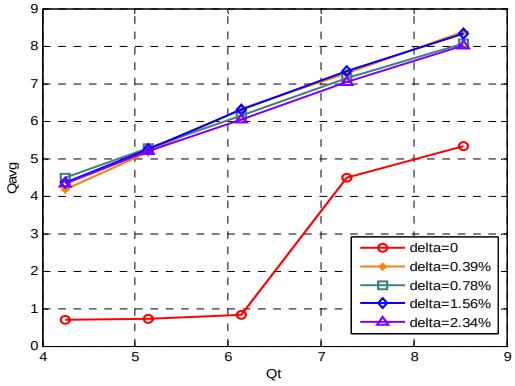

圖十九、在不同 δ 值之下，Q_{avg} 與 Q_t 之關係圖。（N_s=8192）

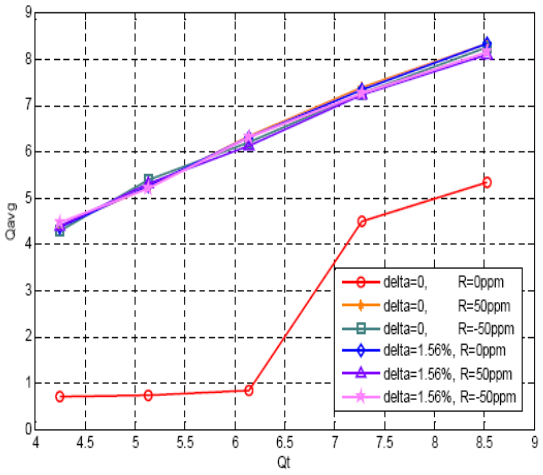

圖二十、在δ=0 與 1.56%，對應不同 R 值之 Q_{avg} 與 Q_t 關係圖。(N_s=8192)

結論與自評

關於本年度的研究成果，在光分碼多工接收機方面，我們已將轉阻放大器、可變增益放大（VGA）與後級放大器與類比相關器整合於同一晶片上，並完成佈局與量測。測試結果顯示，所有電路都能在 1.25Gb/s 的展頻碼下正確工作，且消耗功率僅 452mW。關於非同步光域取樣系統監控方面，我們找出影響取樣所得參數收斂性的條件，同時再提出新的取樣架構，搭配模擬結果驗證其可靠性。經驗證後發現，該架構對取樣之均勻性有明確的改善。

預期近期內本計劃將有論文之發表，擬投稿至 SCI 所收錄之期刊。

參考文獻

【Part A】

1. IEEE Standard 802.3ah, Sep. 2004.

2. Gerry Pesavento,"Ethernet Passive Optical Network (EPON) architecture for broadband access", Optical Networks Magazine Jan./Feb. 2003

3. Chi-Shun Weng and Jingshown Wu,"Perfect Difference Code for Synchronous Fiber-Optical CDMA Communications", IEEE J. Lightwave Technol., vol19, pp.186-194, Feb. 2001.

4. Sung Min Park and Hoi-Jun Yoo, "1.25-Gb/s regulated cascode CMOS transimpedance amplifier for Gigabit Ethernet applications". IEEE JSSC Vol 39, pp.112 - 121, Jan. 2004

5. C. S. Liu, "Design and implementation of analog front-end circuits for optical communication system", National Taiwan Unv, MS thesis, 2003.

6. Galal, S.and Razavi, B., "10-Gb/s limiting amplifier and laser/modulator driver in 0.18- m CMOS technology", IEEE JSSC, Vol 38, pp.2138 – 2146, Dec 2003

【Part B】

7. I. Shake and H. Takara, "Averaged Q-factor method using amplitude histogram evaluation for transparent monitoring of optical signal-to-noise ratio degradation on optical transmission system," IEEE J. Lightwave Technol. Vol. 20, pp. 1367-1373, 2002.

8. H. Takara, S. Kawanishi, A. Yokoo, S. Tomaru, T. Kitoh and M. Saruwatari, "100Gbit/s optical signal eye-diagram measurement with optical sampling using organic nonlinear optical crystal," Electron. Lett., vol. 32, no. 24, pp. 2256-2258, 1996.

9. I. Shake, H. Takara, K. Uchiyama and Y. Yamabayashi, "Quality monitoring of optical signals influenced by chromatic dispersion in a transmission fiber using averaged Q-factor evaluation," IEEE Photon. Technol. Lett., vol. 13, pp. 385-387, 2001.

10. M. Rasztovits-Wiech, K. Studer, and W. R.

Leeb, "Bit error probability estimation algorithm for signal supervision in all-optical networks," Electron. Lett. 30, 71-72, 1994

11. L. Ding, W. Zhong, C. Lu and Y. Wang, "New bit-error-rate monitoring technique based on histograms and curve fitting", Optics Express. vol. 12, pp. 2507-2511, 2004.

12. Z. Li, C. Lu, Y. Dong, Y. Wang,. T. Cheng and F. Yue, "Asynchronous sampling for Q-factor estimation using sampling pulse with wide pulsewidth," IEEE Photon. Technol. Lett., vol. 15, pp. 1749-1751, 2003.

行政院國家科學委員會專題研究計畫期中報告

子計劃五：下世代光子晶體內嵌式光交換器元件設計、製作及應用於寬頻都會與擷取網路平台之研究 (2/3)

Study of Next Generation Photonic Bandgap Embedded Optical Switch Devices and Research of the Applications on Broadband Metro-and Access-Optical Network

計畫編號：NSC 95-2221-E-003-010
執行期限：95 年 8 月 1 日至 96 年 7 月 31 日
主持人：曹士林 教授 國立台灣師範大學 光電科技研究所
計畫參與人員：潘眉秀, 林建宏, 張憲裕,黃俊琪, 劉南新　研究生

一. 中文摘要

在最近幾年，光子晶體光通訊元件設計上已逐漸廣泛的被研究應用，現行在產業及學術研究上也充分的被應用及開發，然而光通信元件之縮小化亦為必然趨勢，因此，本計畫即是以縮小現有光通信元件，並朝向光學能隙晶格光通信元件的技術進行研發為目的。本計畫為“下世代光子晶體內嵌式光交換器元件設計、製作及應用於寬頻都會與擷取網路平台之研究”總計畫之一部份，並分三年進行，第一年已完成光學能隙晶格光子晶體光波導光通信元件系統之研究，並建立模擬環境及測量元件基礎環境，並建立微細光纖抽拉裝置結合設計及模擬矽上微腔盤光記憶儲存單位，以輸入光至微腔盤的共振條件成立與否去決定信號光是否在腔盤中儲存其光能量。本年度為計劃第二年，目前已完成利用矽上絕緣層矽晶元件建立光學讀取系統結合多模干涉型光學能隙波導光分歧器及光子晶體Mach-Zehnder結構，並與第一年之光學能隙晶格光子晶體光波導光通信元件系統整合。進度正常依計劃進行，未來第三年將進行 32x32 矽上絕緣層矽晶為基底奈米光學光波導及波長可交換式微波光子晶體光控開關主動元件光通信元件之研究及整合，以應用於新世代高速光通信系統之中。

本計畫完成研究矽上絕緣層矽晶元件建立光學讀取系統結合多模干涉型光學能隙波導光分歧器及光子晶體Mach-Zehnder結構。我們利用二維光子晶體週期性結構及線狀缺陷的技術並針對不同的能隙結構來控制光在光子晶體波導中行進的路徑，以便達到縮小積體光學元件之體積。多模干涉型光學能隙波導光分歧器是基於自成像現象設計而成。我們利用自成像現象在矽上絕緣層矽晶脊狀光波導設計多模干涉光分歧器並進一步研究自成像現象在光子晶體傳播情形來設計光學能隙波導光分歧器。此外，我們利用六角形晶格光子晶體的Mach-Zehnder結構來達成干涉現象，並藉此設計光學信號讀取系統。

關鍵詞: 光通信元件，光學能隙晶體，波長可交換式光控開關元件，

光學能隙波導光分歧器，矽上絕緣層矽晶，光學讀取頭，光子晶體，光子能隙，多模干涉，脊狀波導。

Abstract:

In recent years, photonic bandgap crystal component with optical communication has been reported for successfully implementing fiber ring laser resonators. In order to fabricate nano optical communication devices, the size reduction of the nano optical communication component to nano scale is a future trend. In this project, we apply nano-photonic bandgap crystal in designing the optical communication components. In order to fabricate nano optical communication devices, the size reduction of the nano optical communication component to nano scale is a future trend. This object of this sub-project is to reduce the existing optical communication component and aims at studying how to apply the photonic bandgap crystal to the optical communication components.

This sub-project is divided into 3 years. At the first year, we have achieved the study for the photonic bandgap crystal applied in active optical communication components serve as optical wavelength switch and we also setup the environment of the simulation and the measurement. In this year, the second year of the sub-project, we study the optical pickup head system by MMI-based PBG waveguide optical splitter with a square-lattice photonic crystal and Mach-Zehnder structure with a hexagonal-lattice photonic crystal building on SOI wafer.

In the future, the third year, we will study and design a 32x32 optical wavelength of Microwave-photonic switch based on SOI which composed of optical unit memory and nano tip fiber components and integration with the optical communication systems developed by others subprojects.

In this project, we design optical pickup head system by MMI-based PBG waveguide optical splitter with a square-lattice photonic crystal and Mach-Zehnder structure with a hexagonal-lattice photonic crystal building on SOI wafer. MMI-based PBG waveguide optical splitter with a square-lattice photonic crystal is based on self-image phenomenon. We design the device according to the self-image phenomenon in MMI optical splitter based on SOI rib waveguide. We use the technique of photonic bandgap and line defect to control the direction of the light wave propagation in a waveguide. Besides, Mach-Zehnder structure with a hexagonal-lattice photonic crystal is also used to design as an interferometer.

Keyword: photonic bandgap crystal, optical communication component, optical switch device, SOI, optical pickup head, photonic crystal, PBG, multimode interference, rib waveguide.

二. 緣由與目的

本子計畫研究方向為下世代光子

晶體內嵌式光交換器元件設計、製作及應用於寬頻都會與擷取網路平台，本計畫主要研發光學能隙晶格結構光通信元件以及矽上微腔盤共振器所設計之光記憶控制儲存單元整合成全光式 32x32 光波長開關交換器。本計畫研究目的是以本實驗室所設計的元件為基礎，整合最新之光控制光的技術來達到全光式光纖通信網路的理想。因此開發光學能隙晶格結構光通信元件之目的在於縮小光通信元件之尺寸，結合奈米製程技術，朝向 PCSOC (photonic communication system on chip)之目標邁進。此子計畫分三年執行，第一年進行之主題為光學能隙晶格光子晶體光波導光通信元件，第二年研究利用矽上絕緣層矽晶元件建立光學讀取系統，製作出全光學式積體化元件，到第三年進一步到微波光子晶體交換器陣列之研究。

此計畫為跨半導體製程技術及光通信領域之不同技術領域整合之新興應用研究，因此，對於國內新研究領域之開發，具有極為重要之必要性光學存儲技術廣泛受到各工程領域之重視與研究 [1-3]。光學讀取頭系統的光點大小則能決定磁碟上的貯存資料得容量。目前有許多方法設計並製作光學讀取頭系統。如使用半導體工技術製作光學讀取頭系統是目前最常使用的方法。而集成式光學讀取頭系統在1986年已經被提出 [4-7]。 S. Ura。提出一個結合光二極體、光柵分光器與偶合器在矽基板上製作出集成式光學讀取頭系統。此讀取系統在聚焦面上的半高寬度是3.5μm，輸入波長為0.79μm [4]，而元件的總尺寸為厘米。 在1991年，H. Ukita提出利用單色同調光結合雷射二極體和光二極體來製作光學讀取頭，在元件總尺寸由之前的厘米平方縮小至微米平方，所使用的波段為1.3μm，聚焦面上的半高寬度為2.4μm[5]。在2001年， S. G.Tang 提出一種光學讀取頭系統，此系統是利用透鏡和圓錐形的非導電性的探針所組成，系統尺寸為厘米平方 、半高寬度在聚焦面上的尺寸為0.2μm，輸入波長為0.488μm [8]。在2004年，T.Liu 和S. L. Tsao 利用光子晶體製作集成式光學讀取頭系統[9-10]。通常，光學讀取頭系統的尺寸都非常大。我們利用半導體製程技術來製作光子晶體式光學讀取頭系統加以縮小尺寸並且有效的縮小聚焦面上光點的尺寸。 我們的研究的目的在矽晶片上利用半導體製程來製作光學讀取頭系統。而利用光子晶體製做光學讀取頭系統的基本概念是 E. Yablonovitch 和S.John在1987年提出的想法 [11-12]。

光子晶體的能隙結構是光子晶體的重要的特徵，為光波是否能在光子晶體中傳播的重要依據。光子晶體波導的能隙結構能提供光場良好的侷限度並且有效縮小光通信設備和光學的存儲設備的體積[13-19]。Meade 最先提出了利用光子晶體能隙[19-24]來製作出光子晶體波導 [24-31]。在本計畫中，我們設計與模擬光學讀取頭利用光子晶體波導和Mach-Zehnder [32]結構製做在絕緣層(SOI)矽晶片上。我們使用OptiFDTD軟體進行模擬研究工作。此軟體裡的演算方法為有限差分時域(FDTD)方法藉由此數值計算模擬光波在波導中傳播方向。當積體電路技術趨於成熟的同時，研究如

何將光學能隙晶格技術應用於主動光通訊元件，於是我們進行模擬測試更進一步利用到積體光學技術製作極小尺寸的波導元件，以期結合光纖通訊之元件，發展出高速光纖通訊所需之關鍵零組件，故光積體元件的發展必然是未來的趨勢。

在本計畫中，我們設計並以光束傳播方法(Beam Propagation Method)分析1x(2N+1)多模干涉植基於SOI脊狀波導之光學分歧器。多模干涉光器件由單模波導和多模態波導所組成。由於多模態波導可以產生自我成像現象，因此我們利用此特性設計在SOI脊狀波導上製作1x(2N+1)的光學分歧器。在材料方面我們研究在SOI脊狀波導在塗佈一層聚合物以及無塗佈時的成效研究。並對矽晶積體光學之結構特性研究，並進行測試傳輸模擬結果，控制矽上微共振腔環的共振條件以決定是否達到耦合的條件做為我們光記憶控制單元的控制機制，我們便可以設計一組光記憶儲存控制單元(OUM)，在未來，我們也將微腔環型光交換器應用在光通信元件上。。

我們利用多模干涉特性，在SOI晶片上設計方形晶格的光子晶體波導之光學分歧器。在設計和分析1x(2N+1)多模干涉光學分歧器時，我們以有限差分時域(FDTD)方法模擬方形晶格排列之光子晶體能帶。由於內部全反射的特性，使得光波能在光纖和波導內部進行傳播而不會消散。而光子晶體是一種週期性的介電材料材料。我們在光子晶體中製造一線缺陷，而在波導中行進的光波不能只僅靠著全反射來傳導，其中必須考量光子晶體能隙，使得波導能將傳導的光波侷限在光子晶體線缺陷中。當光在光子晶體裡面傳播時，對進行一個準確控制光單元來說，是一個具有很高的應用價值，且我們所設計的元件尺寸小，並連同奈米針尖擷取光纖所發射聚焦出之點光源亦相對微小，非常符合我們所設計微小尺寸的光控制單元所要提高精確特性的目的。我們討論自成象現在多模波導與光子晶體結構且使用它在SOI上設計1x(2N+1)光子晶體波導的光學分歧器。

我們並以有限差分時域(FDTD)方法設計和分析在SOI晶片上利用光子晶體波導與 Mach-Zehnder 架構製作光學讀取頭系統，來實現積體光學技術應用於光通訊元件，以利於發展更寬頻都會與擷取光纖通訊系統所需。

三.結果與討論

在光記憶控制單元我們利用矽晶積體光學之結構製做微腔環型光共振腔，其原理結構如同 Fabry-perot 的共振腔體，但它不需要反射的端面，便可以達到自我迴授的目的，利用調整 Gap 之間的距離，去分析最佳的參數，當某些波長的光被耦合進入腔環體時，我們會在腔環中累積共振得到我們所需要的光波長強度，而能達到篩選某特定波段的強度，在研究執行期間，我們研究了如何將矽上微共振腔環所設計之光記憶儲存單位應用於光通信元件當中，圖一為矽上微腔環共振器架構圖，由於矽上微腔環共振器具有非常小的尺寸特性，我們經過模擬並縮小優化元件尺寸，在調動微光環共振器 Gap 參數，將原本 Gap 長度由 200μm 縮減至 0μm 到-200μm，基於我們要設計小尺寸元件的目標，把

它製作成可以控制光傳輸的一個控制單元，我們進行測試傳輸模擬結果如圖二、圖三所示，圖二(a)中為 TE 模態輸出端光場強度圖，當 Gap 由 0nm 縮小至-200nm 時,在 1554.9nm 波段耦合進共振環中，輸出端濾波效果可高達 40 至 50dB，(b) 為 TM 模態輸出端光場強度圖，圖三(a) 中為 TE 模態擷取端光場強度圖，當 Gap 由 0nm 縮小至-200nm 時,在 1554.9nm 波段耦合進共振環中，並由擷取端所測得光場強度，由圖中我們可觀察出當 Gap 趨近於 0nm 時，我們可由擷取端取得越小線寬的波形。(b) 為 TM 模態擷取端光場強度圖，其變化平緩，不受改 Gap 參數影響。

我們利用 SOI 脊狀波導製作 1x(2N+1) 多模干涉光學分歧器，其結構如圖四所示，我們將所設計的 1x(2N+1) 多模干涉光學分歧器的多模波導長度L_{MMI}、寬度W_{MMI}作變化，當我們增加或縮減長度L_{MMI}、寬度W_{MMI}時， 其均勻度與損失會隨著L_{MMI}其變化如圖五、六所示，在 SOI 脊狀深度與均勻度、損失對應變化可由圖七觀察。而均勻度、損失對應波長的變化量由圖八所示。

在設計與分析 1x(2N+1)多模干涉之光子晶體波導光學分歧器，我們將模擬結果與參數列於表格 1。當a/λ=0.4129，我們所設計的 1x(2N+1) 多模干涉之光子晶體波導光學分歧器的多模波導寬度我們可利用式(1)來描述：

$W_{MMI} = 2(2N+1)a$, N=3, 5, 7, 9… (1)

我們所設計的多模干涉光學分歧器，將不同結構做有效結合創新，我們結合了六角型與方形晶格排列的光子晶體來設計 SOI 波導元件。此想法來自於矽晶圓兩不同軸向有相同的晶格常數與半徑，當矽晶軸向晶格常數為 0.64，半徑 0.11μm 的六角形排列光子晶體，其輸入波長為通訊波段 1.55μm 之能帶分析圖如圖九所示。我們並結合我們所研究的多模干涉光學分歧器製作成光學讀取頭系統，圖十為此系統之架構圖，圖中方形晶格至六角型晶格長度為 0.64μm，我們所使用光源為雷射二極體其波段為 1.55μm，在聚焦平面上可測得接收光訊號之半波寬度 0.7μm。在此光學讀取頭系統中，光訊號沿著 Z 軸方向進行傳播其光場分佈圖為圖十一，當光場經過環型光交換陣列平面，光交換面上儲存資訊位元為"1",光波會被直接反射經由光子晶體分歧器符合建設性干涉，在輸出端即聚集建設性干涉點，再利用光學讀取頭系統的檢光器讀取資訊，反之當破壞性干涉光學讀取頭系統的檢光器無法接受到輸出端聚焦盤狀光點，再轉換成"1"、"0"數位位元。在此光學讀取頭系統中由圖十二可得知讀取頭輸出場干涉距 0.45μm，而主波形的旁波帶至次波形旁波帶距離為 1μm。用光學讀取頭系統分析輸出端聚焦光點，可觀察輸出光波經由光環型交換陣列反射後，在輸出端利用檢光二極體偵測建設性干涉與破壞性干涉如圖十三所示產生有、無聚焦點轉換成數位訊號。當有偵測到聚焦光點時則轉會成數位位元"1"如圖十一所示， 當檢光二極體無法接收到光點時時則轉會成數位位元"0" 如圖十四所示檢光二極體無法接收到光環型交換陣列所反射出的光點，以此光儲存分光交換裝置整合成未來寬頻光都會分封交換之關鍵

零組件。

我們所設計和分析在 SOI 晶片上利用光子晶體波導與 Mach-Zehnder 架構製作光學讀取頭系統，在此項研究中我們使用 SOI 材料結合了方形晶格排列光子晶體多模干涉元件與利用六角型晶格排列光子晶體製作 Mach-Zehnder 架構，已成功設計出應用於光交換系統中創新的光交換訊號之光學讀取頭系統。

四.計畫成果自評

在本子計畫第二年執行迄今，我們完成了運用不同結構做有效結合，我們結合了六角型與方形晶格排列的光子晶體來設計 SOI 波導元件，並以有限差分時域(FDTD)方法設計和分析在 SOI 晶片上利用光子晶體波導設計的多模干涉光學分歧與 Mach-Zehnder 架構製作光學讀取頭系統，所設計的元件尺寸小，並連同奈米針尖擷取光纖所發射聚焦出之點光源亦相對微小，非常符合我們所設計微小尺寸的光控制單元來實現積體光學技術應用於光通訊元件以利於發展更高速光纖通訊。我們並完成了運用光學能隙晶格的設計，自行研究以矽上絕緣層矽晶為基底奈米級光學圓環控制元之結構，改變 Gap 參數由正數改變成負參數來縮小光記憶儲存元件體積，並進行模擬設計光通信元件在光儲存元件部分。

設計 1x(2N+1)多模干涉分歧器。並針對 SOI 晶片上利用光子晶體波導與 Mach-Zehnder 架構製作光學讀取頭系統，在此向研究中我們使用 SOI 材料結合了方形晶格排列光子晶體多模干涉元件與利用六角型晶格排列光子晶體製作 Mach-Zehnder 架構，成功設計出創新的光學讀取頭系統。此研究能具體提供在 SOI 光子晶體之大型積體電路整合元件製作良好效能。以未來一年之研究 32x32 埠高速微波光子晶體型光電交換元件在 WDM GPON 及 EPON 平台之整合應用研究及分析，以結合封包交換技術，將可應用於下世代高速光通信系統之中。

最後，在執行計畫期間所發表之相關會議論文達二十四篇[33-56]，期刊論文亦已發表四篇[57-60]，成果豐碩。

五.參考文獻

[1] L. Krusin-Elbaum, T. Shibauchi, B. Argyle, L. Gignac, and D. Weller, “Stable ultrahigh-density magneto-optical recordings using introduced linear defects,” *Nature*, vol. 410, pp. 444-446, 2001.

[2] K. Manoh, H. Yoshida, T. Kobayashi, M. Takase, K. Yamauchi, S. Fujiwara, T. Ohno, N. Nishi, M. Ozawa, M. Ikeda, T. Tojyo, and T. Taniguchi, “Small integrated optical head device using a blue-violet laser diode for Blue-ray Disc system,” *IEEE Optical Memory and Optical Data Storage Topical Meeting*, pp. 386-388, 2002.

[3] N. Kobayashi, and C. Egami, “High-resolution optical storage by use of minute spheres,” *Opt. Lett.*,

vol. 30, no. 3, pp. 299-301, 2005.

[4] S. Ura, T. Suhara, H. Nishihara, and J. Koyama, “An integrated-optic disk pickup device,” *J. Lightwave Technol.*, vol. 4, no. 7, pp. 913-918, 1986.

[5] H. Ukita, Y. Sugiyama, H. Nakada, and Y. Katagiri, “Read/write performance and reliability of a flying optical head using a monolithically integrated LD-PD,” *Appl. Opt.*, vol. 30, no. 26, pp. 3770-3776, 1991.

[6] T. Shiono, and H. Ogawa, “Planar-optic-disk pickup with diffractive micro-optics,” *Appl. Opt.*, vol. 33, no. 31, pp. 7350-7355, 1994.

[7] L. Y. Lin, S. J. Shen, S.S. Lee, M.C. Wu, “Realization of novel monolithic free-space optical disk pickup heads by surface micromachining,” *Opt. Lett.*, 21, pp. 155-157, 1996.

[8] S. G. Tang, T. D. Milster, J. K. Erwin, and W. L. Bletscher, “High-performance readout and recording by a combination aperture,” *Opt. Lett.*, vol. 26, no. 24, pp. 1987-1989, 2001.

[9] T. Liu, A. R. Zakharian, R. Rathnakumar, M. Fallahi, J. V. Moloney, and M. Mansuripur, “Applications of photonic crystals in optical data storage,” *Proceeding of SPIE International Society Optical Engineering*, vol. 5380, pp. 430-438, 2004.

[10] S. L. Tsao and K. C. Lo, “Near field analysis of a compact optical pickup head based on SOI substrate,” *Proceeding of SPIE International Society Optical Engineering*, vol. 5511, pp. 182-191, 2004

[11] E. Yablonovitch, “Inhibited spontaneous emission in solid-state physics and electronic,” *Phys. Rev. Lett.*, vol. 58, pp. 2059-2062, 1987.

[12] S. John, “Strong localization of photons in certain disordered dielectric superlattices,” *Phys. Rev. Lett.*, vol. 58, no. 23, pp. 2486-2489, 1987.

[13] J. D. Joannopoulos, P. R. Villeneuve, and S. Fan, “Photonic crystals: Putting a new twist on light,” *Nature*, vol. 386, pp. 143-149, 1997.

[14] A. Adibi, Y. Xu, R. K. Lee, A. Yariv, and A. Scherer, “Guiding mechanisms in dielectric-core photonic-crystal optical waveguides,” *Phys. Rev. B*, vol. 64, no. 3, pp. 033308, 2001.

[15] M. Notomi, A. Shinya, S. Mitsugi, E. Kuramochi, and H.-Y. Ryu, "Waveguides, resonators and their coupled elements in photonic crystal slabs," *Opt. Express*, vol. 12, no. 8, pp. 1551-1561, 2004.

[16] R. D. Meade, A. Devenyi, J. D. Joannopoulos, O. L. Alerhand, D. A. Smith, and K. Kash, "Novel applications of photonic band materials: Low-loss bends and high Q cavities," *J. Appl. Phys.*, vol. 75, no. 9, pp. 4753-4755, 1994.

[17] P. D. Trinh, S. Yegnanarayanan, and B. Jalali, "Integrated optical directional couplers in silicon-on-insulator," *Electron. Lett.*, vol. 31, pp. 2097-2098, 1995.

[18] E. Cassan, S. Laval, S. Lardenois, and A. Koster, "On-chip optical interconnects with compact and low-loss light distribution in silicon-on-insulator rib waveguides," *J. Selected Topics in Quantum Electron.*, vol. 9, no. 2, pp. 460-464, 2003.

[19] V. Milanovic, "Multilevel beam SOI-MEMS fabrication and applications," *J. Microelectromechanical Systems*, vol. 13, no. 1, pp. 19-30, 2004.

[20] B. Luyssaert, P. Vandersteegen, D. Taillaert, P. Dumon, W. Bogaerts, P. Bienstman, D. Van Thourhout, V. Wiaux, S. Beckx, and R. Baets, "A compact photonic horizontal spot-size converter realized in silicon-on-insulator," *Photon. Technol. Lett.*, vol. 17, no. 1, pp. 73-75, 2005.

[21] U. Fischer, T. Zinke, J. R. Kropp, F. Arndt, and K. Petermann, "0.1dB/cm waveguide losses in single-mode SOI rib waveguides," *Photon. Technol. Lett.*, vol. 8, no. 5, pp. 647-648, 1996.

[22] T. E. Murphy, J. T. Hastings, and H. I. Smith, "Fabrication and characterization of narrow-band Bragg-reflection filters in silicon-no-insulator ridge waveguides," *J. Lightwave Technol.*, vol. 19, no. 12, pp. 1938-1942, 2001.

[23] S. G. Lee, "Study of WDM Optical SOI Waveguide Michelson Interferometer Temperature Sensor Networks," M.S. degree thesis, Taiwan, R.O.C., 2000.

[24] L. Vincetti, A. Cucinotta, S. Selleri and M. Zoboli, "Three-dimensional finite-element beam propagation method: assessments and developments," J. Opt. Soc. Am. A, vol. 17, no. 6, pp. 1124-1131, 2000.

[25] M. D. Feit and J. A. Fleck, Jr., "Light propagation in graded-index optical fibers," *Appl. Opt.*, vol. 17, no. 24, pp. 3990-3998, 1978.

[26] P. Danielsen, "Two-dimensional propagating beam analysis of an electrooptic waveguide modulator," *J. Quantum Electron.*, vol. 20, no. 9, pp. 1093-1097, 1984.

[27] Y. Chung and N. Dagli, "An assessment of finite difference beam propagation method," *J. Quantum Electron.*, vol. 26, no. 8, pp. 1335-1339, 1990.

[28] P. Yeh, *Optical waves in layered media*, chapter 1, Canada, John Wiley & Sons, 1988.

[29] R. Scarmozzino, A. Gopinath, R. Pregla, and S. Helfert, "Numerical Techniques for Modeling Guided-Wave Photonic Devices," *J. Selected Topics in Quantum Electron.*, vol. 6, no. 1, pp. 150-162, 2000.

[30] G. R. Hadley, "Transparent boundary condition for the beam propagation method," *Opt. Lett.*, vol. 16, pp. 624-626, 1991.

[31] W. P. Huang and C. L. Xu, "Simulation of three-dimensional optical waveguides by a full-vector beam propagation method," *J. Quantum Electron.*, vol. 29, pp. 2639, 1993.

[32] N. Takato, T. Kominato, A. Sugita, K. Jinguri, H. Toba, and M. Kawachi, "Silica-based integrated optic Mach-Zehnder multi/demultiplexer family with channel spacing of 0.01dB/250nm," *J. Sel. Areas Communication*, vol. 8, pp. 1120-1127, 1990.

[33] Tz-Yuan Huang, Chih-Ham Ko, and Shyh-Lin Tsao "Experiment Results of Integrated Optical 32x32 Arrayed Waveguide Grating Based on SOI Substrate" International conference on silicon electronics and photonics (ICSEP'06), Taipei, Taiwan. pp.55-56, 2006. (Best student paper award)

[34] Chih-Ta Chu , Chia-Chin Chiang and Shyh-Lin Tsao "Design and Analysis of Microring Optical Wavelength Routing Switches Based on SOI Waveguide ",Internatiomal workshop on multi-project chip(IWMC'06) Taipei, Taiwan. pp.102-103 ,2006. (Best student paper award)

[35] Li-Chiang Hu, Yu-Wei Yang, Chia-Chin Chiang and Shyh-Lin Tsao
"Theoretical and Experimental Study of 50GHz Amplitude Modulated Mode-Locked Figure

Eight Fiber Laser ” International conference on high-speed and broadband network (ICHBNT’06) Taipei, Taiwan. pp.79-80 ,2006. (Best student paper award)

[36] M.Oane,F. Scarlat, Chia-Chin Chiang, Shyh-Lin Tsao, I.N.Mihailescu, C.Oproiu,“The Green function method in laser-multi-layer structures interaction”, International conference on silicon electronics and photonics (ICSEP’06) Taipei, Taiwan. pp.42-44 ,2006. (Best paper award)

[37] Chun-Cheng Lin, Shih-Yung Tsai, Chia-Chin Chiang and Shyh-Lin Tsao“FDTD Analysis of 1x(2N+1) MMI-Based PBG Waveguide Optical Splitter” , International conference on silicon electronics and photonics (ICSEP’06) Taipei, Taiwan. pp.40-41 ,2006.

[38] Chih-Ta Chu, Chia-Chin Chiang, Shu-Fen Hu and Shyh-Lin Tsao “Desiga and Fabrication of Microring Optical Wavelength Switches Based on SOI Waveguide” Symposium on Nano Device Technology(SNDT’06) Taipei, Taiwan. I 1-23, 2006.

[39] Chun-Wei Tsai , Chih-Ta Chu , and Shyh-Lin Tsao “ Study of Integrated Optical Two-Dimensional Photonic Bandgap Sharp Bend Waveguide Based on SOI Waveguide” ,Accept by the Tenth Opto-Electronics and Communications Conference （OECC 2006）

[40] Tz-Yuan Huang, Yen-Heng Lin, Bao-Jen Pong, and Shyh-Lin Tsao “ Silicon-On-Insulator Arrayed Waveguide Grating Erbium Doped Waveguide Cover on” , Accept by the Tenth Opto-Electronics and Communications Conference （OECC 2006）

[41] Chun-Cheng Lin, Shih-Yung Tsai, Chia-Chin Chiang and Shyh-Lin Tsao ” An 1x(2N+1) MMI Optical Splitters Based on SOI Rib Waveguide” , Accept by International Conference on Communications, Circuits and Systems(ICCCS 2006)

[42] Pei-Yuan Chu，Yu-Wei Yang ， Chia-Chin Chiang and Shyh-Lin Tsao “50GHZ optical pulse generation for synchronization of high speed computing signals” SPIE Optics Photonics 13-17 August 2006, San Diego, California USA.

[43] Mao-Tung Weng, Wen-Ching Lee, Chia-Chin Chiang and Shyh-Lin Tsao “Combination of CPW-PBG Cell for Achieving Three band Frequency Division Multiplexer” SPIE Optics Photonics 13-17 August 2006, San Diego, California USA.

[44] Hung-Jen Ke, Jian-Lin Chiu, Chia-Chin Chiang and Shyh-Lin Tsao “A novel two-way wavelength-

division-multiplexed fiber laser" SPIE Optics Photonics 13-17 August 2006, San Diego, California USA.

[45] Yung-Hsien Tsai , Yen-Heng Lin ,Chia-Chin Chiang and Shyh-Lin Tsao"Application of 64 channel laser for free space interconnections" SPIE Optics Photonics 13-17 August 2006, San Diego, California USA.

[46] Chien-Hung Lin ,Chih-Ham Ko, Chia-Chin Chiang and Shyh-Lin Tsao
" Design of photonic switching function of 32×32 arrayed waveguide grating" SPIE Optics Photonics 13-17 August 2006, San Diego, California USA.

[47] Mei-Hsiu Pan, Chih-Ta Chu, Chia-Chin Chiang and Shyh-Lin Tsao
" Design and Analysis of PBG Structure for achieving SOI Buffer" SPIE Optics Photonics 13-17 August 2006, San Diego, California USA.

[48] Chun-Cheng Lin, Chun-Chi Huang, Shyh-Lin Tsao, "Design and Analysis of SOI Devices Application to Optical Pickup Head System" National Symposium On Telecommunications, 2006

[49] Liu Jui-Yu, Kuo Yu-Ti, Tsao Shyh-Lin, "Simulation and Experiments of a HEMT/BJT Cascaded 400MHz-3GHz Broadband Amplifier" National Symposium On Telecommunications, 2006

[50] Chih-Ta Chu, Mei-Hsiu Pan, S.F. Hu and Shyh-Lin Tsao "Design and analysis of nano resonant gap ring structure for electro-optical wavelength switch." International Symposium on Nano Science and Technology 2006

[51] Chun-Cheng Lin, Chun-Chi Huang and Shyh-Lin Tsao "Design of optical pickup head device with MMI-based PBG waveguide on SOI wafer" International Symposium on Nano Science and Technology 2006.

[52] Chien-Hung Lin and Shyh-Lin Tsao "Multimode interference beam splitter based on access nanowire waveguide" International Symposium on Nano Science and Technology 2006.

[53] Yu-Ti Kuo, Wen-Ching Lee, and Shyh-Lin Tsao,"FBG Frequency Response Measurement by Two-Way Optical Frequency Domain Reflection/Transmission Technique", Optics and Photonics Taiwan, Tainan, Taiwan, 2006.

[54] [41] Nan-Hsin Liu, Li-Chiang Hu, Shyh-Lin Tsao, "Pulse Level Equalized Rational Harmonic Mode-Locked Laser", Optics and Photonics Taiwan, Tainan, Taiwan, 2006.

[55] Hsion-Yu Chang, Chih-Ta Chu, and Shyh-Lin Tsao, “Design and Simulation of Integrated 2x2 Electro-Optical Routing Wavelength Switch by Micro-ring Resonators Based on SOI”, Optics and Photonics Taiwan, Tainan, Taiwan, 2006.

[56] Mei-Hsiu Pan, Chih-Ta Chu, Chia-Chin Chiang and Shyh-Lin Tsao, “Design and Analysis of PBG Structure for achieving SOI Buffer” Accept by Photonic Devices and Algorithms for Computing VIII, SPIE Int. Soc. Opt. Pho., 2006.

[57] Y.-H. Lin and Shyh-Lin Tsao “Improved design of a 64×64 arrayed waveguide grating based on silicon-on-insulator substrate” *IEE Proceedings: Optoelectronics*, v 153, n 2, 2006, p 57-62.

[58] Oane, M. Scarlat, F., Shyh-Lin Tsao; Mihailescu, I.N. “Thermal fields in laser-multi-layer structures interaction” *Optics and Laser Technology*, v 39, n 4, June, 2007, p 796-799.

[59] Oane, Mihai, Shyh-Lin Tsao; Scarlat, Florea “Temperature field distribution in multi-layered solid media heated with multi-modes laser beam” Optics and Laser Technology, v 39, n 1, February, 2007, p 179-181.

[60] Chun-Wei Tsai, Chih-Ta Chu, Mei-Hsiu Pan, Shyh-Lin Tsao, “Design and analysis of one-dimensional resonant hexagonal holes photonic bandgap filter waveguide” Optical Engineering, v 45, n 8, August, 2006, p 084601

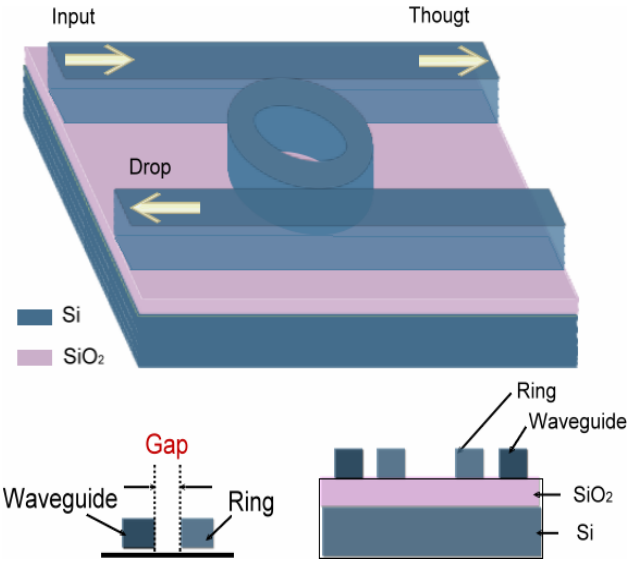

圖一. Structure of microring resonator based on SOI rib waveguide

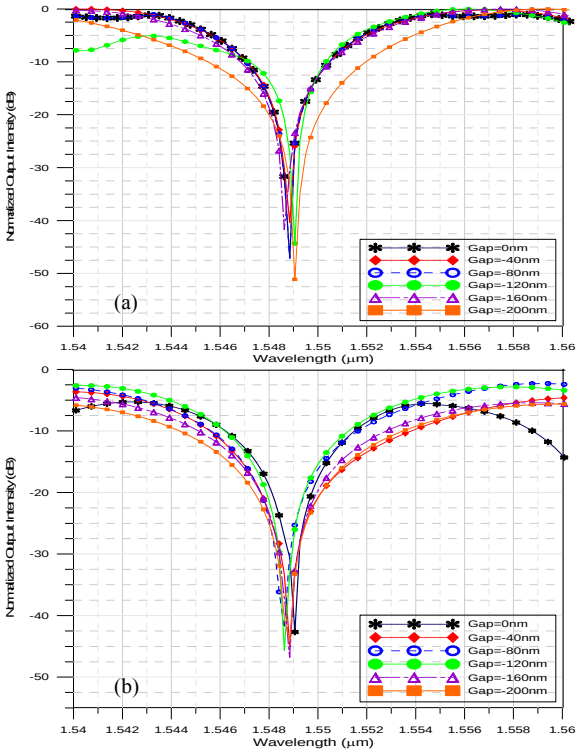

圖三. (a)TE Mode & (b)TM transmission Spectrum of microring resonator with various radius at though port

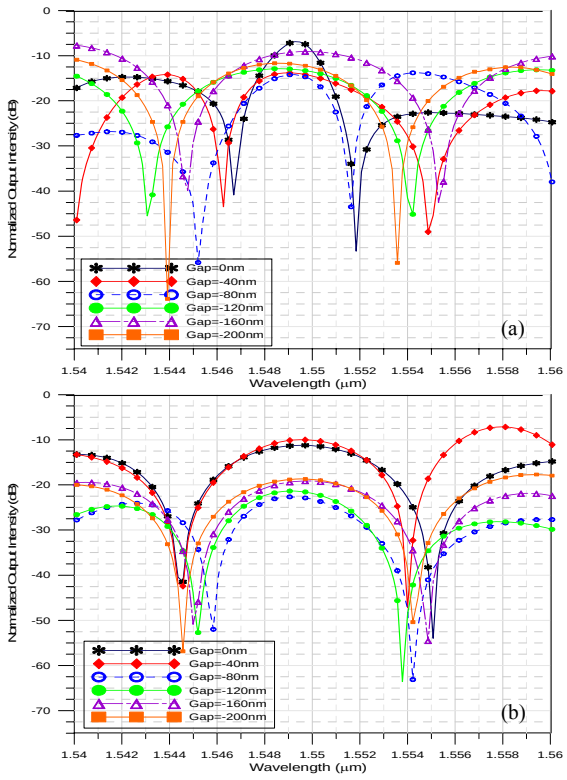

圖二. (a)TE Mode & (b)TM transmission Spectrum of microring resonator with various radius at drop port

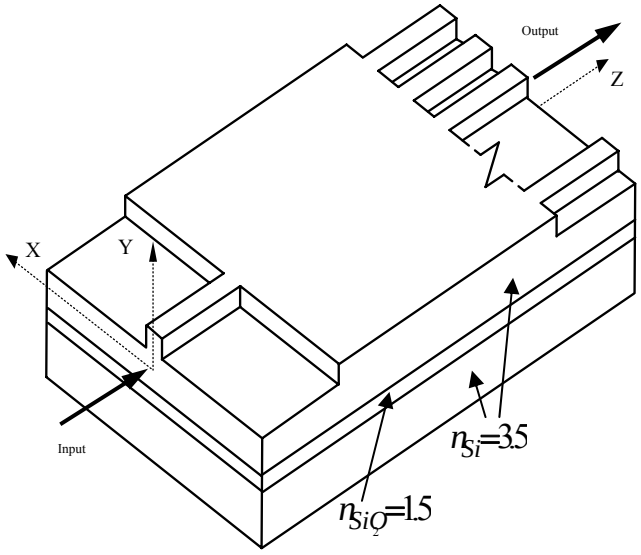

圖四. Structure of 1x(2N+1) MMI optical splitter based on SOI rib waveguide

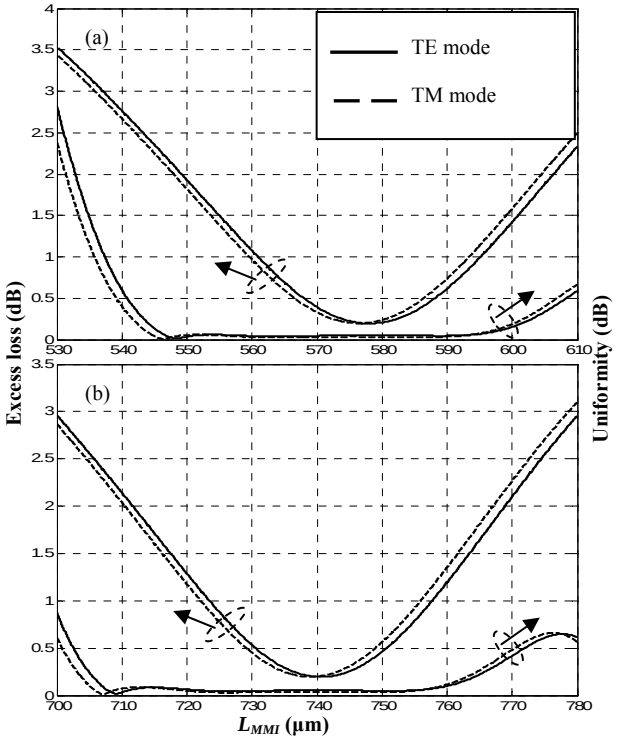

圖五. Length variation of MMI waveguide of a (a) 1x7 & (b) 1x9 MMI splitter

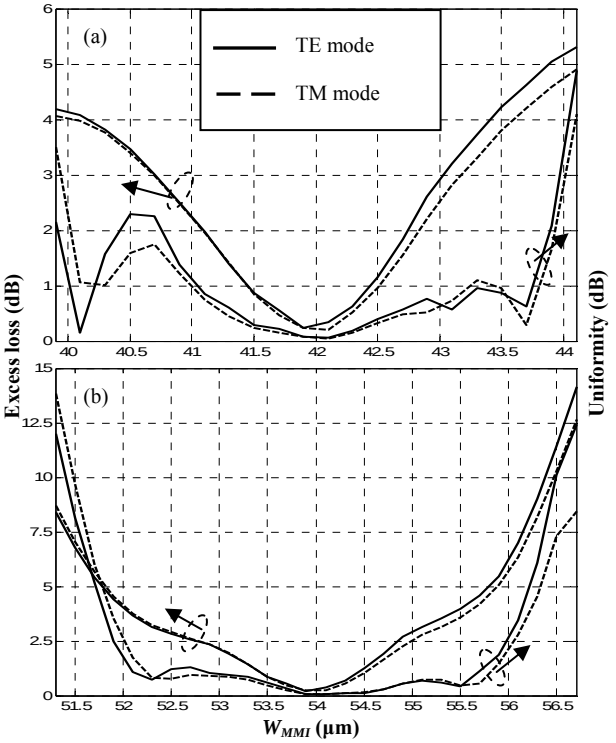

圖六. Width variation of MMI waveguide of a (a) 1x7 & (b) 1x9 MMI splitter

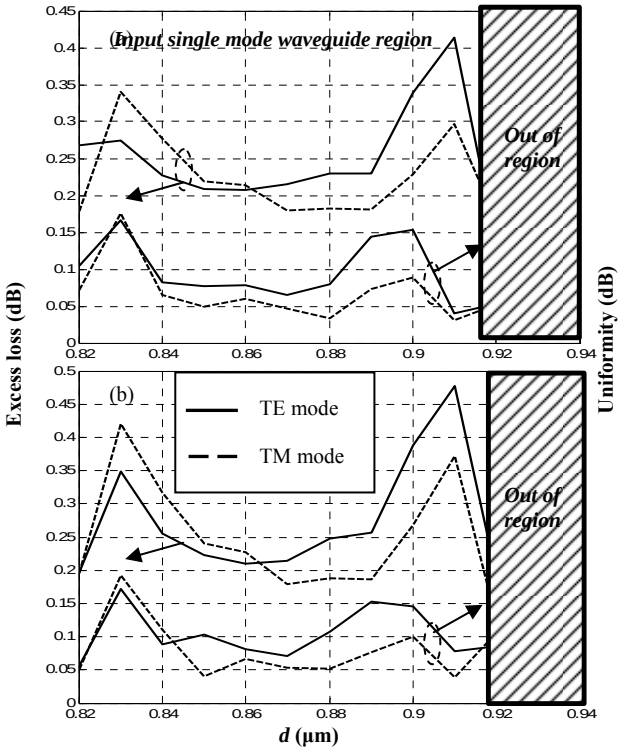

圖七. Etched depth variation of MMI waveguide of a (a) 1x7 & (b) 1x9 MMI splitter

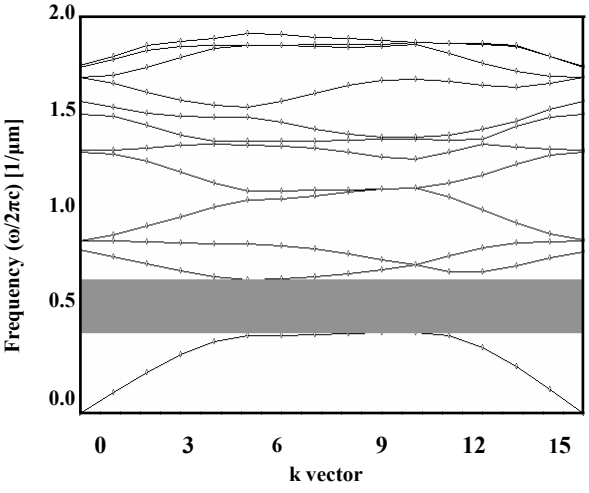

圖八. TE band structure for lattice constant a = 0.64μm and radius r = 0.11μm of Si rod with a hexagonal lattice

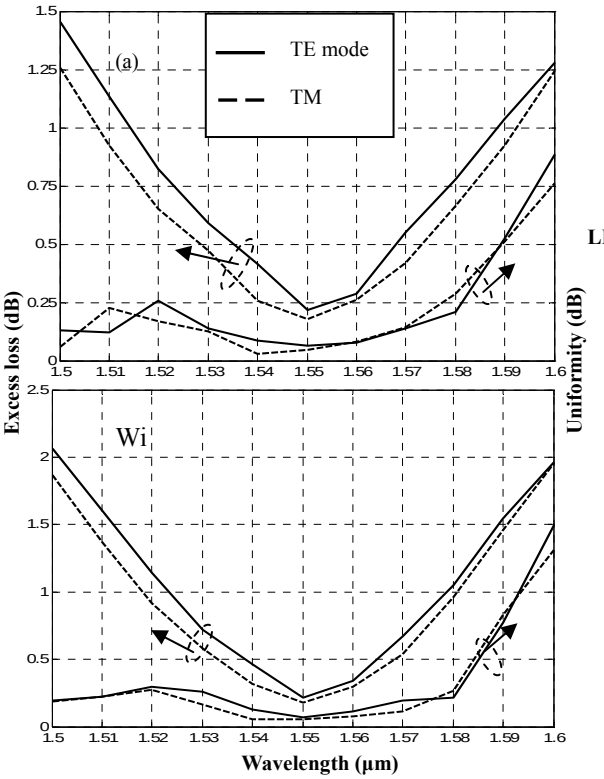

圖九. Response of input wavelength of MMI waveguide of a (a) 1x7 & (b) 1x9 MMI

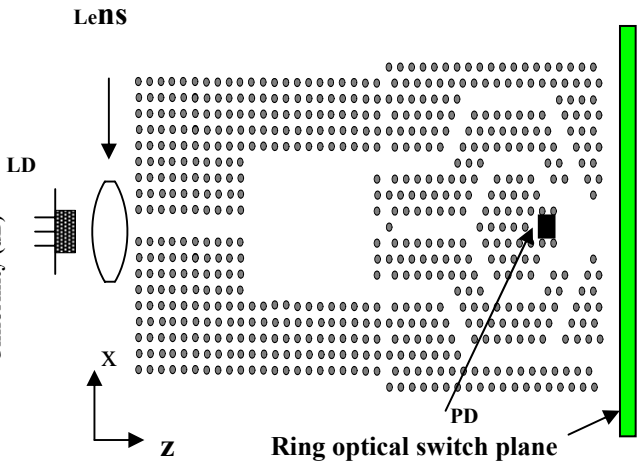

圖十. Structure of our designed optical pickup system based on MMI PBG waveguide

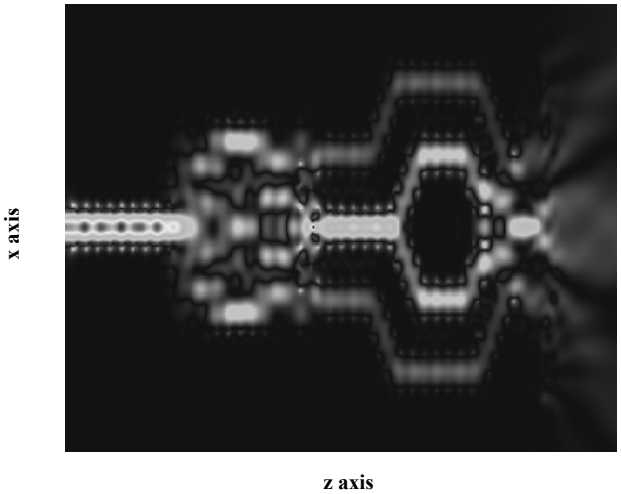

圖十一. Optical field distribution of optical pickup system launched on land region of ring optical switch

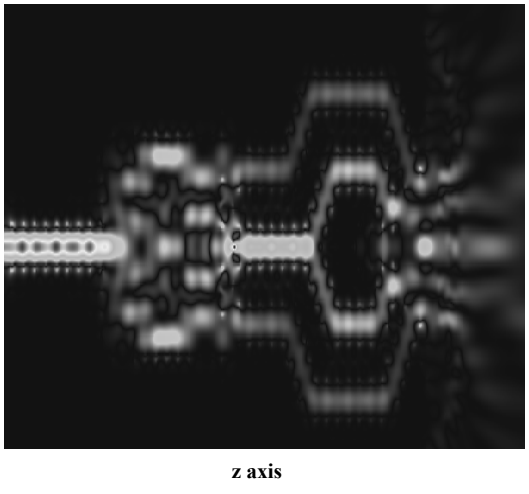

圖十二. Optical field distribution of optical pickup system launched on pit

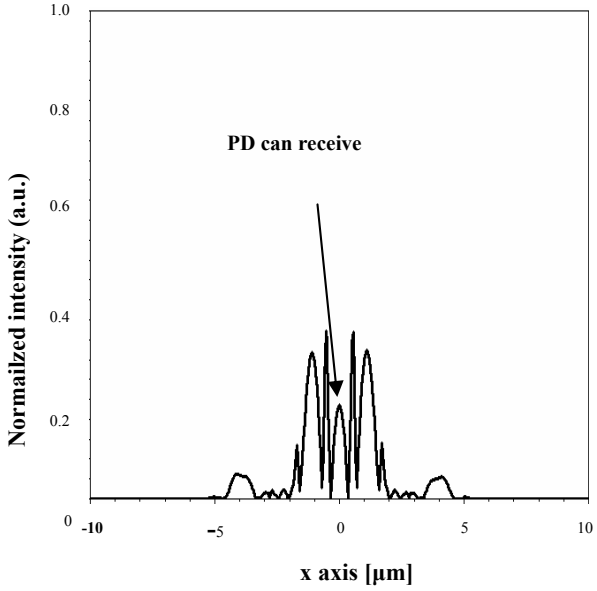

圖十三. Output field intensity of improved system launched on land region of disk

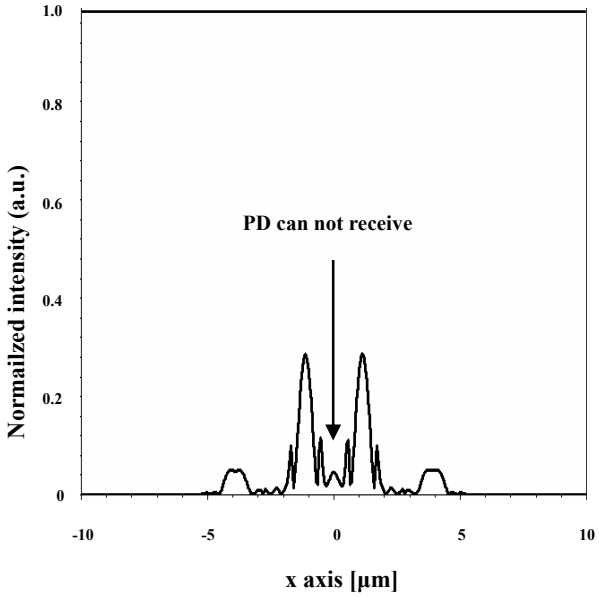

圖十四. Output field intensity of optical pickup system launched on pit region of disk